Efficient Methodology for Roll Prediction on Two Dimensional Bodies in Complete Nonlinear Flows

by

Ratnakar Gadi

in partial fulfillment of the requirements for the degree of

Master of Science
in Ship Hydromechanics

at the Delft University of Technology,
to be defended publicly on Monday December 18, 2017 at 10:30 AM.

Supervisors:	Prof.Dr.ir.R.H.M.Huijsmans,	TU Delft
	Dr.ir.Ido Akkerman,	TU Delft
	Abrari Noor Hashmi	TU Delft
Thesis committee:	Dr.ir.G H Keetels ,	TU Delft

An electronic version of this thesis will be available at
`http://repository.tudelft.nl/`.

Abstract

The accurate computation of hydrodynamic loads on ships is necessary as it dictates the habitability and survivability of a ship. For simple geometries, we can seek for analytical solutions, but as the geometry becomes complex, we needs to resort for numerical solutions. There exists many numerical solution techniques: Finite difference methods, Finite element methods, Finite volume methods and Boundary element methods. Owing to their popularity and simplicity, We employ Boundary Element Methods for our numerical simulations.

Before we carry out the estimation of loads on ship structures, we need to develop a Numerical Wave Tank (NWT). This resembles the physical wave tank in a numerical setting. We have chosen the numerical technique, but the order of the method and the distribution of singularities have not been fixed. Though, Higher Order Boundary Element Methods (HOBEM) ensures higher convergence rate, they require complex coding effort. So, we employ a Lower Order Boundary Element Methods (Constant Panel Method). The singularity distribution is governed by the physics of the problem, minimal discretization error and minimum computational effort. After considering these factors, we choose mixed source distribution (sources and dipoles) for our computation. Thus, employing mixed source distribution, we develop a Constant Panel Method (CPM) for simulating nonlinear waves in our NWT.

After developing NWT, we introduce the body(a 2D barge) into the computational domain. We divide the complete nonlinear program into two programs: a Nonlinear diffraction program, where the body is fixed and the wave impinges on the body, a Nonlinear radiation program, where the body is forced to follow canonical motion in roll mode on an initially undisturbed calm water. We first employ the standard Direct Pressure Integration (DPI), where the generalized load on the structure is obtained as the integration of the pressure along the wetted surface of the body. The computation of

Bernoulli pressure requires an accurate estimation of the temporal and spatial gradients of the velocity potential, which is cumbersome. So, instead we employ Reynolds Transport Theorem (RTT) to the fluid momentum in our closed domain and get an expression for the generalized loads. Such a technique was first introduced by P.D.Sclavonous (2012), but we had to re-derive the theory, since the lateral artificial boundaries (the upstream and downstream boundaries) have not been considered in his derivation. So, we reformulated the Fluid Impulse Theory (FIT). The results of the reformulated FIT have been compared with the results of the DPI.

The results of both the techniques match within a reasonable accuracy, varying depending on the input wave parameters. By employing the reformulated FIT, we circumvent the temporal and spatial gradients of the velocity potential on the body, but the reformulated FIT is quite sensitive to the representation of the free surface.

Acknowledgements

I would like to express my deep gratitude to Prof.Dr.ir.R.H.M.Huijmans for his enthusiastic encouragement and patient guidance during this research work. I would also like to thank Dr.ir.Ido.Akkerman for his useful critiques and assistance in keeping my progress in schedule. My grateful thanks are extended to Mr.Abrari Noor Hashmi(Msc) for his great mathematical intution, without which this research would be an impeccable task, to Dr.ir.J.E.Romate for the initial assistance in the development of the numerical program and to Dr.ir.Henk de Koning gans who was never busy to discuss the details.

I wish to express my very special appreciation to my parents, especially my mother, for her immense support, despite battling cancer. Iwould also like to thank my uncle, aunt and my family for the assistance and their immense faith in me. I would also take this as an oppurtunity and thank my colleagues and friends: Srikar, Prasad, Sai bhaskar, Vinodh, Yue Xie, Harriet, Miltos, Luka, Gian and Teressa for making me feel comfortable and supporting me.

Contents

List of Figures

List of Tables

Nomenclature

ϕ	velocity potential	$[m^2/s]$
g	acceleration due to gravity	$[m/s^2]$
p	pressure	$[N/m^2]$
ρ	Density of sea water	$[kg/m^3]$
U	Velocity of the surfaces	$[m/s]$
S_{BO}	bottom surface, chapter 2	[-]
η	Free surface elevation	[m]
$\frac{\partial \phi}{\partial x}$	horizontal gradient of the velocity potential	[m/s]
$\frac{\partial \phi}{\partial y}$	vertical gradient of the velocity potential	[m/s]
$\frac{\partial \eta}{\partial x}$	horizontal gradient of the free surface elevation(also wave slope)	[-]
c	speed of the wave	[m/s]
$\frac{\partial \eta}{\partial t}$	$temporal gradient of free surface elevation$	[m/s]
$\frac{\partial \phi}{\partial t}$	$temporal gradient of velocity potential$	$[m^2/s^2]$
V_n	Normal gradient of the velocity potential	[m/s]
$\frac{\partial \phi}{\partial n}$	Normal gradient of the velocity potential	[m/s]
UP	Upstream boundary, Chapter 2	[-]
DS	Downstream boundary, Chapter 2	[-]
BO	Bottom boundary, Chapter 2	[-]
FS	Free surface boundary, Chapter 2	[-]
$(Q)_j^n$	Quantity Q at location 'j' evaluated at time step 'n'	units of Quantity Q

N	Outward Normal	[-]
N_x	X component of the outward normal	[-]
N_y	Y component of the outward normal	[-]
k	Wave number	$[m^{-1}]$
ϕ_I	Velocity potential of the incident wave	[-]
A	Amplitude of the incident wave	[m]
ω	wave frequency	$[rad/s]$
h	Depth of the computational domain	[m]
CFL	Courant-Friedrich-Number	[-]
Δt	Time step	[s]
Δx	mesh size	[m]
λ	wavelength	[m]
$\frac{H}{\lambda}$	Wave steepness	[-]
N	Order of the input wave	[-]
φ	acceleration potential	$[m/s]$
$\frac{\partial^2 \phi}{\partial^2 x}$	double derivative of the velocity potential with respect to x	$[m/s^2]$
$\frac{\partial^2 \phi}{\partial^2 y}$	double derivative of the velocity potential with respect to y	$[m/s^2]$
ϕ_D	diffraction potential	$[m^2/s]$
S_{UP}	Upstream boundary(FIT derivation)	[-]
S_{DS}	Downstream boundary(FIT derivation)	[-]
S_{FSL}	Free surface left of the body(FIT derivation)	[-]
S_{FSR}	Free surface right of the body(FIT derivation)	[-]
S_B	Instantaneous body wetted surface(FIT derivation)	[-]
S_{BO}	Bottom surface(FIT derivation)	[-]
B	Beam of the barge, Chapter 3	[m]
T	Draft of the barge, Chapter 3	[m]

$\omega\sqrt{\frac{B}{g}}$	Non-dimensional radiation frequency	[-]
$\frac{M}{\rho B^2 T g/2}$	Non-dimensional moment for the radiation program	[-]
$\frac{\lambda}{B}$	Non-dimensional wavelength	[-]
$\frac{M}{\rho B^2 T g/2H/\lambda}$	Non-dimensional moment for the diffraction program	[-]

Chapter 1

Introduction

The response of a structure, be it freely floating or constrained, to a sea state is the most interesting aspect for the naval architects as it dictates the survivability and habitability of the structure. Therefore, a thorough knowledge of the responses of the structure in the sea states is paramount.

The responses of geometrically simple structures under the excitation of linear sea states(characterized by small wave-height to wavelength ratio) can be found analytically, but as geometry turns out to be complicated or the assumption of linear sea state turns out invalid, one needs to seek numerical solutions. An expensive alternative is to carry out the physical modeling, but scale effects may effect the outcome. On the other hand, the numerical methods, may model finite aspects of the problem at hand which leads to a simplified problems. But, results obtained with these models may be inaccurate in certain situations.

In this thesis, a numerical method is developed and described for evaluating the responses of the structure in steep waves.

1.1 Physical Background

When the characteristic dimensions of the structure under consideration are large and we are interested in the global response of the structure, the flows can be assumed to be inviscid. When the flow is irrotational initially and inviscid, the flow should stay irrotational all times later. These assumptions make the tools of potential theory applicable to characterize the flow field. Thus, the velocity vector can be represented as

a gradient of scalar velocity potential.

When we are dealing with wave-body interactions, in many cases, it is sufficient to linearize the free surface boundary conditions and the solve the linear problem. But, once the waves tend to be steeper, the assumptions of linearity do not hold and one needs to seek to different techniques for solving such problems. These steep waves are characterized by many nonlinear wave effects which include nonlinear wave-wave interactions, overturning of waves and breaking. If a body is introduced, these nonlinear effects may influence the wave-body interactions, thus ruling out the possibility of linearized equations. Typical examples where nonlinear wave body interactions may occur include:

- Overturning and breaking of the wave under excessive body motion.
- Bow wave slamming
- Violent wave sloshing
- Large amplitude motion and capsizing

Though, all the stated examples may not be dealt with the assumption of potential theory in modeling the physical process, but the results from the potential theory computations can give inputs for a more general model.

Though, the goal of the thesis is not to deal with all the stated examples, but instead the author wants to shed light that the nonlinear potential flow models are necessary and useful from engineering point of view.

1.2 Existing Methods to deal with the steep waves

The complete nonlinear potential flow models have evolved over the last three decades. The free surface equations can be derived using a Lagrangian or Eulerian approach. When, a Lagrangian description of flow is used, the time evolution of free surface equations is carried out by following the fluid particles, whereas in Eulerian flows, the horizontal displacement of the points are fixed and the points are allowed to move in vertical direction. A more detailed discusion of the two free surface representation techniques, along with their equations and the technique employed in the thesis is presented in Chapter 2 of the thesis.

The outstanding paper of Longuet-Higgins-Cokelet[1] set the stage for numerical simulation of steep waves where a Lagrangian description of flow was employed. With

the assumption that the flow was periodic, they mapped their physical domain into a closed contour and solved the numerical problem. Following the lines of Longuet-Higgins-cokelet, Vinje and Brevig[2][2] introduced a two dimensional body into the domain. They solved the whole problem in two dimensions, using complex potential. So, the idea of extending the code into three dimensions was discarded, as the stream function could not be defined in a three dimensional flows. They also used the assumptions of periodicity of the solution, which cannot be true, if a body is introduced into the domain as it interacts with the waves. They experienced problems at the intersection of the upstream boundary and the free surface boundary and also at the intersection of free surface and the body. Lin[3] studied about the physics of the flow at the intersection point, by simply looking at the behavior of the flow at the intersection of the wave-maker and free surface in his doctoral thesis. He discovered a weak singularity and stated that this singularity is due to the confluence of boundary conditions at the intersection point between the upstream and free surface boundary. He suggested that both the boundary conditions should be satisfied at the intersection point. The parallel developments in the field were carried out by team of researchers from the Technical University of Twente(Johan Egbert Romate[4],Jan Brooeze[5]). Their works dealt with the development of numerical algorithm for the complete nonlinear gravity wave simulations in three dimensions using a higher order panel method. Their work was followed up by Van Daalen[6], where he introduces a body into the domain. He provides a derivation for setting up an auxiliary intgeral equation for the temporal gradient of the potential. The necessity for such an auxiliary integral equation will be described in the next section.

On the other hand, the wave body interaction using an Eulerian description of flow has very few literature associated. D.Sen[7], in his doctoral thesis, uses a Eulerian description of the flow and finds the forces/moments on the body along with the motions, but only few time traces were simulated after which the program crashed.

The complete nonlinear potential flow models are not the only means of finding the response of the body in steep waves. Decomposing the total potential as the ambient wave potential and disturbance potential, assuming that the disturbance potential is small compared to the ambient wave potential, the complete nonlinear free surface evolution equations can be linearized with respect to the ambient wave potential. This, so called weak-scatter theory, developed by J.D.Pawlouski[8], satisfies the kinematic boundary condition on the body on its instantaneous surface, whereas satisfies the free

surface equations on the ambient wave profile. This can be understood by the following example. Imagine a sharp knife oscillating with a large amplitude in very steep waves. Since, the knife is slender, the disturbance it causes would be small, though it has large motion. But, this weak scatter theory, is mathematically inconsistent. Though, some computations were carried out in the thesis work using the weak scatter approach, they are not reproduced. The body which we consider is two dimensional and not slender, thus the linearization of the free surface equations about the ambient wave profile is not justifiable.

They also exist techniques where the kinematic boundary condition on the body is satisfied on its instantaneous surface, whereas the free surface equations are linearized with respect to the undisturbed free surface(calm water level). This so called body-exact approach, deal with the nonlinearities associated with large amplitude motions, but they cannot predict response of the structure when subjected to steep incident waves. So, we do not carry out any work with these body-exact approaches.

1.3 Methods for finding the Generalized forces

A brief description of the methods for finding the Generalized forces is provided here. A detailed explanation will be provided in chapter 3.

1.3.1 Direct Pressure Integration

The pressure on the body is calculated using by the bernoulli equation(1.1). The integration of the pressure over the wetted surface area(the area of the body immersed in the water) yields the generalized forces(1.2).

$$p = -\rho(\frac{\partial \phi}{\partial t} + \frac{1}{2}\nabla\phi \cdot \nabla\phi + gZ) \tag{1.1}$$

$$F = \int_S pn\mathrm{ds} \tag{1.2}$$

Now, in the beginning, Euler backward differencing was used to find the temporal gradient of potential when free motion simulations were carried out. This leads to the accumulation of numerical error as stated by R.F.Beck[9]. In the case of forced motion simulations, the force can be post-processed and Euler forward differencing can be performed. An alternative is to set up an auxiliary integral equation as explained in chapter 3. This is a computationally demanding task.

1.3.2 Fluid Impulse Theory

Original Fluid Impulse Theory

As explained in previous subsection, the evaluation of the temporal gradients and spatial gradients is often a computationally demanding task. In order to circumvent these terms, P.D.Sclavonous[10] has derived a new theory named Fluid Impulse Theory basing on the application of the Reynolds Transport Theorem to the fluid momentum in a closed domain. The total force on the body is expressed as the summation of nonlinear Froude-Krylov Force(the integration of the nonlinear incident wave profile along the body area below dynamic waterline), nonlinear buoyant force(the integration of the hydrostatic pressure along the body area below the dynamic waterline) and the time derivative of the free surface and body impulse(Impulse is the integral of the product of the potential and normal to the surface taken along the surface(1.3). The Dynamic waterline is defined as the intersection of the body surface and the ambient wave profile.

$$I = \int_S \phi n \mathrm{ds} \tag{1.3}$$

The first application of the theory was carried out using the weak scatterer approach, which will be briefed next. The total potential is decomposed into the incident wave potential and the disturbance potential. The disturbance potential is evaluated using 2.5D+T theory, as potrayed by P.D.Sclavonous and S.Lee[11]. They assume that the incident wave profile is locally horizontal, which leads to the shift of the reference plane at each two dimensional section from the calm water level to the dynamic waterline. This allows them to incorporate Havelock Greens functions. These Green functions satisfy the Laplace equation, linearized free surface boundary conditions and the radiation conditions identically. So, only the body has to be meshed. The final equations, as derived by the authors has no contribution from the control surfaces at infinity.

Reformulations required for the Fluid Impulse Theory

The Fluid Impulse Theory, as original applied deals with weak-scatter flows and this encourages the usage of Havelock Greens functions. As already explained, this weak scatter theory is mathematically inconsistent. So, in the thesis, mathematically consistent approach is undertaken : we invoke the kinematic boundary condition on the instantaneous body location and invoke the complete nonlinear free surface equations

on unknown nonlinear free surface profile. This calls for derivation of Greens functions which satisfy the Laplace equation, complete nonlinear free surface equations and radiation conditions at infinity. This is quite an impeckable task. Instead, simple Rankine Greens functions are used, but the penalty would be meshing of the free surface and the body. These simple Rankine Green funtions satisfy the Laplace equation identically and the radiation condition at infinity. But, one needs a finite computational domain for numerical simulations, this leads to truncation of the free surface by vertical artificial boundaries. Thus, the radiation condition on this truncated domain is not satisfied by the Rankine Greens Function and thus along with the free surface and the body, these artifical vertical boundaries also have to be meshed. This calls for the reformulation of the Fluid Impulse Theory.

1.4 Research Objectives

The main objectives of the research work are:

1. Reformulating the Fluid Impulse Theory using the Reynolds Transport Theorem to the fluid momentum in a closed domain, so that the effect of the computational domain truncation is considered.

2. Develop a code which uses the direct pressure integration, reformulated version of Fluid Impulse Theory to compute nonlinear roll moment on arbitrary two dimensional body. We choose barge as the two dimensional body.

3. Stating the advantages/limitations of the reformulated Fluid Impulse Theory as compared with the Direct Pressure Integration.

1.5 Numerical Techniques

Most of the numerical methods used so far belong to one of the following categories:

- Finite differences methods
- Finite element methods
- Finite volume methods
- Boundary element methods

The first three techniques are field discretization methods. In these methods, the governing field equation is discretized, whereas in Boundary element methods, the governing field equation is not discretized, but an equivalent integral equation representing the governing equation is discretized.

Although every method has its own pros and cons, the Boundary element methods have been the most promising ones and are well established in the field of hydrodynamics. The fact that the computational domain, in these methods is one dimensional lower than the actual spatial dimensionality of the problem has many advantages(e.g. the programming complexity; the number of unknowns in the problem) that the disadvantages of non-sparse matrices are fully compensated. In the work of Jaap-Harm Westhuis[12], a general heuristic comparison between the efficiency of Finite element methods and Boundary Element methods is presented. It was concluded in his work that for two dimensions, Boundary Element Methods are efficient, whereas in three dimensions, both of them are efficient.

In this work, a Boundary integral method is employed as the numerical technique to evaluate the roll moment of two dimensional body in steep nonlinear free surface wavy flows.

1.6 Outline

The chapter 2 of the thesis deals with exact mathematical description of complete nonlinear free surface flows in a computational domain, followed by derivation of the integral equation employed. The results of the linear wave simulations are presented, followed by the nonlinear wave simulations. This is considered as a necessary step, before introducing a body into the computational domain.

The chapter 3 of the thesis introduces the body into the computational domain and presents a clear cut description of the two techniques briefed in the section (1.3). We do not solve free motions of the body, as the goal of the research is to not solve the complete nonlinear problem, but is to compute generalized forces using two different techniques and compare them. So, instead we make two programs: the first one being, diffraction program, where the body is fixed and the wave impinges on the body and the second one being, radiation program, where we make the body follow canonical motion in initially calm undisturbed water. The boundary conditions associated with both problems are dealt independently and then linearized. The linearization is carried as it

serves as a verification step. Once, all the neccessary boundary conditions are stated, we use the standard Direct Pressure Integration(DPI) technique to find the loads on the structure in linear and nonlinear setting. The results are presented and the verifications are carried out. Once, we are confident with the Direct Pressure Integration techinque, we reformulated the Fluid Impulse Theory. Then, we provide an analytical proof of the similarity between the Direct Pressure Integration and the Fluid Impulse Theory for a linearized setting. After that, we simplify our final non-linear expression of the Fluid Impulse Theory, so that it can be implemented in our numerical programs. We, then finally compare the results of the Direct Pressure Integration and the re-formulated Fluid Impulse Theory for two different cases: the first one being the Diffraction case, where the body is fixed and the wave impinges on it and the second one being the Radiation case, where the body is forced to follow canonical motion in roll mode in initially undisturbed calm water.

The chapter 4 provides the conclusions and also throws a light on the recommendations for future work.

Chapter 2

Numerical Wave Tank

In this chapter, a mathematical description of the complete nonlinear free surface flows is presented. The boundary conditions associated with these flows are first discussed. Though, the chapter deals with nonlinear free surface flows in the computational domain without the presence of the body, a brief discussion is provided on the boundary conditions that will be enforced on the freely floating body or fixed body. The numerical algorithm for simulating nonlinear wave propagation is presented. Then, the free surface equations are linearized with respect to undisturbed calm water level. In order to simulate linear waves, the numerical algorithm proposed previously has to be simplified. These simplifications are presented, which are followed by the results of linear wave simulations. These results give the confidence for enhancing the already developed numerical code to incorporate nonlinear terms.

2.1 Description of Flow

The assumption of inviscid and irrotational flows makes it possible to define the velocity vector as a gradient of scalar velocity potential(2.1).

$$\overrightarrow{u} = \nabla\phi \tag{2.1}$$

2.1.1 Governing Equation

To arrive at the governing equation for the potential flows, we need to impose the conservation of mass over a control volume V(2.2).

$$\frac{\mathrm{d}}{\mathrm{dt}} \int_V \rho \mathrm{dv} = 0 \tag{2.2}$$

Now, applying the Reynolds Transport theorem reduces the integrand into two integrals, one over the control volume V and the other on the surface S bounding the control volume V(2.3).

$$\int_V \frac{\partial \rho}{\partial t} \mathrm{dv} + \int_S \rho (U \cdot n) \mathrm{ds} = 0 \tag{2.3}$$

Now, applying the stokes theorem to the second integral on the left side of the (2.3) leads to an integral over the control volume V(2.4).

$$\int_V (\frac{\partial \rho}{\partial t} + \nabla(\rho U)) \mathrm{dv} = 0 \tag{2.4}$$

With the assumption of incompressibility of flow, which is quite good approximation except in the regions of the cavitating flows and regions of high pressure gradients, (2.4) simplifies to (2.5).

$$\int_V \nabla(\rho U) \mathrm{dV} = 0 \tag{2.5}$$

Since, the equation (2.5) has to be true for any arbitrary volume, the integrand of the integral has to be identically zero. Since, the flow is characterized by uniform density, this leads to the simplified equation(2.6).

$$\nabla U = 0 \tag{2.6}$$

If the notation for U as depicted in (2.1) is used, this leads to the Laplace equation, which governs any inviscid, irrotational and incompressible flow(2.7).

$$\nabla^2 \phi = 0 \tag{2.7}$$

2.1.2 Boundary Conditions

The Laplace equation has many solutions, but we are looking for solutions of the Laplace equation which generate waves on the undisturbed water surface. So, we need to specify certain boundary conditions which augment the Laplace equation. Before, we provide the mathematical expressions for the boundary conditions, we want to introduce the

computational domain(Fig 2.1). Strictly, speaking the free surface extends to infinity in space, but in order for numerical computations to be carried out, this has to be truncated by vertical artificial boundaries(the upstream and downstream boundaries). The computational domain has four boundaries: Bottom boundary, Free surface, Upstream Boundary and Downstream boundary. The boundary conditions on the various segments are described next.

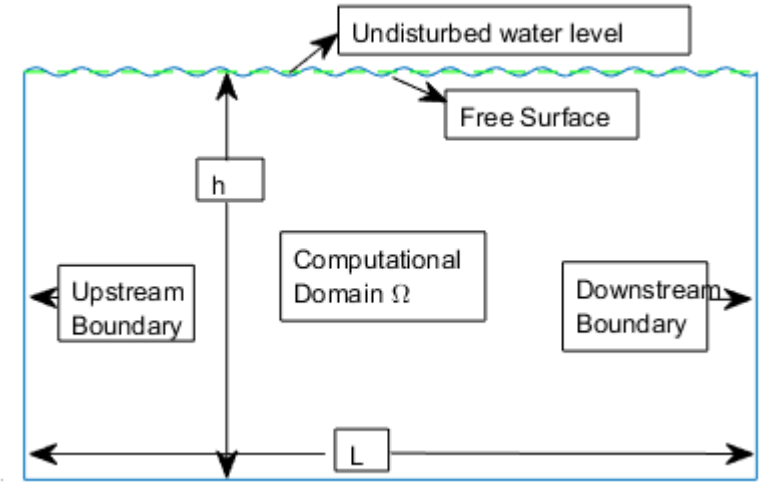

Figure 2.1: Computational Domain

Bottom Boundary condition

The thesis does not aim at studying the influence of sloping bottoms, porous bottom or bottoms with undulations on the motion of the two dimensional bodies. Instead, to meet with the goals of the thesis, a simple rigid bottom is employed. Thus, the flux of the flow across the bottom should be zero(2.8).

$$\frac{\partial \phi}{\partial n} = 0 \text{ on bottom } S_{BO} \tag{2.8}$$

Free Surface Boundary condition

Before specifying the conditions to be satisfied by the flow on the Free surface, it would be wise to have a glance at the two representation of the free surface: Eulerian and Lagrangian. In the Lagrangian description of the free surface, the time stepping of the equations of the free surface is following the fluid particles(material points), whereas

the Eulerian description of the free surface restricts the particles(not material points) from any horizontal motion. So, in Eulerian flows, the potential cannot be multi-valued at a fixed horizontal position. Thus, overturning of the waves, which occur before the breaking of waves cannot be predicted using Eulerian description of the flow. Though, the Lagrangian description of flow can predict the overturning of waves, but that comes with an additional penalty. In Lagrangian flows, the particles may leave the computational domain or additional particles may enter the computational domain through the artificial vertical boundaries(upstream and downstream boundaries). In computational sense, after every time step, few particles(points) have to be deleted or added, which calls for additional care and complicated algorithms. Also, keeping in mind that the goal of thesis is to deal with steep waves and not with extreme breaking waves, an Eulerian description of the flow is given preference. Though, it does not match with present discussion, the author wants to point out that in case of bodies with small freeboard(the difference between the depth and draft of the vessel) performing large roll(rotations about the Y-Z plane, defined in chapter 3) motions in the waves, points may leak into the body, in Eulerian description of the flows. This can be dealt by choosing bodies having high freeboard, so that the goals of the thesis could be still satisfied. Thus, an Eulerian description of the flow is chosen for the derivation of the free surface boundary conditions.

Unlike the bottom surface, the free surface shape is not known forehand and should be part of the solution. This adds to the unknown potential on the free surface and calls for two boundary conditions on the free surface.

Kinematic Free Surface Boundary Condition The Free surface is the interface between the water and the air. Thus, the free surface separates the fluid particles from the air particles. So, none of the fluid particles can cross the free surface. Thus, when the free surface moves with a velocity, all the fluid particles associated with the free surface need to move with the same velocity. To put it in other words, the free surface is a material surface. If we represent the free surface with a function F as shown in (2.9), then the material derivative of the function should be zero(2.10).

$$F = y - \eta(x,t) \tag{2.9}$$

$$\frac{\mathrm{DF}}{\mathrm{Dt}} = 0 \tag{2.10}$$

The material derivative is related to the partial temporal and partial spatial gradients through (2.11).

$$\frac{\mathrm{D}}{\mathrm{Dt}} = \frac{\partial}{\partial t} + \nabla\phi \cdot \nabla \tag{2.11}$$

So, expanding (2.10) using the definition of material derivative leads to the kinematic free surface boundary condition to be invoked on the unknown free surface location.

$$\frac{\partial \eta}{\partial t} + \nabla\phi \cdot \nabla\eta = \frac{\partial \phi}{\partial y} \text{ on y=}\eta \tag{2.12}$$

Dynamic Free Surface Boundary Condition As explained, the Free surface is an interface between the air and water. The pressure on any such surface has to be invariant, if not there will be force that restricts the motion of the free surface. This will lead to the Dynamic Free Surface Boundary Condition. The pressure at point in the ideal fluid(irrotational, inviscid and incompressible) can be expressed by Bernoulli equation(2.13).

$$\frac{p - p_a}{\rho} = -\frac{\partial \phi}{\partial t} - \frac{1}{2}\nabla\phi \cdot \nabla\phi - gY + C(t) \tag{2.13}$$

If we choose the arbitrary constant C, such that the constant pressure(in the case of free surface, atmospheric pressure p_a) is made zero, then the Dynamic Free Surface Boundary Condition on the free surface can be obtained.(2.14)

$$\frac{\partial \phi}{\partial t} + \frac{1}{2}\nabla\phi \cdot \nabla\phi + g\eta = 0 \text{ on y=}\eta \tag{2.14}$$

The set of equations (2.12) and (2.14) provide the conditions to be invoked on the unknown free surface in Eulerian description of flow.

Upstream Boundary Condition

The incident wave is introduced into the computational domain through the upstream boundary. For, the case where the computational domain is free of a rigid body, prescribing the incident wave potential or its normal gradient would be sufficient. If the body is present, the boundary conditions may not be that simple and they will be discussed further in the next chapter.

Downstream Boundary Condition

The downstream boundary should not reflect the waves simulated in computational domain, otherwise the solution in the computational domain is contaminated by the

reflected wave from the downstream boundary. For periodic waves, Sommerfeld radiation conditions can be invoked on the downstream boundary. The wave equation is a good approximation for the free surface flows. It is a second order equation, which has two characteristics(the lines along which information travels). One characteristic resembles ϕ^+(the wave travelling towards the downstream boundary in the positive x-direction) and the other resemble ϕ^-(the reflected wave, which travels along negative x-direction). We do not want the ϕ^- component to contaminate the solution. Mathematically, this can be stated as shown in (2.15).

$$\frac{\partial \phi}{\partial t} - c\frac{\partial \phi}{\partial x} = 0 \tag{2.15}$$

But, as the solution turns out to be non-periodical(may be when we introduce the body into the computational domain), the accuracy of Sommerfeld radiation condition in ensuring non reflecting downstream boundaries is reduced and one needs to resort to numerical beaches in conjunction to the specified Sommerfeld radiation condition. In (2.15), we see that we require the speed of the wave, which is obtained as an output from the Rienecker & Fenton Algorithm.

This brings to the end of discussion on the conditions to be invoked on boundaries for simulation of waves over the computational domain. These conditions have been pictorally presented in Figure 2.2.

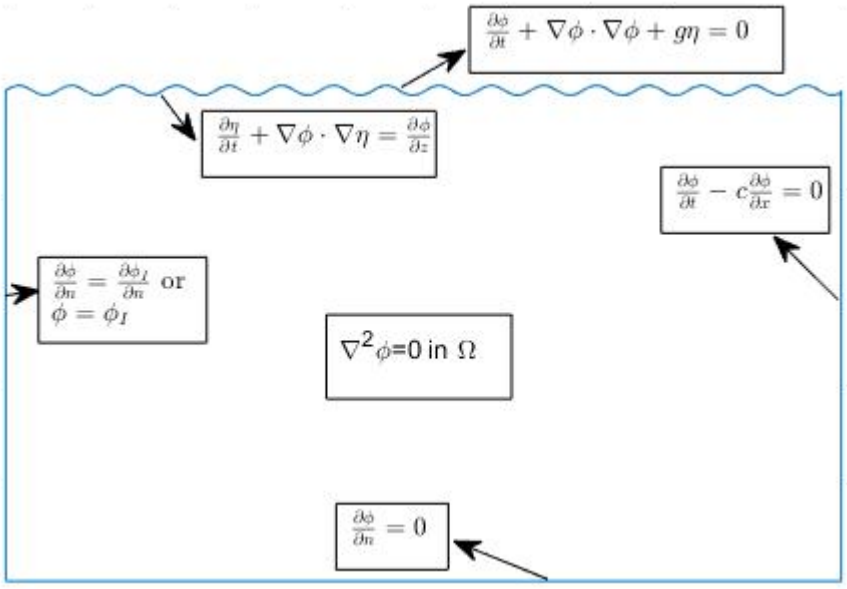

Figure 2.2: Computational Domain with Boundary conditions

Body Boundary Condition The normal velocity of the fluid particles on the wetted surface of the body should be equal and opposite to the normal velocity of the body itself. If this condition were not satisfied, then they will be a resultant flux, in or out of the body and in that case, the body will not represent a watertight entity. Mathematically, this is depicted in (2.16).

$$\frac{\partial \phi}{\partial n} = V_n \text{ on body } S_B \tag{2.16}$$

If the body is fixed, in that case the normal velocity(V_n) of the body is zero. Then, (2.16) reduces to the (2.8).

2.1.3 Linearized Free Surface Boundary Conditions

When the steepness of the wave(defined as the product of the wavenumber(k) and wave height(H)) is considerably small(kH<<1) and the wavelength is small enough that the waves do not feel the bottom(kd>>1), the equations governing the free surface wave propagation can be simplified considerably. Under this conditions, any nonlinear term in the equations that involves the product of the gradients of the functions(free surface elevation and velocity potential) can be relaxed and the equations can be satisfied on the undisturbed calm water level, instead of the unknown free surface. Thus (2.12) and (2.14) reduce to (2.17) and (2.18) respectively.

Linearized Kinematic Free Surface Boundary Condition

$$\frac{\partial \eta}{\partial t} = \frac{\partial \phi}{\partial y} \text{ on y=0} \tag{2.17}$$

Linearized Dynamic Free Surface Boundary Condition

$$\frac{\partial \phi}{\partial t} = -g\eta \text{ on y=0} \tag{2.18}$$

2.2 Boundary Integral Method

The use of boundary integral equations to solve problems of physical interest dates back to 1950's. The sound theoretical basis of potential theory[13] and the knowledge of Fredholm boundary integral equations made these techniques a good competitor to other numerical methods.

In this section, a brief reformulation of integral equations is carried out. For a more rigorous mathematical treatment of the potential theory, readers are referred to Kellogg[13] and Courant and Hilbert[14], whereas Jaswon and Symm[15] and Hunt[16] give an excellent introduction to the use of integral equations in potential theory.

The complete derivation of the Boundary integral equation is provided in Appendix-A. We just brief the procedure here. Considering a simply connected region and applying Greens theorem to any two scalar functions u,v which are second order continuous in the domain leads to (2.19).

$$\iiint_{\Omega}(u\nabla^2 w - w\nabla^2 u)\mathrm{d}\Omega = \iint_{S}[-w\frac{\partial u}{\partial n_\zeta} + u\frac{\partial w}{\partial n_\zeta}]\mathrm{dS}_\zeta \tag{2.19}$$

Now, if we choose u to be an unknown potential and w to be Rankine Greens function(a homogenous solution to boundary value problem with infinite domain, that will be discussed later), and follow along the lines provided in Appendix-A, one ends up with (2.20).

$$\frac{\phi(x)}{2} = \iint_{dS}[\phi(\zeta)\frac{\partial G(\zeta;x)}{\partial n_\zeta} - \frac{\partial \phi(\zeta)}{\partial n_\zeta}G(\zeta;x)]\mathrm{dS}_\zeta \tag{2.20}$$

The gradient applied to (2.20) leads to (2.21), i.e. the gradient can be bought under an integral sign by considering the regularity of the integral.

$$\frac{\nabla_x\phi(x)}{2} = \iint_{dS}[\phi(\zeta)\nabla_x(\frac{\partial G(\zeta;x)}{\partial n_\zeta}) - \frac{\partial \phi(\zeta)}{\partial n_\zeta}\nabla_x(G(\zeta;x))]\mathrm{dS}_\zeta \tag{2.21}$$

The boundaries of our computational domain also serve as interior boundaries to the exterior simply connected region that extends to infinity. Let S_e denote a circle centered at x and radius large enough to include all the boundaries, one can apply Greens theorem to the part of the domain bounded by S and S_e, this leads to (2.22), where $\hat{phi}$ is the fictitious potential. The procedure, to be followed is clearly explained in the works of J.E.Romate[4], Van Broeze[5] and Van Daalen[6].

$$\frac{\hat{\phi}(x)}{2} = \iint_{dS}[\hat{\phi}(\zeta)\frac{\partial G(\zeta;x)}{\partial n_\zeta} - \frac{\partial \hat{\phi}(\zeta)}{\partial n_\zeta}G(\zeta;x)]\mathrm{dS}_\zeta \tag{2.22}$$

Applying the gradient to the (2.22) leads to (2.23).

$$\frac{\nabla_x\hat{\phi}(x)}{2} = \iint_{dS}[\hat{\phi}(\zeta)\nabla_x(\frac{\partial G(\zeta;x)}{\partial n_\zeta}) - \frac{\partial \hat{\phi}(\zeta)}{\partial n_\zeta}\nabla_x(G(\zeta;x))]\mathrm{dS}_\zeta \tag{2.23}$$

Adding (2.20) and (2.22), (2.21) and (2.23) yields (2.24) and (2.25) respectively.

$$\frac{(\phi+\hat{\phi})}{2}(x) = \iint_{dS}((\phi-\hat{\phi})\frac{\partial G}{\partial n}(\zeta;x) - (\frac{\partial \phi}{\partial n} - \frac{\partial \hat{\phi}}{\partial n})G(\zeta;x))\mathrm{dS} \tag{2.24}$$

$$\frac{(\nabla_x\phi + \nabla_x\hat{\phi})}{2}(x) = \iint_{dS}((\phi - \hat{\phi})\nabla_x(\frac{\partial G}{\partial n}(\zeta;x)) - (\frac{\partial \phi}{\partial n} - \frac{\partial \hat{\phi}}{\partial n})\nabla_x G(\zeta;x))\mathrm{dS} \tag{2.25}$$

Now, posing

$$\sigma(\zeta) = \frac{\partial \phi}{\partial n} - \frac{\partial \hat{\phi}}{\partial n} \tag{2.26}$$

$$\nu(\zeta) = -(\phi - \hat{\phi}) \tag{2.27}$$

We can rewrite the expressions (2.24) and (2.25) in terms of surface source distribution and surface distribution of normal dipoles, leading to (2.28) and (2.29).

$$\frac{(\phi + \hat{\phi})}{2} = -\iint_{dS}(\sigma G + \nu\frac{\partial G}{\partial n})\mathrm{dS} \tag{2.28}$$

$$\frac{(\nabla_x\phi + \nabla_x\hat{\phi})}{2} = -\iint_{dS}(\sigma\nabla_x G + \nu\nabla_x(\frac{\partial G}{\partial n})\mathrm{dS} \tag{2.29}$$

All the formulations derived so far look same as those derived by J.E.Romate[4]. The only difference being the sign ahead of the right hand side integrals. This difference is due to their choice of Greens function G, negative of the function generally chosen in three dimensions. Since $\hat{\phi}$ is a fictitious potential, we can choose any value for the potential $\hat{\phi}$, as long as the exterior problem is well posed. Different choices of the fictitious potentials leads to different integral formulations. Three examples of the problem are provided:

1. If $\phi = \hat{\phi}$, $\nu = 0$ and source only formulation follows:

$$\phi(x) = -\iint_{dS}\sigma G\mathrm{dS} \text{ ,if x is on S} \tag{2.30}$$

2. If $\frac{\partial\phi}{\partial n} = \frac{\partial\hat{\phi}}{\partial n}$, $\sigma = 0$ and dipole only formulation follows:

$$\phi(x) = \frac{1}{2}\nu(x) + \iint_{dS}\nu\frac{\partial G}{\partial n}\mathrm{dS} \text{ ,if x is on S} \tag{2.31}$$

3. If $\hat{\phi} = 0$ on S, implying $\frac{\partial\hat{\phi}}{\partial n} = 0$, $\sigma = \frac{\partial\phi}{\partial n}$ and $\nu = -\phi$. This leads to a mixed source formulation:

$$\frac{\phi}{2}(x) = \iint_{dS}(\phi\frac{\partial G}{\partial n} - G\frac{\partial\phi}{\partial n})\mathrm{dS} \tag{2.32}$$

2.2.1 Choice of Singularity

Now, all the three forms as described in the last section(2.30-2.32) can be used as a Boundary integral equations. The choice of the representation is governed by the physics of the problem, minimal discretization error and minimum computational effort.

The source only formulation can be used when one only wants flux entering into the computational domain, whereas the dipole only distribution is used in the case of lifting bodies/circulation. Since, we have a free surface, the fluid particles follow an elliptical/circular motion(depending on the water depth) along with mass convection. To enforce an accurate desription of such a motion, we need source and dipole distribution. We also have few other factors which decide in the choice of singularity. So we deal with these factors next.

The boundary integral equation is discretized at certain points(collocation points). But, in between the collocation point, the equations are not satisfied exactly and this leads to leakage. Hunt[16] states that the leakage error can be reduced considerably by the usage of mixed source distribution(sources and dipoles) and one can achieve a higher accuracy than the source only or dipole only formulations of the same order. Though, it was not clear, we believe the reason may be that the leakages due to sources are counterbalanced by the leakages due to dipoles in some sense. Also, Henk de Koning Gans[18], in his doctoral thesis, gives a proof that source only or dipole only formulations cannot be accurate enough when they are convex surfaces in the computational domain. But, apart from the above points, the mixed source formulation has other advantages as pointed out by J.E.Romate[4] and will be referred here. Since in the mixed source formulation, $\hat{\phi} = 0$ on the boundary S, this fictitious solution does not introduce singularities in the solution. Another advantages is that, in mixed source formulations, we are dealing with quantities of physical interest, unlike source-only or dipole-only formulation, where quantities of physical interest are not dealt with, often making the understanding of the numerical solution difficult.

All the points discussed previously attracted the mixed source integral equation representation(2.32) as the integral formulation to be employed in this thesis.

2.2.2 Order of Panel Method

We choose a lower order panel method for the solution of the problem, since it does not require complex coding effort. The higher order panel methods lead to higher accuracy

than the lower order panel methods, but at the cost of complex coding effort(Not always true, as Hunt[16] states that the lower order mixed source distribution(constant) has lower leakages than first order mixed source distribution). Since, the goal of the thesis is to evaluate the moments on the bodies using two different techniques and compare the re-formulated Fluid Impulse Theory with the standard Direct Pressure Integration technique, we are looking for qualitative results rather than quantitative results. Also, the time framework of the thesis should be taken into consideration. Thus, a lower order panel method should do as good as a higher order panel method. There is always confluence of boundary conditions at intersection point when Dirichlet-Nuemann Boundary conditions are imposed on either side of the body. We expect that this will cause some numerical problems, which will be explained in detail in the next chapter. But, in this work, the potential and the normal gradient of the potential are assumed constant over each panel

$\frac{\partial \eta}{\partial t} + \nabla\phi \cdot \nabla\eta = \frac{\partial \phi}{\partial z}$ on the Free surface

$\frac{\partial \phi}{\partial t} + \nabla\phi \cdot \nabla\phi + g\eta = 0$ on the Free surface

$\frac{\partial \phi}{\partial n} = 0$ on the bottom

$\frac{\phi}{2}(x) = \int_S (\phi \frac{\partial G}{\partial n} - G\frac{\partial \phi}{\partial n})$dS on all boundaries

$\frac{\partial \phi}{\partial n} = \frac{\partial \phi_I}{\partial n}$ or $\phi = \phi_I$' on the upstream boundary

$\frac{\partial \phi}{\partial t} - c\frac{\partial \phi}{\partial x} = 0$ on the downstream boundary

ϕ_I refers to the incident wave potential

Figure 2.3: Summary of Equations

2.3 Method of lines Approach

The summary of the equations to be satisfied are provided in Figure 2.3. The surface S, which bounds the computational domain Ω is divided into N straight line segments(panels) clockwise from the lower end of the upstream boundary. The functions desired(ϕ, $\frac{\partial\phi}{\partial n}$) are assumed to be constant over each panel, with a collocation point(points where the equations are satisfied exactly) at the panel centre.

If the discretized integral equation is applied at x=x_i(i=1,...N) collocation points, this leads to N system of linear equations with 2N variables(N potential values and N normal gradient of the potential values). If the boundary conditions at each of the collocation point eliminates the N variables, one is left with a system of N linear equations for the N unknowns(2.33).

$$C(\overrightarrow{x})\phi(\overrightarrow{x}) - \int_{\mathrm{d}\Omega} \phi(\overrightarrow{\epsilon})\frac{\partial G}{\partial n}(\overrightarrow{\epsilon};\overrightarrow{x})\mathrm{dS} = \int_{\mathrm{d}\Omega} \frac{\partial\phi}{\partial n}(\overrightarrow{\epsilon})G(\overrightarrow{\epsilon};\overrightarrow{x})\mathrm{dS} \tag{2.33}$$

where:

$$C(\overrightarrow{x}) = \begin{cases} 1 & \text{if } \overrightarrow{x} \text{ is within the domain } \Omega \\ 1/2 & \text{if } \overrightarrow{x} \text{ is on a smooth boundary of } \Omega \\ 0 & \text{if } \overrightarrow{x} \text{ is outside the domain } \Omega \end{cases}$$

Before we venture into further details, the verification of the boundary element method is to be carried out. This is carried out by introducing a constant potential along the boundaries of the domain. Then, these boundaries act like a streamline and from the fundamentals of fluid flow, we know that they cannot be a flow across a streamline. This implies that the flux across these surfaces is zero. Thus, the Boundary Element Method devised should produce zero normal velocity. This has been checked.

In order for a solution to exist, each surface of the domain should be imposed with a potential(Dirichlet Boundary Condition) or with the normal gradient of the potential(Neumann Boundary Condition) or with a equation combining the potential and the normal gradient of the potential(Robin Conditions).

Then, one can solve the system of equations for the N variables. Once, the unknowns are evaluated using the discretized boundary integral equation, we time step the equations on the free surface. In this way, the discretization in space and time can be separated, resulting in so-called method of lines approach.

The global procedure for complete nonlinear simulations is briefed first.

1. Subdivide the boundary surfaces into N linear segments.

2. At time step 'n', $(\phi)^n_{UP}$, $(\phi)^n_{FS}$, $(\phi)^n_{DS}$, $\left(\frac{\partial\phi}{\partial n}\right)^n_{BO}$ and $(\eta)^n_{FS}$(UP-Upstream boundary, DS-Downstream boundary, FS-Free surface, BO- Bottom) known.

3. If A represents the matrix associated with the potential(Dipole) and B represents the matrix associated with the normal gradient of the potential(Source), subdividing these matrices leads to a system of equations(2.34).

$$\begin{pmatrix} A^n_{1,1} & A^n_{1,2} & A^n_{1,3} & A^n_{1,4} \end{pmatrix} \begin{pmatrix} \phi^n_{UP} \\ \phi^n_{FS} \\ \phi^n_{DS} \\ \phi^n_{BO} \end{pmatrix} = \begin{pmatrix} B^n_{1,1} & B^n_{1,2} & B^n_{1,3} & B^n_{1,4} \end{pmatrix} \begin{pmatrix} \left(\frac{\partial\phi}{\partial n}\right)^n_{UP} \\ \left(\frac{\partial\phi}{\partial n}\right)^n_{FS} \\ \left(\frac{\partial\phi}{\partial n}\right)^n_{DS} \\ \left(\frac{\partial\phi}{\partial n}\right)^n_{BO} \end{pmatrix} \tag{2.34}$$

The co-efficients of these matrices change in time as the evaluation of its constituent elements depends on the shape of the domain at the present time instant. Now re-arranging these matrices by bringing the knowns to the right hand side leads to the system of equations(2.35).

$$\begin{pmatrix} -B^n_{1,1} & -B^n_{1,2} & -B^n_{1,3} & A^n_{1,4} \end{pmatrix} \begin{pmatrix} \left(\frac{\partial\phi}{\partial n}\right)^n_{UP} \\ \left(\frac{\partial\phi}{\partial n}\right)^n_{FS} \\ \left(\frac{\partial\phi}{\partial n}\right)^n_{DS} \\ \phi^n_{BO} \end{pmatrix} = \begin{pmatrix} -A^n_{1,1} & -A^n_{1,2} & -A^n_{1,3} & B^n_{1,4} \end{pmatrix} \begin{pmatrix} \phi^n_{UP} \\ \phi^n_{FS} \\ \phi^n_{DS} \\ \left(\frac{\partial\phi}{\partial n}\right)^n_{BO} \end{pmatrix} \tag{2.35}$$

Carrying out the inverse of the matrix on the left hand side, we can evaluate the unknowns. Since, we are dealing with 2D problem, we use direct techniques for evaluation of the inverse.

4. After the finding the unknowns, we need few variables for time stepping the equations of the free surface. These include: $\left(\frac{\partial\phi}{\partial x}\right)^n_{FS}$, $\left(\frac{\partial\eta}{\partial x}\right)^n_{FS}$, $\left(\frac{\partial\phi}{\partial y}\right)^n_{FS}$ and $\left((\nabla\phi)^2\right)^n_{FS}$. To evaluate the first two, a finite difference first order upwind scheme(upwind with respect to direction of wave propagation) is used. They will be problem in applying this scheme to the end points of the free surface collocation points(especially the left most one). A fictitious point is introduced at half panel distance from the left most collocation point on the free surface. The free surface elevation and the

potential at the fictitious collocation point were initially supplied by an extrapolation of the nearby free surface values. But, lead to the development of wiggles, so for these fictitious points, the potential and the free surface elevation are specified from the input incident wave(where the potential is specified from the Rienecker and Fenton Algorithm[17]). Then, the difference schemes are applied.

$$\left(\frac{\partial\phi}{\partial x}\right)_j^n = \frac{\phi(x_j) - \phi(x_{j-1})}{x_j - x_{j-1}} \tag{2.36}$$

$$\left(\frac{\partial\eta}{\partial x}\right)_j^n = \frac{\eta(x_j) - (x_{j-1})}{x_j - x_{j-1}} \tag{2.37}$$

5. The last step dealt with the evaluation of gradients of potentials and free surface in the horizontal direction. We are yet to evaluate the vertical gradient of potential. For this, the following two step technique is used. Using $\left(\frac{\partial\phi}{\partial x}\right)_{FS}^n$ and $\left(\frac{\partial\phi}{\partial n}\right)_{FS}^n$, $\left(\frac{\partial\phi}{\partial s}\right)_{FS}^n$ is estimated by co-ordinate transformation equations(2.38). Then, using the gradients of ϕ in the s-n plane, $\left(\frac{\partial\phi}{\partial y}\right)_{FS}^n$ is estimated through(2.39). It may be quite puzzling why we had to employ this two step technique. An idea that may be implemented is evaluating the tangential gradient of the potential through first order upwind scheme and then evaluating the gradients in X-Y plane. This was followed in the beginning, but avoided later. The reason is explained as follows: The free surface is not re-gridded uniformly in the tangential direction and if the tangential derivative of the potential is evaluated using the upwind finite difference scheme, they are instances where the length between two collocation points is larger than the horizontal separation between the collocation points. This may lead to unnecessary artificial dissipation of the gradients of the functions. Thus, we had to follow the two step procedure.

$$\left(\frac{\partial\phi}{\partial s}\right)_{FS}^n = \frac{N_x\left(\frac{\partial\phi}{\partial n}\right)_{FS}^n + \left(\frac{\partial\phi}{\partial x}\right)_{FS}^n}{N_z} \tag{2.38}$$

$$\left(\frac{\partial\phi}{\partial y}\right)_{FS}^n = N_x\left(\frac{\partial\phi}{\partial s}\right)_{FS}^n + N_z\left(\frac{\partial\phi}{\partial n}\right)_{FS}^n \tag{2.39}$$

N_x,N_y are respectively the components of the outward normal(2.40,2.41).

$$N_x = -\frac{(y_2 - y_1)}{\sqrt{(x_1 - x_2)^2 + (y_1 - y_2)^2}} \tag{2.40}$$

$$N_y = \frac{(x_2 - x_1)}{\sqrt{(x_1 - x_2)^2 + (y_1 - y_2)^2}} \tag{2.41}$$

where(x_1, y_1) and (x_2, y_2) refer to the end points of the panel taken clockwise.

6. The values in the previous two steps are required to evaluate $\left((\nabla\phi)^2\right)^n_{FS}$. This quantity is required in the time stepping of Dynamic Free Surface Boundary Condition.

$$\left((\nabla\phi)^2\right)^n_{FS} = \left((\frac{\partial\phi}{\partial y})^n\right)^2_{FS} + \left((\frac{\partial\phi}{\partial x})^n\right)^2_{FS} \tag{2.42}$$

7. All that requires is the time stepping of the free surface equations and Sommerfeld radiation condition for the downstream boundary(2.43-2.45).
   Kinematic Free Surface Boundary Condition(KFSBC) for η:

$$(\eta)^{n+1}_{FS} = (\eta)^n_{FS} + \Delta t \left(\frac{\partial\phi}{\partial y}\right)^n_{FS} - \Delta t \left(\frac{\partial\eta}{\partial x}\right)^n_{FS} \left(\frac{\partial\phi}{\partial x}\right)^n_{FS} \tag{2.43}$$

   Dynamic Free Surface Boundary Condition(DFSBC) for ϕ:

$$(\phi)^{n+1}_{FS} = (\phi)^n_{FS} - g\Delta t\,(\eta)^{n+1}_{FS} - \Delta t\frac{1}{2}\left((\nabla\phi)^2\right)^n_{FS} \tag{2.44}$$

   Sommerfeld Radiation boundary condition for ϕ on Downstream Boundary:

$$(\phi)^{n+1}_{DS} = (\phi)^n_{DS} - c\Delta t \left(\frac{\partial\phi}{\partial x}\right)^n_{DS} \tag{2.45}$$

8. The location of end points of each panel has to be updated as they are required for the evaluation of the integrals associated with the Boundary Integral representation at the next time step. We know the free surface elevation of the collocation points. A cubic spline interpolation(using the MATLAB smoothing spline function) is carried out for evaluating the free surface elevation of all the end points of the panel which are present in between the collocation points. The left most end point free surface elevation is provided from the nonlinear incident wave potential obtained from the Rienecker and Fenton algorithm[17], whereas the right most end point used a second order extrapolation procedure. An extrapolation procedure was used for both the end points in the beginning, but avoided later on, as it lead to the development of wiggles.After we find the new free surface elevations at the ends of the free surface, we re-grid the upstream and downstream boundary, accordingly. This is considered as necessary to keep the length of the panels constant all along

the boundaries. Since, the upstream boundary uses an explicit expression for the specification of the potential, the re-gridding should not cause any problem, but at the downstream boundary, the potential is estimated after time stepping the Sommersfeld Radiation condition at collocation points before re-gridding and these values have to be transfered to the new collocation point after re-gridding. A cubic spline interpolation, as used for the free surface elevation is used to find the potentials at new grid points on the downstream boundary from the ones existing previously.

9. Repeat the steps 1-8 until desired.

All that remains is to explain the starting of the algorithm. The free surface and downstream boundary are initially assumed to be at rest. The upstream boundary is provided with nonlinear wave computed from the Reinecker and Fenton algorithm[17] and is slowly introduced into the domain by using a time modulation function. This time modulation function was picked up from the work of D.sen[7].

$$T = \begin{cases} 0.5(1 - \cos(\frac{\pi t}{\sigma}) & \text{if } t < \sigma \\ 1 & \text{if } t >= \sigma \end{cases}$$

The choice of the parameter σ depends on the steepness of the wave being simulated, so that transients do not cause any wiggles. The value of σ of four time periods seemed to work well upto the wave steepness of 0.03. This time modulation is necessary as we do not want an impulsive start. Many researchers(Lin[3], Cointe[18], Greenhow and Lin[19]) have proved that an impulsive start(depending on the acceleration) may lead to a weak or strong singularity. If it was weak singularity, the free surface elevation would be bounded, but they would be wiggles developed and if it were strong singularity, the free surface elevation is not bounded. So, as to avoid wiggles and ensure the boundedness of the free surface elevation, such a time modulation was required. We do not need any space modulation, as that carried in the work of D.Sen[7]. The reason why such a space modulation was used in his thesis was because he prescribes a linear Airy wave potential on the upstream boundary, whereas he uses nonlinear free surface equations. This caused an incompatibility in the potential at the intersection of the free surface and the upstream boundary where wiggles developed. But, in our case, we provide a complete nonlinear wave potential on the upstream boundary and seek for a complete

nonlinear wave solution on the free surface. Thus, we do not have any incompatibility issue and do not need any space modulation.

The simplifications for the case of the linear wave simulations will be presented next. The first three steps remain unchanged for the linear wave simulations. Hence, for the sake of brevity are not repeated again. The global procedure for the linear wave simulations is as follows:

1. Steps 1-3 of the nonlinear wave simulations, but with the only difference that the co-efficients of the matrices(2.34-2.35) are time independent(since all the boundary conditions are satisfied over the mean positions of the bounding surfaces). So, these co-efficients are computed, once for all.

2. Once, the normal gradient of potential is evaluated, the free surface elevation can be updated using the linearized Free Surface Boundary Condition(because in a linear setting, the direction of the normal matches with the positive y direction). This updated free surface elevation is used, to time step the Free surface potential using the linearized Dynamic Free Surface condition. The time stepping technique will be discussed in detail in the following section. Thus, the values of free surface elevation and free surface potential are evaluated at time $t_0 + \Delta t$.

3. Repeat steps 1-2 until desired.

2.4 Smoothing of the solution

The free surface had wiggles($2\Delta x$ oscillations) after a few time steps 'T' at the crests of the wave. The value of T decreased as the steepness increased. For low wave steepness(kH<=0.03), the diffusive ability of the total algorithm dampened these wiggles and for wave simulations of about 100 wave periods, they do not contaminate the solution. But, as the steepness increased, these wiggles do not suppress and contaminate the solution. Here, the details about the wiggles and the technique for suppression is described.

Initially, the potential prescribed on the upstream boundary was linear and the potential computed on the free surface was nonlinear. This was assumed to be the cause of wiggles in the beginning, as an impulsive pressure will be generated because of the incompatibility of the potential on both sides of the intersection point between

the upstream and free surface. So, in order to avoid this incompatibility, the upstream was prescribed with a complete nonlinear potential. A similar reasoning was seen in the work of D.Sen[7], but by using a smoothing function, he matches the nonlinear free surface solution to the linear wave solution on the upstream boundary. But, doing this, itself did not removes wiggles. So, there is more to it.

Also, by specifying the free surface elevation at the intersection point(between the free surface and upstream boundary) explicitly as the complete nonlinear solution obtained by the Rienecker and Fenton algorithm[17], we ensured the compatibilty of free surface elevation. This does not completely remove the wiggles, when high steepness waves are simulated, but delays their occurence in time.

A first order accurate spatial and temporal discretization along with constant panel method may be an attributing factor to the development of wiggles. In view of the goals of the thesis and the restriction of the time framework, the free surface can be smoothed(whenever necessary, but seldom used in the case of wave-body interactions) using the following technique:

1. After every 'm' time steps, the free surface collocation points are smoothed by finding them from the end points using 2.46. The elevation of the free surface end points is obtained from the algorithm at every time step.

$$\overrightarrow{X}_j = \frac{\overrightarrow{Xe}_j + \overrightarrow{Xe}_{j+1}}{2} \tag{2.46}$$

   where $\overrightarrow{Xe}_j$,$\overrightarrow{Xe}_{j+1}$ refer to the position vectors of the left and right end points of the panel and $\overrightarrow{X}_j$ is the position of the collocation point(panel center).

2. The values of the free surface potential available, have to be interpolated in order to obtain the values at these new points. A smoothing spline interpolation is used for these points from the potential available at 'm-1' time step.

The choice of the 'm' also depends on the steepness of the wave generated. As the value of steepness increases, the value of 'm' has to decrease. On the other hand, a smaller value of 'm' causes huge numerical dissipation(around 20%) in the simulations. The solution loses its accuracy, setting a limitation of the wave steepness predicted.

An other choice which has been tried is using a low pass filter to remove the high frequency oscillations. Unfortunately, this causes a phase shift in the waves and thus

waves get reflected from the downstream boundary(the speed of the wave changes). But, this technique can be handy later on, if numerical beaches are to be employed.

Many researchers provide some local smoothing for these wiggles, but these formulas have not been tried upon. The main reason, being that these smoothing functions would lead to messy terms in our reformulation of the Fluid Impulse Theory.

2.5 Time marching scheme

The time evolution of the free surface equations depends on the results obtained from the solution of the integral equation, whose eigenvalues are imaginary. Due to the nonlinearity of the problem, waves of all frequencies are present eventually, even though one starts with waves of single frequency.

As the eigenvalues of the discrete system are expected to have a wide range, close to the imaginary axis of the system, and may have negative real parts(due to the space discretization), the stability regimes of the time stepping technique should be such that they cover the region R=($\Delta t\lambda$— $-\alpha < Re(\Delta t\lambda) < 0$, $-\beta < Im(\Delta t\lambda) < \beta$), with $\alpha, \beta > 0$ and real.

This calls for A-stable methods, which have stability region covering the entire left half space, like implicit Euler scheme. Also, though explicit RK methods do not satisfy the A-stability condition, they can still be used.

Following the works of Vada and Nakos[20], we use Explicit-Implicit scheme for the time evolution of the free surface equations. Off-course, fourth order RK method can also be applied, but we wanted some diffusivity in the code and thus resorted to partly implicit method.

The Explicit Euler scheme integrates the kinematic boundary condition to obtain the new wave elevation at each time step, according to (2.47)

$$\frac{{\eta_j}^{n+1} - {\eta_j}^n}{\Delta t} = \frac{\partial \phi}{\partial y}^n - \frac{\partial \eta_j}{\partial x}^n \frac{\partial \phi_j}{\partial x}^n \tag{2.47}$$

Then, a semi-implicit Euler scheme is used to integrate the dynamic boundary condition to obtain the velocity potential at the new step, according to (2.48).

$$\frac{{\phi_j}^{n+1} - {\phi_j}^n}{\Delta t} = -g{\eta_j}^{n+1} - \frac{1}{2}\nabla{\phi_j}^n \cdot \nabla{\phi_j}^n \tag{2.48}$$

In the case of the linear wave simulations, (2.47) and (2.48) simplify into (2.49) and

(2.50).

$$\frac{{\eta_j}^{n+1} - {\eta_j}^n}{\Delta t} = (\frac{\partial \phi}{\partial y})_j^{\ n} \tag{2.49}$$

$$\frac{{\phi_j}^{n+1} - {\phi_j}^n}{\Delta t} = -g{\eta_j}^{n+1} \tag{2.50}$$

The implicit nature of (2.48) and (2.50) will ensure some diffusion to the scheme. Thus, any numerical disturbance can be partly smoothed out. Using an complete implicit scheme(implicit-implicit) will be rather computationally expensive because one needs to use iterative process for the solution and at each iteration, the right hand side of these equations(contributions from the boundary integral equations) should be evaluated.

2.6 Incident Wave potential

2.6.1 Linear unsteady wave simulations

The incident wave potential serves as an input to the computational domain. For, the case of linear wave simulations, linear Airy wave potential(2.51) is specified at the upstream boundary. This wave potential satisfies the linearized free surface boundary condition.

$$\phi_I = \frac{Ag}{\omega} \frac{\cosh k(h+y)}{\cosh(kh)} \cos(\omega t - kx) \tag{2.51}$$

2.6.2 Nonlinear Unsteady wave simulations

Using (2.51), for the case of nonlinear waves simulations, creates instability after few time steps(number of time steps for the initiation of the instability depends on the wave steepness) at the free surface panel adjacent to the intersection point of the upstream and free surface boundary. The linear Airy wave solutions satisfy the linearized free surface conditions on the undisturbed free surface. But, in the case of nonlinear wave simulations, the nonlinear free surface conditions are to be satisfied on the actual unknown free surface. Since we slowly introduce the wave into the computational domain, both the upstream and free surface potentials are initially compatible(they satisfy same free surface conditions), but in later time instants, the upstream boundary is provided with linear wave potentials, whereas the free surface boundary conditions are completely nonlinear. Imagine that there is a free surface to the left of the upstream boundary and one is specifying a linear wave solution on this free surface, but on the right of the upstream boundary, the numerical scheme provides as a nonlinear solution. Thus, at the

upstream boundary, there is a jump of the potential. This jump of potential behaves like an impulsive pressure, causing excessive free surface elevations and finally breaking of the solution, if not checked for.

We have used Taylors expansion and computed the wave potential upto fourth order by considering the linear Airy wave potential(For Details,refer Appendix-B) and this is given as the input to the computational domain. Though, this did not resolve the problem for all steepness, it worked well up to medium steepness(kH<=0.01). But, as this limit is crossed, the $2\Delta x$ instabilities are developed in the computational domain at the collocation points close to the free surface and upstream boundary intersections.

This was believed to the effect of confluence of boundary conditions. So, as to avoid it, a wave potential, computed by the Rienecker and Fenton algorithm[17] was used as a incident wave potential. Though this did not remove the instabilities for medium steepness(kH=0.04), but it postponed the occurrence of these instabilities. This was considered sufficient for our computations as we are employing a low order numerical technique and keping in mind, that the goal of the research work was not to develop a 2D Numerical Wave Tank(NWT).

2.7 Results of the wave simulations

For both the linear and nonlinear wave simulations, the length of the domain was chosen as 100m and the height of the domain was chosen as 50m.

2.7.1 Linear waves

The results of steady wave propagation are first presented, followed by the unsteady wave propagation.

Steady Wave propagation

The table 2.1 presents the details of the input wave.

Variable	Value
η	0.8m
λ	20m
Δx	1m
Δt	0.1s

Table 2.1: Choice of wave conditions

The free surface elevation is updated using an explicit Euler time stepping scheme and by carrying on von-Neumann stability analysis, it is easy to prove that there exists a limitation on Courant-Freidrich-Lewy(CFL) number. This limits the time step that can be chosen for the analysis.

$$CFL = \frac{c\Delta t}{\Delta x} <= 1 \tag{2.52}$$

The plots of the free surface elevation in space are provided in Fig(2.4) along with the expected free surface elevation(computed from the analytical expression obtained using Linear Airy Wave theory).

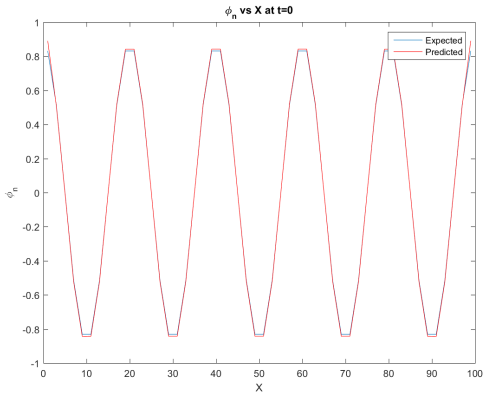

(a) At T = 0s

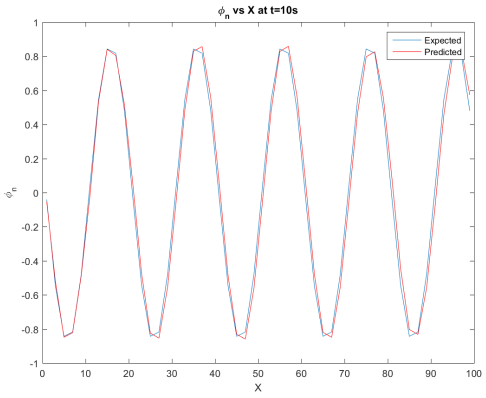

(b) At T = 10s

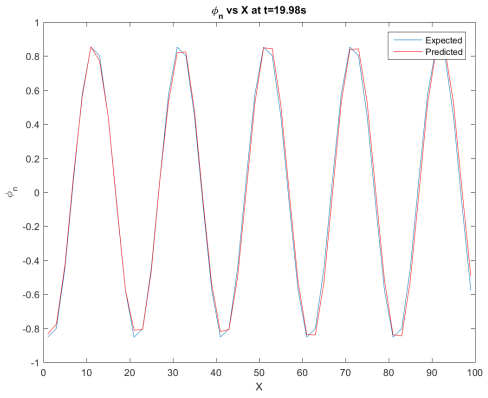

(c) At T = 20s

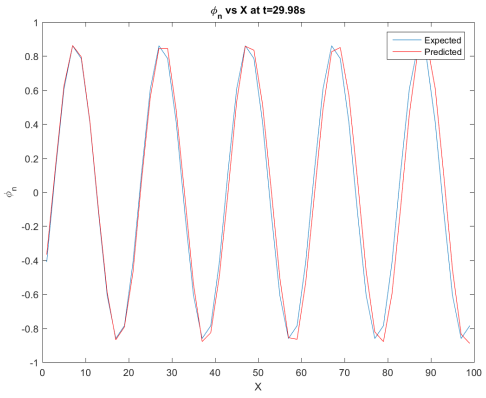

(d) At T = 30s

Figure 2.4: Free Surface Elevation plots

As can be seen from the figure(2.4), the actual and predicted free surface correspond quite well. The time traces of the free surface wave elevation are provided in (2.5).

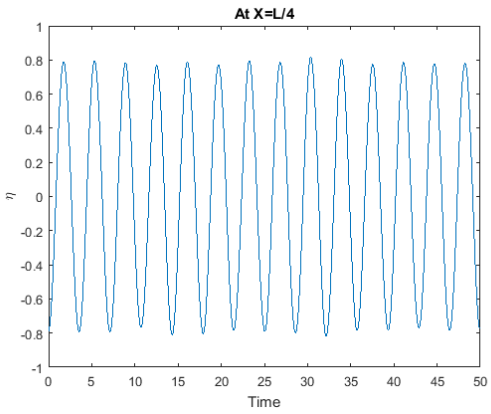

(a) At X = 25m

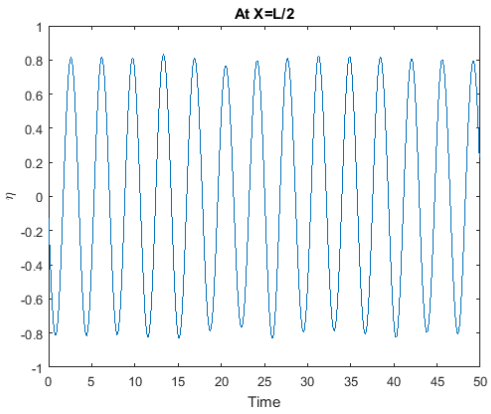

(b) At X = 50m

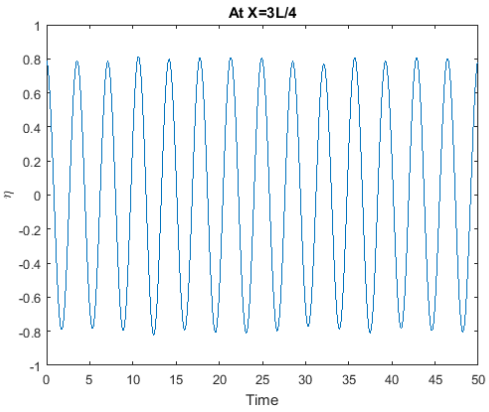

(c) At X = 75m

Figure 2.5: Time traces of free surface elevation at various locations

Another check on the code can be that there should be no mean flux(mean in time) flowing or leaving the domain. If that were not the case, there is mean rise or fall in water in the domain, which is not true in the case of linear waves. The main flux is very close to zero.

By changing the wavelengths and predicting the numerical wave frequencies(At X = L/2), we can arrive at the numerical dispersion relation(Fig 2.6(a)) at that location. The number of panels per wavelength(30 panels/λ) is always kept constant, along with the same non-dimensional time(ratio of the time step to the Time period of the wave) for all the computations. The results match quite well(The maximum difference between the Numerical and Analytical wavength is 3.2% and the maximum difference between

the Numerical and Analtyical wavefrequencies is 2.2%).

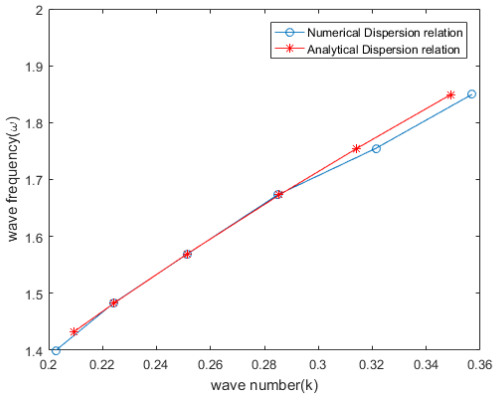

(a) Numerical dispersion relation compared with analytical dispersion relation(At X = 50m)

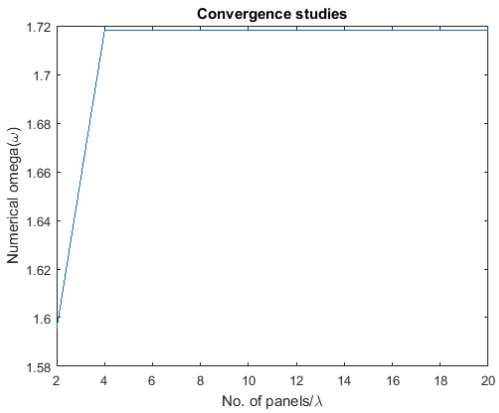

(b) Sensitivity of numerical frequency with panels/λ

Figure 2.6: Verifiication of Linear wave simulator

The number of panels per wavelength plotted against numerical frequency is shown in Fig(2.6(b)) and shows that having around 10-20 panels per wavelength is sufficient for accurate results.

Unsteady Wave Simulations

The unsteady wave simulations have been carried out and the results are reported here for the case of the input wave with parameters as in Table-2.2. The waves slowly develop in the domain and the plots of the predicted wave elevation is compared with the expected

Variable	Value
η	2m
λ	20m
Δx	1m
Δt	0.1s

Table 2.2: Wave inputs for unsteady wave simulations

wave profile(computed by the analytical expression from the linear Airy wave theory). As we can see from the fig(2.7), these almost are indistinguishable. There is slight

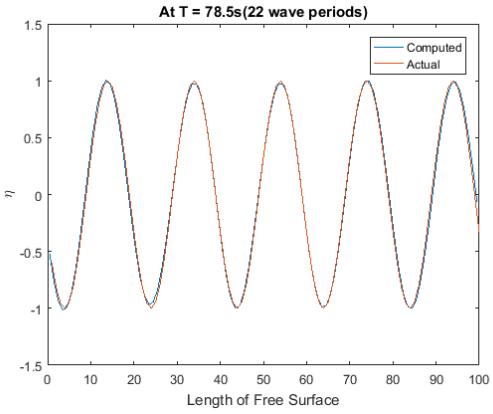

(a) At T = 78.5s(22 wave periods)

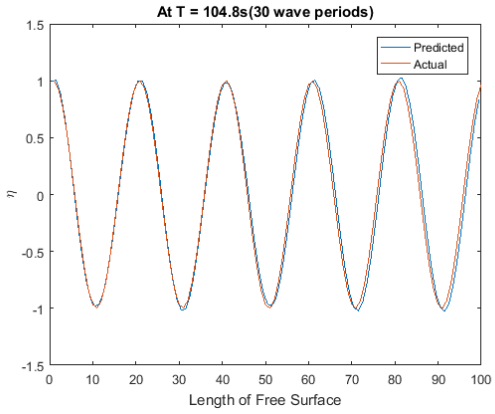

(b) At T = 104.8s(30 wave periods)

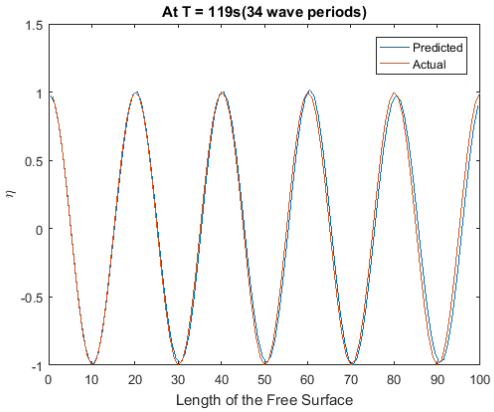

(c) At T = 119s(33 wave periods)

Figure 2.7: Free Surface Elevation plots

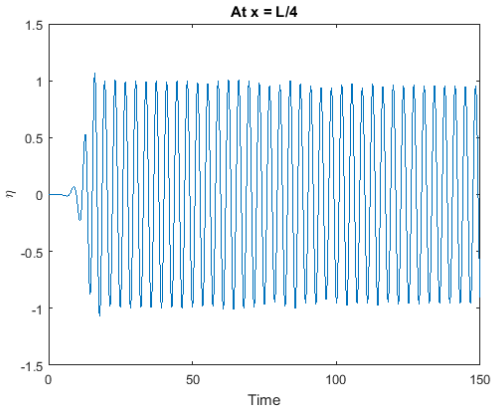

(a) At X=25m

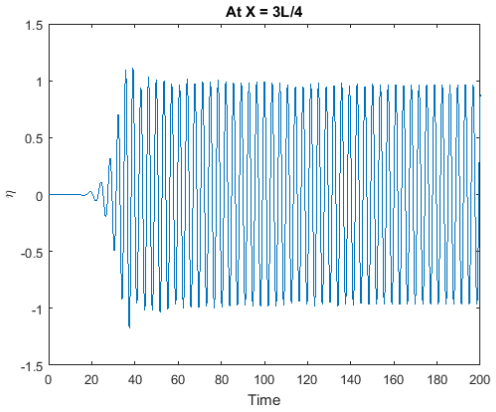

(b) At X=50m

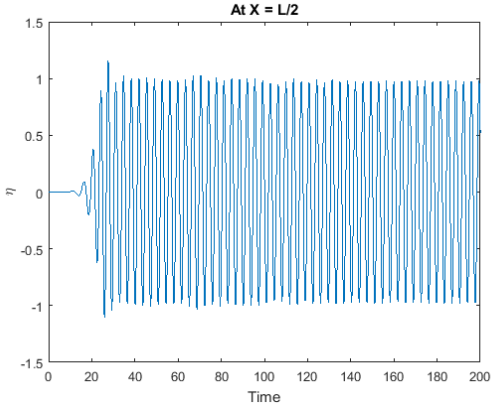

(c) At X=75m

Figure 2.8: Free Surface Elevation Time traces

numerical dispersion(but less than 1%). Also, in Fig(2.8), the time traces are provided.

2.7.2 Nonlinear waves

The steady nonlinear wave simulations were not carried out, but directly we proceeded to the unsteady wave simulations with the upstream boundary provided with a Nth order(depending on the wave steepness, max N = 20) wave potential obtained by the Rienecker and Fenton algorithm[17]. Waves up to a steepness ratio of 0.04 have been predicted and the results of the plots are depicted in Fig(2.9). As we can see from

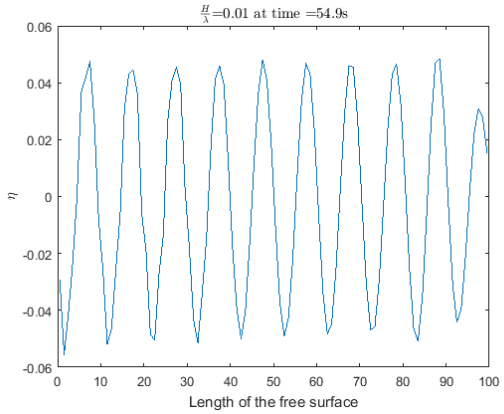

(a) At $\frac{H}{L}$=0.01 and T=54.9s

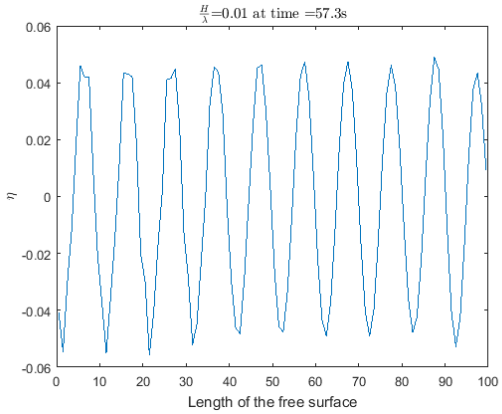

(b) At $\frac{H}{L}$=0.01 and T=57.3s

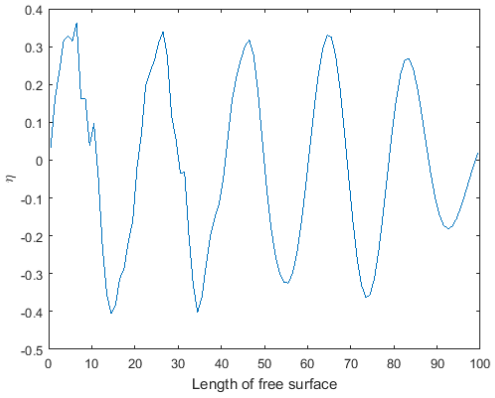

(c) At $\frac{H}{L}$=0.04 and T=40s

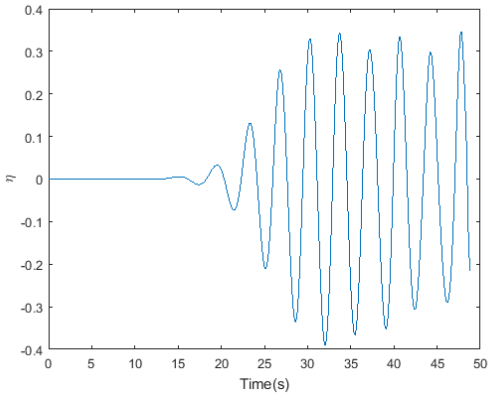

(d) At $\frac{H}{L}$=0.04 and X=L/2

Figure 2.9: Free surface Elevation plots

2.9(c), the wiggles are developing and these contaminate the solution. These wiggles actually look like propagating in the backward direction and do take some time before they occur at the middle of the domain. A lot of time has been invested in understanding their occurrence, but this still seems to be a mystery. We believe that these are mostly associated with the accuracy of the method itself(first order in space and time, constant strength of desired functions). Another contributing factor could be the incompatibility of the boundary conditions between the lateral boundaries and the bottom boundary. The bottom should always behave like a streamline, but as the steepness increases, there is a accumulation of horizontal potential gradient(the potential is no longer constant) and thus violating the assumption. Simply, the bottom boundary can not represent the

convection of flow. If deeper depth is used for simulation, these wiggles are generated for higher steepness.

A more detailed calculation is performed on the wave parameters provided in table 2.3. The plots of the free surface at various time instants is provided in Fig 2.10.

Parameter	Value
Wave Height(H)	0.04m
Wave length(λ)	20m
Wave Steepness(H/λ)	0.02
Length of domain	100m
height of the domain	50m

Table 2.3: Particulars of the Nonlinear wave simulation

The validation of the results is carried out by finding the energy under the wave at location(middle of the domain) and comparing the values with the energy per unit length of the Nth order nonlinear wave from the Rienecker and Fenton Algorithm[17]. The Rienecker and Fenton algorithm[17] provides the energy under a wave per unit length as an output. For finding the energy under the wave in our simulation, we choose the middle of the domain and find the energy at that location. The time trace of the free surface elevation is used for finding the energy spectral density of the wave and we find the area under this spectrum to get the energy at that location. The comparison of the energy per wavelength from the Rienecker and Fenton algorithm[17] with the estimation of energy per wavelength from the numerical simulation with varying steepness of the wave is shown in Fig 2.11(a) and tabulated in Table 2.4. The difference in the energy is

Steepness	Energy from R&F Algorithm	Energy from Numerical Simulation	% Difference
0.01	50.2125	50.1337	0.157
0.0125	78.446	77.8339	0.78028
0.015	112.9426	111.768	1.04
0.02	200.6967	195.175	2.75
0.0225	253.937	244.53	3.7
0.025	313.4029	296.94	5.25298

Table 2.4: Energy comparison

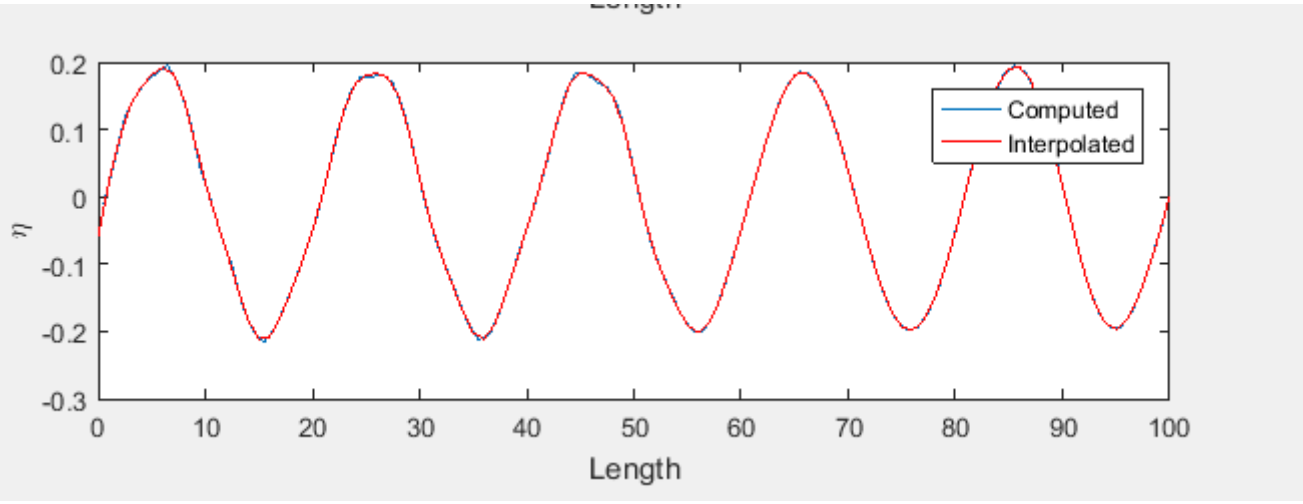

(a) $\frac{H}{\lambda}$=0.02 at T=46.7s

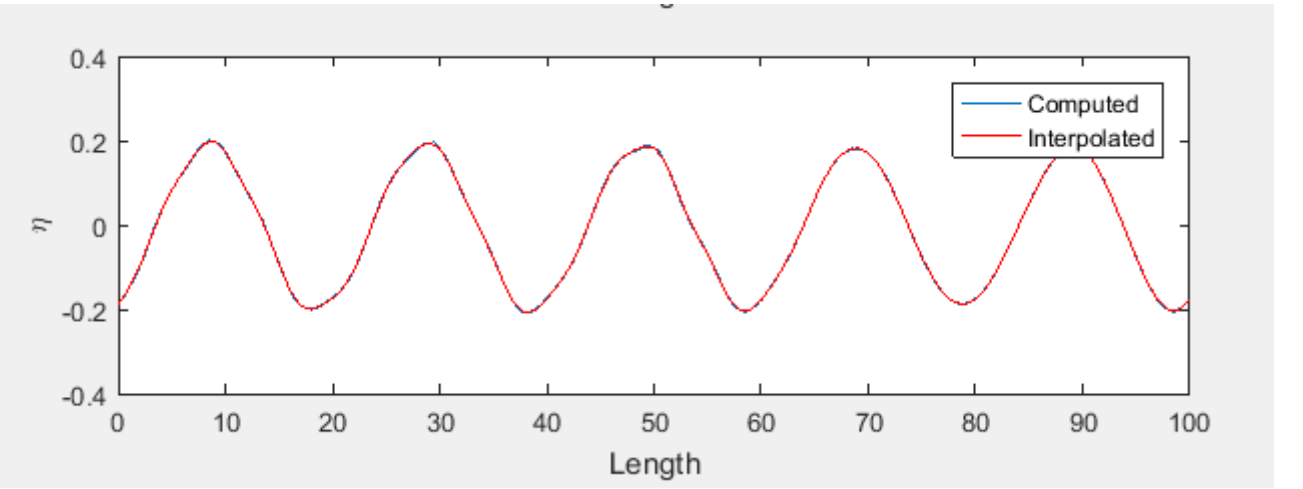

(b) $\frac{H}{\lambda}$=0.02 at T=51.7s

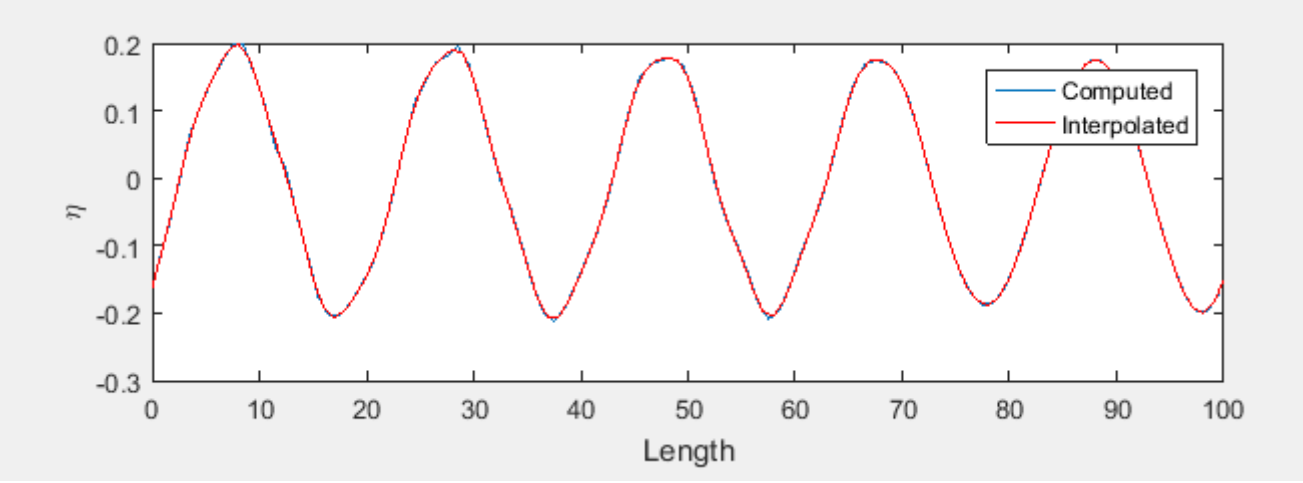

(c) $\frac{H}{\lambda}$=0.02 at T=55s

Figure 2.10: Free Surface Elevation plots

expressed as a percentage according to (2.53) and this is plotted against varying steepness in 2.11(b).

$$\%\ \text{diff. in energy} = \frac{(\text{Energy from R\&F} - \ \text{Numerical predicted Energy})}{\text{Energy from R\&F}} * 100 \quad (2.53)$$

Using an another location for evaluating the energy under the wave, produces results which are quite similar to the results presented and our research goal is not to develop a complete 2D NWT(Numerical Wave Tank) that can predict waves upto breaking limit, but is to compare two different techniques of evaluating generalized forces on structures. Also, wiggles develop as the steepness of the wave is increased beyond 0.03 and these

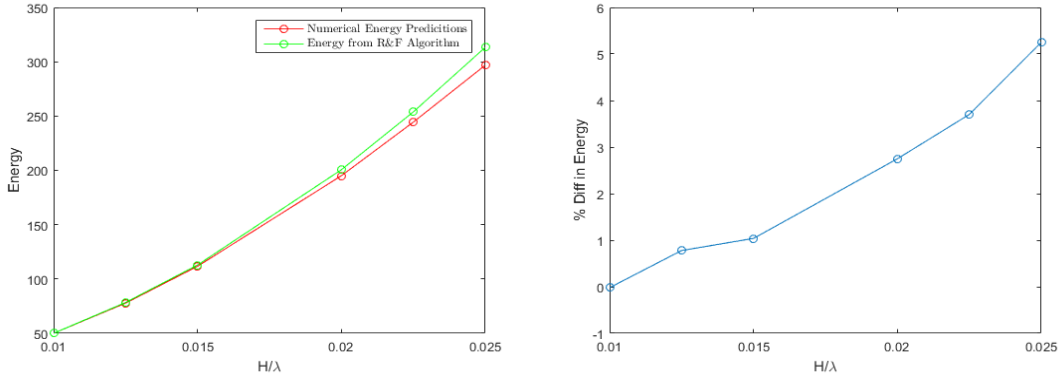

(a) Comparison of energy between the numerical code and the Rienecker and Fenton Algorithm[17] as a function of steepness

(b) % difference in energy as a function of steepness

Figure 2.11: Verification of the 2D Numerical Wave Tank(NWT)

wiggles can be suppresed by smoothing functions, if necessary. But the usage of smoothing functions complicates the derivation of the re-formulated Fluid Impulse Theory and thus, will not be encouraged in this thesis work.All the results presented here so far, do not use any such smoothing. Keeping in mind that Constant Panel Method(CPM) is employed, along with first order accurate formula for spatial derivatives and time evolution, the accuracy of the solution can be considered to sufficient enough and we can proceed further by introducing the body into the domain in the next chapter.

Chapter 3

Wave-body Interactions

We have already dealt with complete nonlinear free surface flows. In this chapter, we introduce a body into our computational domain. We follow and build up along the lines followed in the last chapter. We begin with throwing light on the work of previous researchers, building up the theoretical/mathematical framework for the nonlinear wave body interaction and linearize the various equations with valid assumptions. The linearized solutions can be verified which gives us confidence that we are dealing with the proper physics. Then, we extend the code further to deal with nonlinear wave-body interactions.

The results are presented, whenever necessary. First, we deal with the Direct Pressure Integration(DPI) that is a standard technique in dealing with wave-body interactions, as described in Chapter-1. Then, we provide re-derivation of the Fluid Impulse Theory using Reynolds Transport Theorem(RTT) to the fluid momentum in closed domain for reasons specified in Chapter-1. A small and simple analytical proof is provided which shows the similarity between the standard Direct Pressure Integration(DPI) and the re-formulated Fluid Impulse Theory(FIT) in the linear case.Then, we implement this technique to get in results for simulations in complete nonlinear setting and compare the results with results from Direct Pressure Integration technique.

3.1 Existing techniques to deal with nonlinear wave body interactions

Koo and Kim[21] have described four methods to deal with wave-body interaction problem:

1. Mode decomposition method, proposed initially by Vinje and Brevig[2] and followed by Cointe[18][22] and Koo and Kim[21].

2. Iterative methods of D.Sen[7] and Cao et. al[23].

3. Indirect method of Wu and Eatock Taylor[24].

4. Implicit Method of Van Daalen[6] and Tanizawa[25].

In all the methods described above, the potential and the temporal gradient of the potential are obtained as solutions of the Laplace problem in the computational domain at each time step, except the indirect method of Wu and Eatock Taylor[24], where the accelerations of the body are obtained directly at each time step. Except the indirect method of Wu and Eatock Taylor, all the other methods rely on an accurate estimation of the temporal gradient of potential, which plays an important role in the pressure evaluation as stated by various researchers([18], [21], [22], [25]). The use of backward differences for the estimation of the temporal gradient of potential is not the most accurate and may lead to instabilities for bodies in large amplitudes.

The body and water should find dynamic equilibrium at each and every time step. Using backward differences implies that the information from previous time step is employed to find the new dynamic equilibrium at the present time step, which may lead to instabilities. An overview of the four methods is given hereafter:

The mode decomposition method was proposed by Vinje and Brevig[2] in their 2D-Numerical Wave Tank(NWT). It was later used by Cointe[18], [22] and Koo and Kim[21] in their 2D-NWT. The time derivative of the potential is estimated basing on a linear decomposition into four modes corresponding to three unit accelerations for sway-heave-roll and acceleration due to the velocity field. The four modes are calculated at each time step and lead to the estimation of the temporal gradient of the potential. The loads are predicted and the equations of motion are time integrated to find the new positions. The main drawback of the technique is that we need to solve four boundary integral equations; each for one mode, just to obtain the temporal gradient of the potential. This would lead to an inevitable time consuming algorithm.

The iterative methods of D.Sen[7] and Cao et al[23] use predictor-corrector loop to converge on the values of accelerations at current time step. The values of the accelerations at the present time step are first predicted basing on the their values from past time step for the first iteration. Then, the potential is evaluated using the boundary

integral equation to yield the forces/moments, through which the accelerations are calculated. These accelerations are compared with their values from previous iteration and convergence checks are carried out. The new body positions are finally evaluated by integrating the equations of motion. This approach is also time consuming, but is better than mode decomposition method. However, the equations of motion are not strictly verified, but only up to an order of convergence. Choosing a lower convergence criterion would inevitably lead to high number of iterations and a larger CPU time.

The indirect method was introduced by Wu and Eatock-Taylor[24] in 3D and used by Kashiwaga in his 2D-NWT[26]. They introduce an artificial potential(φ) for each degree of motion and set up a boundary value problem for each degree. The hydrodynamic forces and moments can be expressed as function of artificial potential, its normal derivative and apart from known quantities, body acceleration. By injecting these relations, Wu and Eatock-Taylor establish a relation between body acceleration and potential and the artificial potential, with its spatial derivatives. At each time step, the boundary value problem for potential and boundary value problem for each artificial potential is solved and the equations of motion are time integrated to yield new positions of the body for the next time step. This method is clearly efficient than the mode decomposition method as it has one boundary value problem lower, but since the temporal gradient of the potential is not calculated explicitly, the hydrodynamic pressure cannot be evaluated explicitly.

Finally, the implicit method proposed by Van Daalen[6], also called the acceleration potential method as used by Tanizawa[25], uses the body motion equations in order to yield an extra boundary integral equation which links the potential and the temporal gradient of the potential on the body boundary. This relation is added to the Laplace equation for the temporal gradient of the potential so that the number of equations equals the number of unknowns. Now, integrating the equations of motion, new displacements and velocities are estimated for next time step.

We suggest interested readers to the works of Koo and Kim[21] for further details. The table 3.1 illustrates the number of Laplace problems to be solved at each time step for each method.

The implicit method is apparently less time expensive compared to the other methods, as two boundary value problems are to be solved per each time step and also, the hydrodynamic pressure can be calculated, once temporal gradient of potential is esti-

mated. We, therefore choose the implicit method for its efficiency. The mathematics associated with it is detailed in later sections.

method	authors	artificial potential	Number of equations in 2D
mode decomposition	Vinje & Brevig, Cointe	Yes	5
Iterative	D.Sen, Cao et al	No	1+i
indirect	Wu & Eatock-Taylor	Yes	4
implicit	Van Daalen, Tanizawa	No	2

Table 3.1: Comparison of the methods for wave-body interaction, in the scope of fully nonlinear potential flow theory. For iterative method, i stands for the number of iterations necessary for convergence(i>=1)

3.2 Theoretical Framework for Wave-Body Interaction

The body along with the computational domain is presented in Fig 3.1. They are two frame of references: one is the earth fixed co-ordinate system used to describe the translation of the body(which is zero in our case, X-Y co-ordinate system) and the other is the body fitted frame of reference(centered at center of gravity, X'-Y' co-ordinate system). At the mean position, these two frame of references coincide. We have already explained the boundary conditions in the previous section, but we reproduce them for the sake of clarity. Then, we discuss about the acceleration potential and provide the boundary conditions for the acceleration potential. Then, we look into the assumptions of linear theory and solve a set of linear problems: linear radiation, and linear diffraction. The results are documented and then we proceed into complete nonlinear wave-body interactions.

3.2.1 Boundary Conditions for velocity potential

As stated in the previous chapter, each and every boundary should have a Dirichlet condition or a Neumann condition or a linear combination of velocity potential and normal gradient of the velocity potential(Robin condition) in order to ensure a unique solution. The computational domain has five boundaries: Upstream boundary, Downstream boundary, Free Surface, Body boundary and the bottom boundary. We will specify the

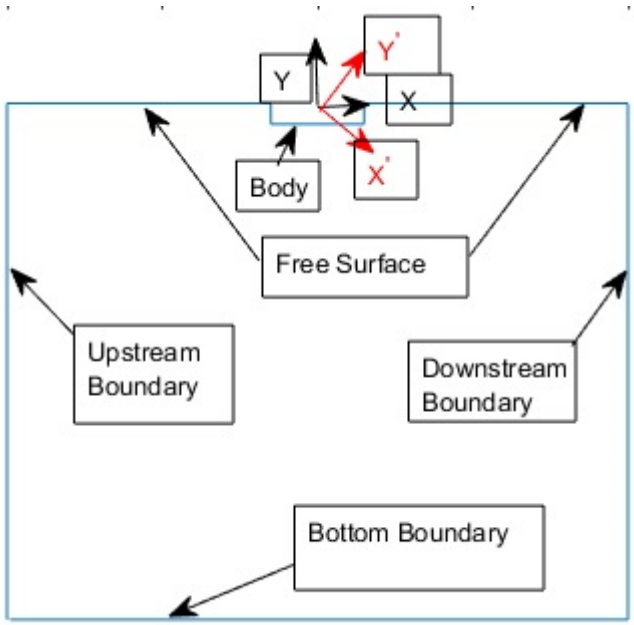

Figure 3.1: Co-ordinate system for wave-body interaction along with the various boundaries of the Computational Domain

boundary conditions on the various boundaries.

Free Surface Boundary Conditions

The free surface has two unknowns: its shape and the velocity potential. Thus, it requires two boundary conditions: Kinematic Free Surface Boundary Conditions(KFSBC) and Dynamic Free Surface Boundary Conditions(DFSBC).

Kinematic Free Surface Boundary Condition

$$\frac{\partial \eta}{\partial t} + \nabla\phi \cdot \nabla\eta = \frac{\partial \phi}{\partial y} \text{ on y } = \eta \tag{3.1}$$

Dynamic Free Surface Boundary Condition

$$\frac{\partial \phi}{\partial t} + \frac{1}{2}\nabla\phi \cdot \nabla\phi + g\eta = 0 \text{ on y} = \eta \tag{3.2}$$

Upstream Boundary Condition

The boundary condition to be invoked on the upstream boundary depends on the type of problem at hand. If, we are dealing with the diffraction program, where the body is fixed and waves impinge on it, the Upstream boundary should allow the incident waves to enter the computational domain and should not allow the diffracted wave to reflect from the boundary. It is quite difficult to arrive at a boundary condition that would ensure complete non-reflective boundaries. We use a Generating Absorbing Boundary Condition(GABC) to generate and absorb the waves, which are periodic and travel at a speed(c). We expect the efficiency of the boundary to behave as a non reflective boundary to reduce, with nonlinear wave body interactions.

$$\frac{\partial \phi}{\partial t} + c\frac{\partial \phi}{\partial n} = \frac{\partial \phi_I}{\partial t} + c\frac{\partial \phi_I}{\partial n} \tag{3.3}$$

If we are dealing with forced nonlinear radiation program, the upstream boundary should absorb the radiated waves and we employ the Sommersfeld radiaition condition(3.4).

Downstream Boundary Condition

The Downstream boundary has to behave such that waves do not reflect and enter back into the computational domain. As stated already, deriving a boundary condition which has 100% effectiveness in absorbing waves is quite difficult due to the presence of body. We employ the Sommersfeld Radiation boundary condition on the downstream, which absorbs waves travelling at speed c(3.4).

$$\frac{\partial \phi}{\partial t} - c\frac{\partial \phi}{\partial n} = 0 \tag{3.4}$$

Bottom Boundary Condition

Without loss of generosity, we assume the bottom to be rigid and the flux across should be, thus zero as stated mathematically in (3.5).

$$\frac{\partial \phi}{\partial n} = 0 \tag{3.5}$$

Body Boundary Condition

The body should represent an watertight entity and this calls for no flux across the body. This is ensured if the normal velocity of the body surface equals the normal velocity of

the fluid on the body surface. Basing on the problem at hand, different Nuemann conditions are employed for the potential on the body. In the case of fixed body(diffraction program), the normal velocity of the body is zero, whereas in the case of forced motion(radiation program), the body moves with a normal velocity V_n. Mathematically, these conditions are depicted in (3.6).

$$\frac{\partial \phi}{\partial n} = \begin{cases} 0 & \text{if diffraction program} \\ V_n & \text{if radiation program} \end{cases} \tag{3.6}$$

The computational domain along with its boundary conditions for the velocity potential is presented in Fig 3.2.

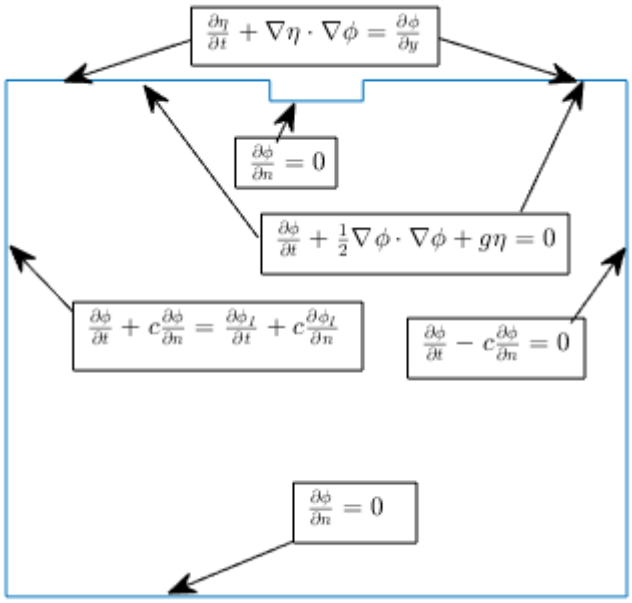

Figure 3.2: The boundaries of the computational domain, along with the associated boundary value problems for the velocity potential

3.2.2 Techniques for Moment Evaluation

Keeping in mind the research objectives and the time framework, we decided that we will not solve the equations of the motions of the body. This implies that the generalized force on the body will not determine the position, velocity nor the acceleration of the body. So, we can post process the generalized force. As already stated, we decompose

the problem into two segments: Diffraction program and the Radiation program. In the Diffraction program, we keep the body fixed and allow the incident wave to impinge on it, whereas in the Radiation program, the body is made to follow forced canonical motion in the roll mode in calm water. We use two techniques to evaluate the generalized moment on the structure:

1. Direct Pressure Integration.

2. Fluid Impulse Theory.

We would like to begin with the brief introduction of the two techniques, before we provide deep insight into these techniques. In Direct Pressure Integration, the pressure is integrated along the wetted surface of the body, as shown in (3.7).

$$M = \int_{S(t)} p\hat{n}\mathrm{ds} = \int_{S(t)} (\frac{\partial \phi}{\partial t} + \frac{1}{2}\nabla\phi \cdot \nabla\phi + gZ)\hat{n}\mathrm{ds} \tag{3.7}$$

In the previous subsection, we have presented a boundary value problem for evaluating the velocity potential of the body, but an examination of (3.7) clearly shows that we do not need the velocity potential on the body, but we are interested in the gradients of the potential(temporal as well as spatial). We have already discussed the methodology that will be employed for evaluating the temporal gradient of the potential in the begining of the chapter, though we did not give a complete description. For the estimation of the spatial gradients of the potential, first order finite difference schemes are employed. So, to evaluate the moment, we need to solve an another boundary value problem which makes this computationally expensive.

P.D.Sclavounous[10] has developed an alternative technique for estimating the generalized forces on the structures by using Reynold Transport Theorem and applying it to the fluid momentum in a closed domain. We use the same idea, but we had to re-derive it for reasons that have been explained in Chapter 1 and will be briefed again in the section on Fluid Impulse Theory. But the whole idea is that we can circumvent the gradients of the potential(temporal and spatial) on the body and estimate the generalize force on the body.

We will first try to apply the direct pressure integration for the estimating the generalized forces on the body and verify the program. Once, we are confident that the nonlinear programs using Direct Pressure Integration provide reasonable results, we provide a derivation of the Fluid Impusle Theory, implement it and compare the results with the Direct Pressure Integration.

3.3 Direct Pressure Integration

We first provide a definition of the acceleration potential, then set up an boundary Integral equation for the temporal gradient of the potential and specify the boundary conditions on the various segments of our computational domain.

3.3.1 Acceleration potential

The Euler momentum equations are reproduced in (3.8).

$$a = \frac{\mathrm{Dv}}{\mathrm{Dt}} = \frac{\partial v}{\partial t} + (v \cdot \nabla)v = -\frac{\nabla p}{\rho} - g\nabla Y \tag{3.8}$$

By following along the lines of Tanizawa[25], substituting v=$\nabla\phi$ leads to (3.9).

$$a = \frac{\mathrm{Dv}}{\mathrm{Dt}} = \frac{\mathrm{D}\nabla\phi}{\mathrm{Dt}} = \frac{\partial\nabla\phi}{\partial t} + (\nabla\phi \cdot \nabla)\nabla\phi = \nabla(\frac{\partial\phi}{\partial t} + \frac{1}{2}\nabla\phi \cdot \nabla\phi) \tag{3.9}$$

We introduce the acceleration potential(φ), whose gradient yields the acceleration of a fluid particle.

$$\varphi = \frac{\partial\phi}{\partial t} + \frac{1}{2}\nabla\phi \cdot \nabla\phi \tag{3.10}$$

A point that is noteworthy is the nonlinear nature of the acceleration potential, along with its inability to satisfy the Laplace equation. So, this is inappropriate to numerical methods like BEM. This nonlinear part of the acceleration field can be evaluated explicitly from the solution of the velocity field(solution of the Boundary value problem for the velocity potential, as detailed in the previous subsection). So, we can leave out the nonlinear part and deal with the temporal gradient of the potential. Since, the temporal gradient of the potential does solve the Laplace problem, it is easy to set up a boundary value problem and use numerical methods to evaluate it. But it has to be noted that this temporal gradient does not give the acceleration of the fluid particle itself. For a more detailed discussion on the acceleration potential, the readers are referred to the work of Tanizawa[25].

3.3.2 Boundary Integral Equation for the temporal gradient of potential

The Boundary Integral equations(2.33) derived for the velocity potential can be differentiated with respect to time and noting the regularity of the integrals, the time

derivative can be bought inside the integral expressions, yielding a Boundary Integral representation for the temporal gradient of the velocity potential(3.11).

$$\frac{1}{2}\frac{\partial\phi(\overrightarrow{x})}{\partial t} = \int_{\partial \mathrm{S}} (\frac{\partial\phi(\overrightarrow{\epsilon})}{\partial t}\frac{\partial G(\overrightarrow{\epsilon};\overrightarrow{x})}{\partial n} - \frac{\partial^2\phi(\overrightarrow{\epsilon})}{\partial t \partial n} G(\overrightarrow{\epsilon};\overrightarrow{x}))\mathrm{dS} \tag{3.11}$$

In (3.11), $\overrightarrow{x}$ and $\overrightarrow{\epsilon}$ refer to the field point and source point respectively, G refers to the Rankine Green function that satisfies the Laplace equation. Since, neither the temporal gradient of the potential nor its normal gradient are known on the body forehand, the Robin condition linking these two quantities serves as an auxiliary equation.

Discretizing the domain and using constant strength singularities along each panel, leads to a matrix that connects the 2N variables(N variables associated with the temporal gradient of the potential and N associated with its normal gradient) and using the same discretization for the Robin boundary, we can get a matrix representation, similar to that of the Berkvens[27] and Van Daalen[6]. (3.12) provides a matrix description, after arranging the knowns to the right hand side.

$$\begin{pmatrix} C_s^{ij} & C_d^{ij} - \frac{1}{2}\delta_{ij} & C_d^{ij} - \frac{1}{2}\delta_{ij} & C_s^{ij} \\ 0 & 0 & C_f^{ij} & \delta_{ij} \end{pmatrix} \begin{pmatrix} \left(\frac{\partial\phi}{\partial n}\right)_t^j \\ \left(\frac{\partial\phi}{\partial t}\right)^j \\ \left(\frac{\partial\phi}{\partial t}\right)^j \\ \left(\frac{\partial\phi}{\partial n}\right)_t^j \end{pmatrix} = \begin{pmatrix} C_d^{ij} - \frac{1}{2}\delta_{ij} & C_s^{ij} & 0 & 0 \\ 0 & 0 & 0 & \gamma^i\delta_{ij} \end{pmatrix} \begin{pmatrix} \left(\frac{\partial\phi}{\partial t}\right)^j \\ \left(\frac{\partial\phi}{\partial n}\right)_t^j \\ 0 \\ 1 \end{pmatrix} \tag{3.12}$$

Now, let us look into the boundary conditions associated with boundaries of the computational domain.

3.3.3 Boundary Conditions for evaluating temporal gradient of the potential

Fig 3.3 gives a pictoral description of the various boundaries and their respective boundary conditions.

Free Surface Boundary Condition

The boundary condition on the Free surface is obtained by re-arranging the Dynamic Free Surface Boundary Condition(DFSBC) and is a Dirichlet boundary condition for the temporal gradient of the velocity potential(3.13).

$$\frac{\partial\phi}{\partial t} = -\frac{1}{2}\nabla\phi\cdot\nabla\phi - g\eta \tag{3.13}$$

Body Boundary

Using the condition that the normal acceleration of the fluid particle is to be equal to the normal acceleration of the body and using the equations of the motion leads to a dynamic boundary condition linking the temporal gradient of the velocity potential to its normal gradient. The derivations have been carried out and provided in the Appendix. The boundary conditions is of the Robin type and stated in (3.14).

$$\frac{\partial^2 \phi}{\partial t \partial n} + C\frac{\partial \phi}{\partial n} = \gamma \tag{3.14}$$

But since, we are not solving the free motions of the body, we can further simplify (3.14). In case of fixed body(diffraction), a simple time derivative of (3.6) will yield (3.15), whereas for the forced radiation program, the derivation is provided in the Appendix-C(the formula is reproduced in (3.15)).

$$\frac{\partial^2 \phi}{\partial t \partial n} = \begin{cases} 0 & \text{if diffraction program} \\ \ddot{x} \cdot n - ((\dot{x} \cdot s) - \frac{\partial \phi}{\partial s})\dot{\theta} - (\dot{x} \cdot s)\left[\frac{\partial \phi}{\partial s}\frac{1}{R} + \frac{\partial^2 \phi}{\partial s \partial n}\right] + (\dot{x} \cdot n)\left[\frac{\partial^2 \phi}{\partial^2 s} - \frac{1}{R}\frac{\partial \phi}{\partial n}\right] & \text{if radiation program} \end{cases} \tag{3.15}$$

Upstream Boundary Condition

Re-arranging the Generating Absorbing Boundary Condition leads to a Dirichlet boundary condition for the temporal gradient of the potential(3.16) for the diffraction program. For the radiation program, the Sommersfeld radiaition boundary condition has to be re-arranged to arrive at Dirichlet boundary condition on the Upstream boundary(3.17). In either cases, we have a Dirichlet Boundary Condition.

$$\frac{\partial \phi}{\partial t} = \frac{\partial \phi_I}{\partial t} + c\frac{\partial \phi}{\partial n} - c\frac{\partial \phi}{\partial n} \tag{3.16}$$

Downstream Boundary Condition

Re-arranging the Sommersfeld Radiation condition provides with a Dirichlet boundary condition for the temporal gradient of the velocity potential(3.17).

$$\frac{\partial \phi}{\partial t} = c\frac{\partial \phi}{\partial n} \tag{3.17}$$

Bottom Boundary

Taking the time derivative of the (3.5), leads to a Neumann Boundary condition for the temporal gradient of the velocity potential(3.18) on the bottom.

$$\frac{\partial^2 \phi}{\partial t \partial n} = 0 \tag{3.18}$$

After we find the temporal gradient of the velocity potential on the body, we just need to evaluate the hydrodynamic pressure and find the moments on the structure.

3.3.4 Algorithm for Wave-Body Interaction

The algorithm for wave body interaction is enumerated below.

1. Subdivide the boundary surfaces into N linear segments.

2. At time step 'n', $(\phi)^n_{UP}$, $(\phi)^n_{FS}$, $(\phi)^n_{DS}$, $\left(\frac{\partial \phi}{\partial n}\right)^n_B$, $(\eta)^n_{FS}$, $(\zeta)^n_B$ and $\left(\frac{\partial \phi}{\partial n}\right)^n_{BO}$ are known(UP-Upstream, DS- Downstream, BO-Bottom, B - Body, FS - Free Surface).

3. If A represents the matrix associated with the potential(Dipole) and B represents the matrix associated with the normal gradient of the potential(Source), subdividing these matrices leads to a system of equations(3.19).

$$\begin{pmatrix} A^n_{1,1} & A^n_{1,2} & A^n_{1,3} & A^n_{1,4} & A^n_{1,5} \end{pmatrix} \begin{pmatrix} \phi^n_{UP} \\ \phi^n_{FS} \\ \phi^n_{DS} \\ \phi^n_B \\ \phi^n_{BB} \end{pmatrix} = \begin{pmatrix} B^n_{1,1} & B^n_{1,2} & B^n_{1,3} & B^n_{1,4} & B^n_{1,5} \end{pmatrix} \begin{pmatrix} \left(\frac{\partial \phi}{\partial n}\right)^n_{UP} \\ \left(\frac{\partial \phi}{\partial n}\right)^n_{FS} \\ \left(\frac{\partial \phi}{\partial n}\right)^n_{DS} \\ \left(\frac{\partial \phi}{\partial n}\right)^n_B \\ \left(\frac{\partial \phi}{\partial n}\right)^n_B \end{pmatrix} \tag{3.19}$$

The co-efficients of these matrices change in time as the evaluation of its constituent elements depends on the shape of the domain at the present time instant(stated generically, not the case for linear case). Now re-arranging these matrices by

bringing the knowns to the right hand side leads to the system of equations(3.20).

$$\begin{pmatrix} -B^n_{1,1} & -B^n_{1,2} & -B^n_{1,3} & A^n_{1,4} & -B^n_{1,5} \end{pmatrix} \begin{pmatrix} \left(\frac{\partial\phi}{\partial n}\right)^n_{UP} \\ \left(\frac{\partial\phi}{\partial n}\right)^n_{FS} \\ \left(\frac{\partial\phi}{\partial n}\right)^n_{DS} \\ \phi^n_B \\ \phi^n_{BB} \end{pmatrix} =$$

$$\begin{pmatrix} -A^n_{1,1} & -A^n_{1,2} & -A^n_{1,3} & B^n_{1,4} & A^n_{1,5} \end{pmatrix} \begin{pmatrix} \phi^n_{UP} \\ \phi^n_{FS} \\ \phi^n_{DS} \\ \left(\frac{\partial\phi}{\partial n}\right)^n_B \\ \left(\frac{\partial\phi}{\partial n}\right)^n_B \end{pmatrix} \tag{3.20}$$

Carrying out the inverse of the matrix on the left hand side, we can evaluate the unknowns. Since, we deal with a 2D problem, use of direct inverse has been used.

4. After the finding the unknowns, we need few variables for time stepping the equations of the free surface and few variables for invoking the Nuemann boundary condition for the temporal gradient on the body. These include: $\left(\frac{\partial\phi}{\partial x}\right)^n_{FS}$, $\left(\frac{\partial\eta}{\partial x}\right)^n_{FS}$, $\left(\frac{\partial\phi}{\partial y}\right)^n_{FS}$, $((\nabla\phi)^2)^n_{FS}$, $\left(\frac{\partial\phi}{\partial x}\right)^n_{BB}$, $\left(\frac{\partial\phi}{\partial y}\right)^n_{BB}$, $\left(\frac{\partial^2\phi}{\partial^2 x}\right)^n_{BB}$ and $\left(\frac{\partial^2\phi}{\partial^2 y}\right)^n_{BB}$. The way, the first two quantities are estimated is given in the section about the algorithm for nonlinear wave simulations. Here, we do not reproduce all the details, but we specify the formulaes(3.21-3.22) for the sake of clarity.

$$\left(\frac{\partial\phi}{\partial x}\right)^n_j = \frac{\phi(x_j) - \phi(x_{j-1})}{x_j - x_{j-1}} \tag{3.21}$$

$$\left(\frac{\partial\eta}{\partial x}\right)^n_j = \frac{\eta(x_j) - (x_{j-1})}{x_j - x_{j-1}} \tag{3.22}$$

5. The next step dealt with the evaluation of gradients of potentials and free surface in the horizontal direction. We are yet to evaluate the vertical gradient of potential. For this, two step procedure employed in the section about the algorithm of nonlinear wave simulations is employed. Again, for the sake of clarity, the formulae(3.23-3.26) are specified.

$$\left(\frac{\partial\phi}{\partial s}\right)^n_{FS} = \frac{N_x \left(\frac{\partial\phi}{\partial n}\right)^n_{FS} + \left(\frac{\partial\phi}{\partial x}\right)^n_{FS}}{N_z} \tag{3.23}$$

$$\left(\frac{\partial\phi}{\partial z}\right)^n_{FS} = N_x\left(\frac{\partial\phi}{\partial s}\right)^n_{FS} + N_z\left(\frac{\partial\phi}{\partial n}\right)^n_{FS} + \tag{3.24}$$

N_x,N_y are respectively the components of the outward normal(3.24,3.25).

$$N_x = -\frac{(y_2 - y_1)}{\sqrt{(x_1 - x_2)^2 + (y_1 - y_2)^2}} \tag{3.25}$$

$$N_y = \frac{(x_2 - x_1)}{\sqrt{(x_1 - x_2)^2 + (y_1 - y_2)^2}} \tag{3.26}$$

where(x_1, y_1) and (x_2, y_2) refer to the end points of the panel taken clockwise.

6. We require quanitites of interest on the body, which are estimated by employing first order schemes, so as to be consistent with the technique used for estimation of quatities on the free surface. For estimation of $\left(\frac{\partial\phi}{\partial x}\right)^n_{BB}$ and $\left(\frac{\partial\phi}{\partial y}\right)^n_{BB}$, (3.21) and (3.27) are employed. Using the quantities evaluted in the last sentence and employing a first order scheme, $\left(\frac{\partial^2\phi}{\partial^2 x}\right)^n_{BB}$ and $\left(\frac{\partial^2\phi}{\partial^2 y}\right)^n_{BB}$ are predicted((3.28) and (3.29)). These quantities are only required in the case of radiation program(body following a forced motion). So, in the case of diffraction program, this step is skipped completely.

$$\left(\frac{\partial\phi}{\partial y}\right)^n_j = \frac{\phi(y_j) - \phi(y_{j-1})}{y_j - y_{j-1}} \tag{3.27}$$

$$\left(\frac{\partial^2\phi}{\partial^2 x}\right)^n_{BB} = \frac{\frac{\partial\phi}{\partial x}(x_j) - \frac{\partial\phi}{\partial x}(x_{j-1})}{x_j - x_{j-1}} \tag{3.28}$$

$$\left(\frac{\partial^2\phi}{\partial^2 y}\right)^n_{BB} = \frac{\frac{\partial\phi}{\partial y}(y_j) - \frac{\partial\phi}{\partial y}(y_{j-1})}{y_j - y_{j-1}} \tag{3.29}$$

7. The values employed in steps 4 and 5 are required to evaluate $\left((\nabla\phi)^2\right)^n_{FS}$. This quantity is required in the time stepping of Dynamic Free Surface Boundary Condition.

$$\left((\nabla\phi)^2\right)^n_{FS} = \left((\frac{\partial\phi}{\partial y})^n\right)^2_{FS} + \left((\frac{\partial\phi}{\partial x})^n\right)^2_{FS} \tag{3.30}$$

8. Now, we set up a similar Boundary Integral equation as of (1.18) for the temporal gradient of the potential . All the quantities which have been evaluated so far are used. The solution of this boundary value problem provides with the temporal gradient of the potential($\left(\frac{\partial\phi}{\partial t}\right)^n_{BB}$) on the body. The Moments on the body are evaluated using (16).

9. Time marching of the various equations: The Kinematic Free Surface and the Dynamic Free Surface. For the free surface, the scheme described in previous chapter is employed. Evaluate $(\eta)_{FS}^{n+1}$, $(\phi)_{FS}^{n+1}$, $(\phi)_{DS}^{n+1}$ and $(\phi)_{UP}^{n+1}$.

10. The wetted surface of the body changes due to the motion of the body and its encounter with the incident waves. Thus, for every time step, keeping the number of panels on the body constant, re-griding is carried out. If re-griding were not carried out and new points were added/deleted, we expect pressure spikes as stated in the work of D.Sen[6]. In order to carry out re-gridding, we need to evaluate the intersection point(between the water and body) first. We use cubic spline fit along the free surface and extrapolate the free surface elevation on the body in the case of diffraction as the body is stationary(This is quite simple to carry out with the MATLAB in-buit command). In the case of radiation program, it gets a bit tricky for finding the intersection point. We take advantage of the linear geometry of the barge by fitting a line that represents the side of the barge and then find the intersection of this line with the cubic spline fit on the free surface. Once, we have found the intersection points, then we need to think about the re-gridding to be carried out on the body. Again, we try to take advantage of the linear geometry and try using the principles of FEM(with linear basis functions) to find the new points. Let (X_i, Y_i) and (X_B, Y_B) be an intersection point and the corner point of the barge, then any X,Y location between this points is given by:

$$X = \frac{1}{2}(1-\zeta)X_i + \frac{1}{2}(1+\zeta)X_B \tag{3.31}$$

$$Y = \frac{1}{2}(1-\zeta)Y_i + \frac{1}{2}(1+\zeta)Y_B \tag{3.32}$$

where we map everything between these corner points into a ζ plane of unit length. For the diffraction program, the X-location of the intersection point always remains the same and thus, we do not need any re-gridding on the free surface, whereas in the radiation program, the X-location of the intersection also changes, thus the free surface has to be re-gridded. Once, the free surface is re-gridded, the values of the potential and the free surface elevation are interpolated on the new grid(obtained after re-gridding) using the data obtained after time stepping from the previous time step. Use of cubic spline interpolation has been employed.

11. We repeat 1-10 till desired.

3.3.5 Linearization of the Wave-body Interaction problem

Assuming that the motion of the body is small(in the case of radiation program) and that the wave amplitude impinging on the vessel is small compared to its wavelength(in the case of diffraction), leads to huge simplification of the equations. In this segment, we first, provide the linear versions of the boundary conditions for diffraction and radiation programs. Both the boundary conditions are compared in table 3.1 for the velocity potential and in table 3.2 for the temporal gradient of the velocity potential. Then, we go about by finding the roll excitation moment(Froude Krylov moment and diffraction moment) and roll radiation moment.

Boundary Conditions

Free Surface Boundary Conditions The nonlinear terms in the (3.1) and (3.2) can be dropped due to the assumptions stated in previous paragraph and the equations need not be imposed on the unknown free surface elevation, instead they can be invoked on mean water level(calm water surface). The simplified equations are depicted by (3.33) and (3.34) respectively.

$$\frac{\partial \phi}{\partial t} = -g\eta \text{ on y=0} \tag{3.33}$$

$$\frac{\partial \eta}{\partial t} = \frac{\partial \phi}{\partial y} \text{ on y=0} \tag{3.34}$$

Body Boundary Condition Now, here we specify two different boundary conditions, basing on whether we are dealing with the radiation or the diffraction problem. In both the boundary conditions, the main principle is the same, the flux of the flow should be zero, so as to ensure that the body represents a water tight entity.

$$\frac{\partial \phi}{\partial n} = V_n \tag{3.35}$$

In the case of forced motion(Radiation problem), body moves with a normal velocity(V_n) and we require the fluid particles attached to the body to move with the same normal velocity. For the radiation problem, the temporal gradient of the velocity potential should satisfy the Neumann boundary condition on the body surface(3.35). A simple time derivative of (3.34) yields this expression, where the normal is time independent(a consequence of linear theory is that the boundary conditions are always invoked at the

mean position).

$$\frac{\partial^2 \phi}{\partial n \partial t} = \ddot{x} \cdot n \tag{3.36}$$

The normal is time independent in a linear setting, thus by time derivative of (3.35), we end up with (3.36). The complete nonlinear equation that will be used later on, is derived in the Appendix.

$$\frac{\partial \phi}{\partial n} = 0 \tag{3.37}$$

In the case of diffraction problem, the body is stationary and hence the fluid particle, adjacent to the body should have no normal velocity(3.37). For the diffraction problem, we also have no normal acceleration of the fluid particle(3.38). This is a Neumann boundary condition for the temporal gradient of the velocity potential.

$$\frac{\partial^2 \phi}{\partial n \partial t} = 0 \tag{3.38}$$

Upstream Boundary Conditions The diffraction and the radiation program have different boundary conditions on the upstream boundary. So, we first specify the boundary conditions for the radiation and then follow it up with the boundary conditions for diffraction problem. In the case of radiation problem, the upstream boundary need not allow an incident wave to pass through the domain. Thus, a simple Sommersfeld Radiation Boundary condition(3.39) can be invoked, so that the wave radiated by the body does not reflect from the upstream boundary.

$$\frac{\partial \phi}{\partial t} + c \frac{\partial \phi}{\partial n} = 0 \tag{3.39}$$

For the diffraction boundary, waves are introduced into the domain through the upstream boundary and the diffracted wave is not supposed to be reflected from the upstream boundary. Thus, the Generating Absorbing Boundary Conditions can be invoked on the upstream boundary, as in (3.3).

Downstream Boundary Conditions In the both, radiation and the diffraction problem, the downstream boundary is supposed to behave like a non-reflective boundary and since we assume linear, the Sommersfeld Radiation boundary condition(3.39) can be invoked.

Bottom Boundary In both the cases, we assume a rigid bottom(3.5), without loss of generosity.

Boundary	Radiation problem	Diffraction Problem
Free Surface	$\frac{\partial \eta}{\partial t} = \frac{\partial \phi}{\partial y}$	$\frac{\partial \eta}{\partial t} = \frac{\partial \phi}{\partial y}$
Free Surface	$\frac{\partial \phi}{\partial t} = -g\eta$	$\frac{\partial \phi}{\partial t} = -g\eta$
Upstream	$\frac{\partial \phi}{\partial t} + c\frac{\partial \phi}{\partial n} = 0$	$\frac{\partial \phi}{\partial t} + c\frac{\partial \phi}{\partial n} = \frac{\partial \phi_I}{\partial t} + c\frac{\partial \phi_I}{\partial n}$
Downstream	$\frac{\partial \phi}{\partial t} - c\frac{\partial \phi}{\partial n} = 0$	$\frac{\partial \phi}{\partial t} - c\frac{\partial \phi}{\partial n} = 0$
Body	$\frac{\partial \phi}{\partial n} = V_n$	$\frac{\partial \phi}{\partial n} = 0$
Bottom	$\frac{\partial \phi}{\partial n} = 0$	$\frac{\partial \phi}{\partial n} = 0$

Table 3.2: Boundary conditions for solving the velocity potential in a linear body-wave interaction problem

Boundary	Radiation problem	Diffraction Problem
Free Surface	$\frac{\partial \eta}{\partial t} = \frac{\partial \phi}{\partial y}$	$\frac{\partial \eta}{\partial t} = \frac{\partial \phi}{\partial y}$
Free Surface	$\frac{\partial \phi}{\partial t} = -g\eta$	$\frac{\partial \phi}{\partial t} = -g\eta$
Upstream	$\frac{\partial \phi}{\partial t} = -c\frac{\partial \phi}{\partial n}$	$\frac{\partial \phi}{\partial t} = -c\frac{\partial \phi}{\partial n} + \frac{\partial \phi_I}{\partial t} + c\frac{\partial \phi_I}{\partial n}$
Downstream	$\frac{\partial \phi}{\partial t} = c\frac{\partial \phi}{\partial n}$	$\frac{\partial \phi}{\partial t} = c\frac{\partial \phi}{\partial n}$
Body	$\frac{\partial^2 \phi}{\partial n \partial t} = \ddot{x} \cdot n$	$\frac{\partial^2 \phi}{\partial n \partial t} = 0$
Bottom	$\frac{\partial^2 \phi}{\partial n \partial t} = 0$	$\frac{\partial^2 \phi}{\partial n \partial t} = 0$

Table 3.3: Boundary conditions for solving the temporal gradient of the velocity potential in a linear body-wave interaction problem

As already stated, assuming small motions of the vessel, small amplitudes of the incident waves impinging on the vessel, linearizations can be carried out, which simplifies the problem and at the same time, provides with verification techniques to employed with sound theoretical basis. The complete nonlinear wave-body interaction algorithm can be considerably simplified and the simplifications are listed below:

1. All the co-efficients(source and dipole co-efficients)in the boundary integral equations are time independent. Thus, they can be computed, once for all.

2. For the free surface, we do not require any gradients of the potential and the free surface elevations.

3. A simple explicit-implicit scheme is used for the time stepping the free surafce elevation and the potential on the free surface.

4. Since, all boundary conditions are invoked on the mean positions of the various boundaries, we do not require any re-griding techniques and hence, no interpolation of data is required.

3.3.6 Results of Linear simulations

We present the results of linear diffraction simulations first and follow it up by the results of linear radiation problem.

Linear diffraction problem

A rectangular barge was chosen to be the 2D body in the presence of the incident waves. The dimensions of the body, along with the dimensions of the computational domain are presented in table-3.4. A wave amplitude of 1m with a frequency of 0.78rad/s(close

Variable	Value
Beam of the barge	30m
Draft of the barge	6m
Length of computational domain	200m
Depth of the computational domain	150m
CFL number	0.5

Table 3.4: Dimensions of the body and the domain used for linear simulations

to the natural frequency of roll) is used for performing a convergence study of the roll diffraction moment with number of panels on the body(The diffraction moment of the roll is calculated using the Code-B, which will be explaned later in this section). The results are plotted in Fig 3.3. Having around 200 panels provides results which are quite converged. So, for all the results to be followed hereafter, the number of panels on the body, where chosen to be 200, unless stated. We use two techniques for finding the temporal gradient of the velocity potential: backward differences and the implicit technique of Van Daalen[6]. The integration of pressure was carried out using the rectangle method. This was chosen as the potential is assumed to be constant over each panel. We want to remind the readers that we are only interested in the computation of hydrodynamic pressure and not the hydrostatic component. The results of both the techniques are plotted in Fig 3.4. As we can see in the figure, both the

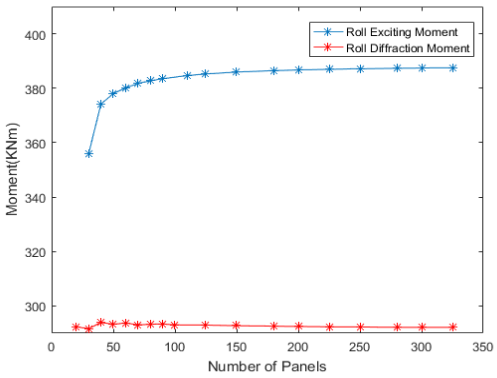

Figure 3.3: Convergence of the Roll excitation moment with the number of panels on the body wetted surface

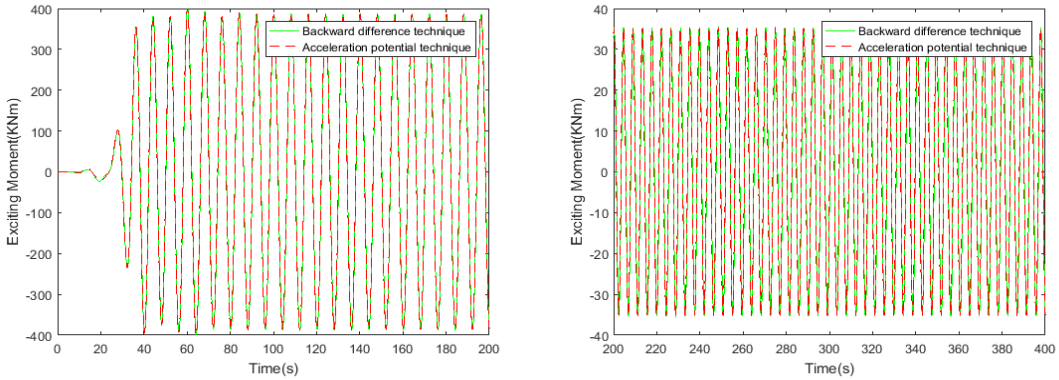

(a) Roll excitation moment on Barge due to an incident wave of η=1m and ω=0.7854rad/s

(b) Roll excitation moment on Barge due to an incident wave of η=1m and ω=1.43rad/s

Figure 3.4: Roll excitation moment on barge

techniques yield same results to the naked eye. The wave frequencies were chosen such that one is close to the roll natural frequency of the barge(0.76rad/s) and the other one represents a condition where, wavelength equals Beam of the barge. The first choice of the frequency is quite trivial, but the latter is chosen, as it resembles a condition, where nonlinear effects are significant. Some verification checks that were carried on the model include the conservation of energy under the wave: The energy of the incident wave should be equal to the energy of the reflected and transmitted wave as the body does no work(only true in the linear case). This was checked and was the case. To carry

this out, since we input the wave, we do know the energy under the incident wave. We pick up a location(say 10m from the body's left end) and substract from the free surface elevation, the expected incident wave elevation. Then, we process the obtained time series, to get a power amplitude spectrum, which yields the amplitude of the reflected wave. We pick up another location(say 10m from the right end of the barge) and process the time trace of the free surface elevation to get a power amplitude spectrum, which provides us with the amplitude of the transmitted wave. Then, we find the energy of the various components and check the conservation of energy.

Another check that could be performed and was carried out is the variation of the exciting roll moment with the amplitude of the incident wave(all carried out at roll natural frequency). Since, its the linear theory, we expect the variation to be a straight line. As, we can see from Fig 3.5, we get a linear variation between the Roll excitation moment and the amplitude of the incident wave. Also, we wanted to be more sure of

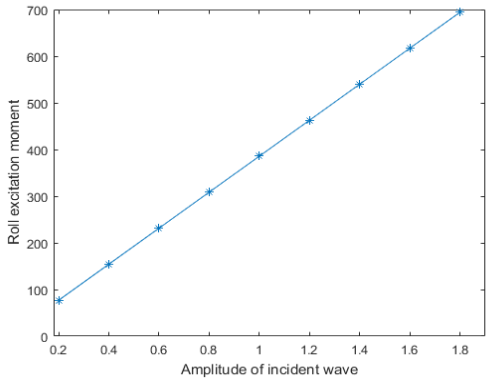

Figure 3.5: Variation of the Roll excitation moment with the amplitude of the incident wave

our predictions, so we reformulate the problem in such a way that we can compare our computational results with that of ANSYS AQWA. Strictly speaking, ANSYS AQWA is a three dimensional panel code, so it cannot be used to compare results with our code. The only way we can compare is by modelling an infinitely long rectangular barge, but this is not possible. So, instead we model barge having same cross section, but length of the barge is made 40m. We could have gone for even higher lengths, but there is a limitation on the number of nodes as we are using a student license. So, we modelled a barge of length 1m and length of 40m. We wanted to prove that as the length becomes

more and more larger, ANSYS AQWA and our results converge. The results of ANSYS AQWA are divided by the length of the vessel to achieve the 2D load. Now, it becomes evident that if the length is small, the ends of the barge effect the 2D load estimation from 3D ANSYS AQWA results.

So, as to compare with ANSYS AQWA, we require the froude-krylov force and the diffraction force independently. We need to reformulate the boundary value problem by decomposing the total potential as the sum of the incident wave potential(ϕ_I) and the diffraction potential(ϕ_D). The numerical wave tank, already explained can be used to estimate the froude-krylov force(the force on the body by undisturbed incident wave potential), whereas for the diffraction potential, a new boundary value problem is set up. The upstream and the downstream boundary should absorb the diffracted waves and thus, a Sommerfeld Radiaition condition is imposed on them. The diffracted wave needs to satisfy the same linerarized free surface boundary condition and the bottom boundary condition as the incident wave. The boundary conditions that are used for evaluating the diffraction potential are provided in table 3.5. As we can see from the table that for the

Boundary	Boundary Condition
Upstream boundary	$\frac{\partial \phi_D}{\partial t} + c\frac{\partial \phi_D}{\partial n} = 0$
Downstream boundary	$\frac{\partial \phi_D}{\partial t} + c\frac{\partial \phi_D}{\partial n} = 0$
Free Surface	$\frac{\partial \phi_D}{\partial t} + g\eta_D = 0$
Body Boundary	$\frac{\partial \phi_D}{\partial n} = -\frac{\partial \phi_I}{\partial n}$
Bottom Boundary	$\frac{\partial \phi_D}{\partial n} = 0$

Table 3.5: Boundary Conditions for the velocity potential in the linear diffraction program

body boundary condition, we require the normal gradient of the incident wave potential. We have explained in the Appendix how we will evaluate the normal gradient of incident wave potential. What we have not explained is how we solve the problem. First, the incident wave profile is generated using the Linear Numerical Wave Tank(developed in the last chapter) without the presence of the body. We require the evaluation of the normal gradient of the incident wave potential on the body. we create an artificial body with sides parallel to the actual body and evaluate potentials on this artificial body, then use finite differences to estimate the normal gradients of the potentials(refer appendix).

From now on, we refer this as Code-B. An another way to solve the same problem is by not decomposing the total velocity potential as the incident wave potential and the diffraction potential. . From now this is refered to as Code - A.

The figure 3.6 provides the plots of the Froude-Krylov roll moment, diffraction roll moment and the exciting roll moment. The results are provided for wave conditions tabulated in table 3.6. We provide in table 3.7, the results from our Numerical program -

Variable	Value
Amplitude(η_I)	0.1m
Wave length(λ)	20m
CFL number	0.28
Δx(Length of panel on free surface)	1m
Δt	0.05

Table 3.6: Wave conditions used for Linear diffraction simulations

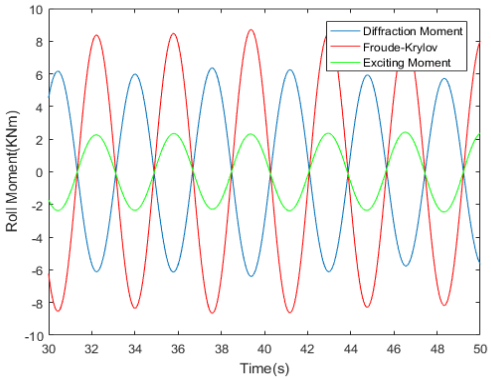

Figure 3.6: Froude-Krylov,Diffraction and Total exciting moment on barge due to an incident wave of amplitude 0.1m and wavelength 20m

A, Numerical program - B and ANSYS AQWA results. Along with them, we also provide results of ANSYS AQWA(L=80m model), but since we use a student license, there is a limitation on the number of panels and thus we used a coarse gird, so the results may not be that accurate. But, the general trend can be seen that if we take more and more longer body, the total exciting force from ANSYS AQWA comes closer and closer. This provides us with enough confidence to proceede further.

Code	Diffrac moment(KNm)	Exciting moment(KNm)
Code - A	-	2.45
Code - B	6.02	2.22
ANSYS AQWA(L=40m)	4.21	3.575
ANSYS AQWA(L=1m)	0.13	8.43
ANSYS AQWA(L=80m)	5.42	3.14

Table 3.7: Comparison of the various programs for the magnitudes of the Diffraction(Diffrac) roll moment and the Total exciting roll moment for waves of amplitude 0.1m and wavelength of 20m

Linear Radiation program results

The dimensions of the domain remain unchanged from the ones used in the linear diffraction problem. We use two techniques for the evaluation of the roll radiation moment as was done in the case of the linear diffraction studies: Backward differences and the implicit tecnhique of Van Daalen[6]. We make the barge, follow sinusoidal motion in roll mode with an amplitude of 0.005rad at natural frequency of roll(0.76rad/s). The amplitude is taken so small, as it has to satisfy the assumptions of linearity. The convergence of the solution with respect to number of panels is shown in Fig 3.7(a).From the figure, 200 panels on the body, seems to be suficient(independent of the technique). The non dimensional differences(eq) in the values are shown in the Fig 3.7(b), along with the number of panels. The difference in the both techniques is small(less than 0.5%).

Again, for the verification of results, we can look into the conservation of volume flux in the computational domain. The volume flux can be estimated through formula given in (3.40).

$$V = \int_{\partial \mathrm{S}} \frac{\partial \phi}{\partial n} \mathrm{dS} \tag{3.40}$$

This should be conserved quantity over a wave period, as can be seen from the fig 3.8(a). As a last step for verification of roll radiation problem, the behavior of the solution with varying roll amplitudes at a particular frequency(roll natural frequency) should be linear, as seen in Fig 3.8(b).

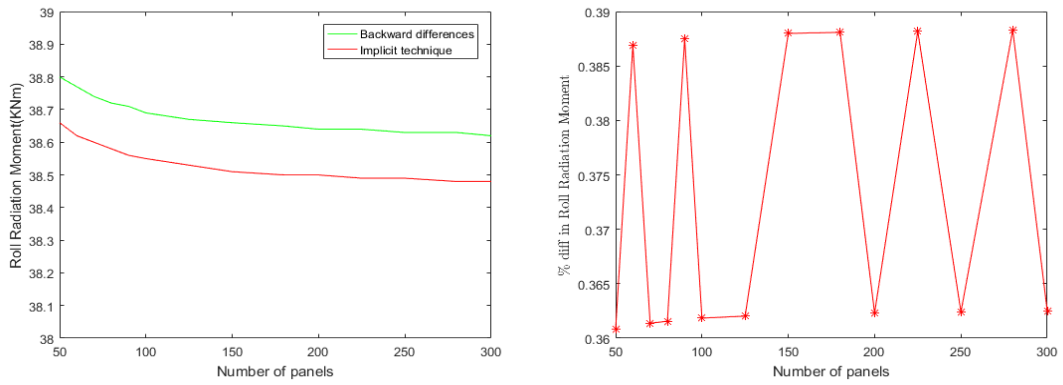

(a) Roll radiation moment convergence with number of panels on the body

(b) Difference in the two techniques for roll radiation moment with respect to the number of panels

Figure 3.7: Roll radiation moment on barge

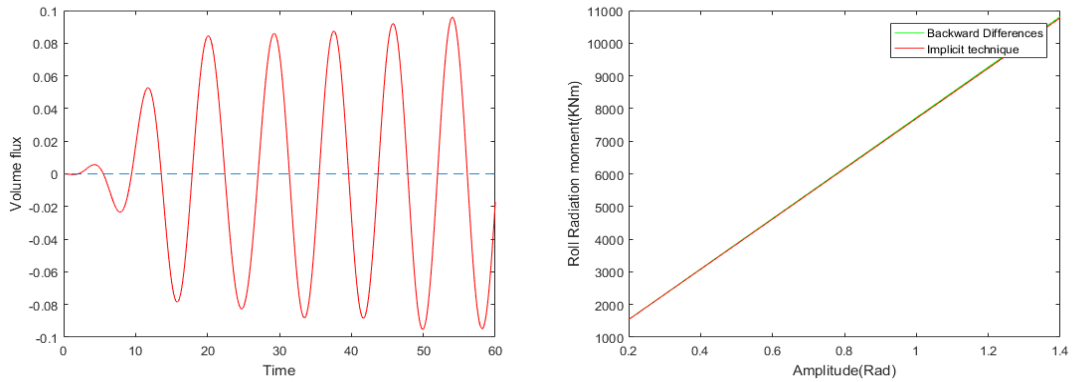

(a) Volume flux in the computational domain(dotted line- mean)

(b) Variation of Roll radiation moment with amplitude of roll motion

Figure 3.8: Verification checks for linear radiation programs

3.3.7 Nonlinear wave-body interactions

In this section, we go about the results of complete nonlinear wave body interaction in the roll mode. We first, develop a pure diffraction program(body fixed), follow it up with the radiation program(body moving), carry out simulations by providing inputs such that we can compare the results with our linear programs.

Nonlinear diffraction program

All the boundary conditions for the velocity potential follow from the theorethical framework for wave-body interactions section and we do not intend to reproduce them for the sake of brievity. We breifly specify the steps that are undertaken at each time step:

1. First, we use constant panel methods to evaluate the velocity potential field. This is required for time stepping the evolution equations on the free surface and lateral boundaries.

2. Using the input from present time step, we set up the boundary value problem for the acceleration potential and evaluate the roll exciting moment associated with it.

3. Step 1-2 repeated until desired.

We choose a wave such that it is in the realms of linear wave theory(small wave steepness) and see the behaviour of the program. The conditions of the wave are: wave height of 0.2m and wavelength of 20m. In fig 3.9, we provide a time series and the frequency plot of the Roll exciting moment. We can interpret much information from the frequency plot of the roll exciting moment. They are three components: a mean component(zero frequency component) and two frequency components(for the irregular waves, we will also have an another component, which equals the difference of frequency between the consituent waves. Since, its periodic we only have sum component): one at the wave frequency and other at twice the wave frequency. The results of the ANSYS AQWA(L=40m), our linear diffraction Numerical code-A(no decomposition of the velocity potential), our linear diffraction Numerical code-B(velocity potential is decomposed into the incident wave and diffraction potential), weak scatterer diffraction code and the complete non linear diffraction code(the amplitude at the wave frequency) are tabulated in table3. 8. As we can see, our nonlinear diffraction moment results match quite well with the linear results and the mean drift moment comes close to the results of ANSYS AQWA(L=40m). On the other hand, the weak scatter diffraction results do not match quite well. The reason being that we do not satisfy the assumptions of the weak scatter theory, i.e. the diffracted wave is not small compared to the incident wave. We also tabulate the results of the nonlinear diffraction moment in Table-3.9 for the wave conditions specified already: wave height of 0.2m and wavelength of 20m. To perform further verification, we

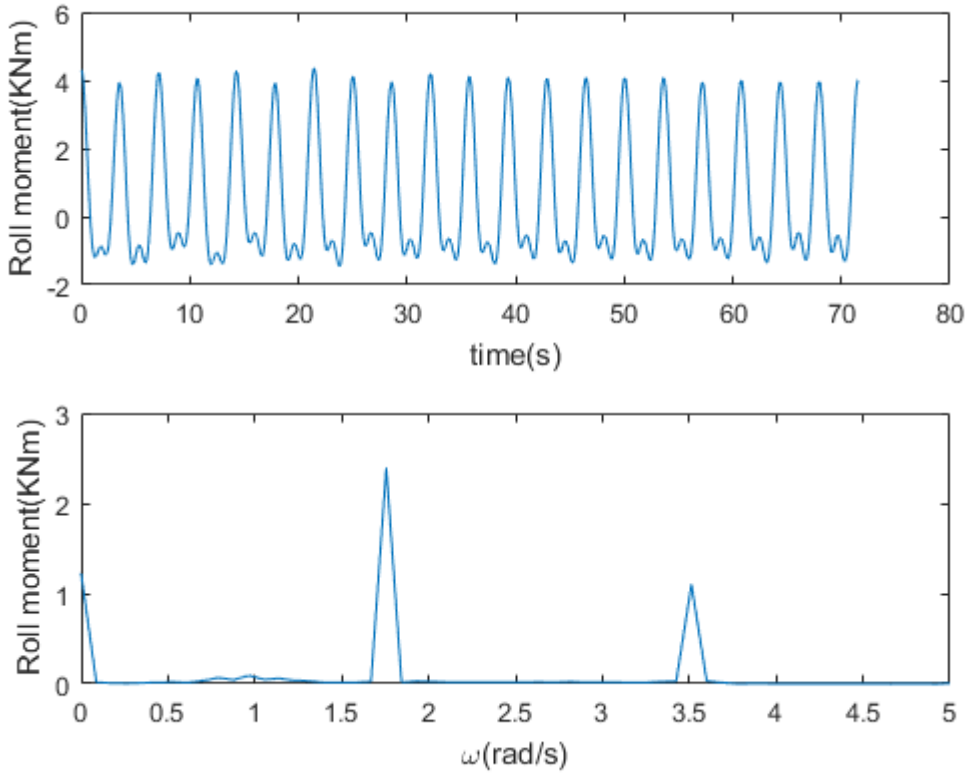

Figure 3.9: (Top): Time series plot of the roll exciting moment and (Bottom): frequency spectrum of the roll exciting moment

Code	Mean moment(KNm)	Amplitude(KNm)
ANSYS AQWA(L=40m)	1.1	3.4
Linear diff code-A	-	2.45
Linear diff code-B	-	2.25
Weak scatt. diff	-	4.6
Nonlin. diff	1.225	2.4

Table 3.8: Comparison of the results from the various numerical code(Mean and the amplitude of the motion at wave frequency

carry out the simulation with twice the wave amplitude and see whether the following occur:

Moment type	Amplitude(KNm)
Mean drift moment	1.225
Linear component	2.4
Sum frequency component	1.104

Table 3.9: Complete output of the nonlinear diffraction program for waves of wavelength 20m and amplitude 0.1m

1. The moment at the wave frequency should behave linearly with the wave amplitude. Offcourse, we cannot expect the exact linear trend in a nonlinear numerical code, due to the inherent simple first order time stepping techniques, but we expect the result to be quite close to linear trend.

2. The steady drift moment(zero frequency component) and the sum frequency component(component at double the wave frequency) of the moment should behave quadratically with the wave amplitude.

These points are well explained in chapter 9 of the course textbook of offshore hydromechanics[28] at TU Delft. So, we double the wave amplitude from 0.1m to 0.2m and carry out simulations with the wavelength being 20m. The time traces along with its frequency content is depicted in 3.10. We have presented the frequency component of two simulations in table 3.10, the second one having twice the steepness of the first one and we can see the expected behaviour.

Steepness	Mean(KNm)	Linear(KNm)	Sum comp.(KNm)
0.01	1.225	2.4	1.104
0.02	5	4.6	4.051

Table 3.10: Verification of nonlinear diffraction program

We obtain the numerical order of convergence of the nonlinear diffraction program by carrying out the procedure as explained by L.Eca and M.Hoekstra[29]. Since, we use the first order time stepping techniques and first order upwind schemes for spatial gradients, we expect the order of convergence of the method to be 1. This is precisely the order of convergence we obtain after we employ technqiue of Eca and Hoekstra[29] for the linear component of the moment(the contribution to the total moment at wave

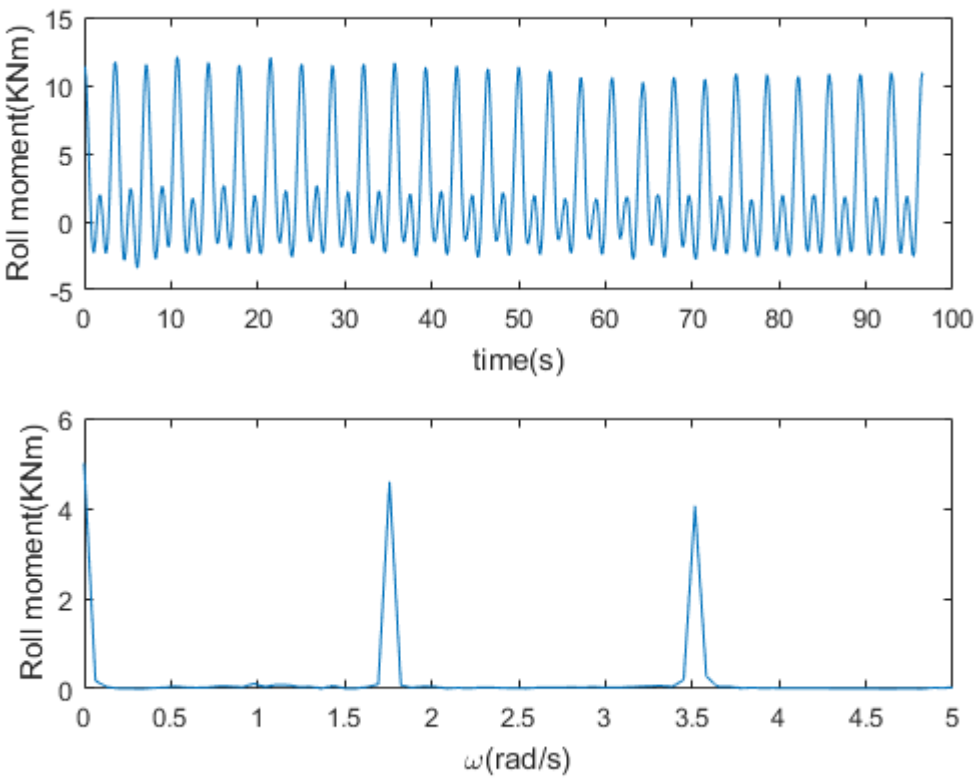

Figure 3.10: (Top): Time series plot of the roll exciting moment and (Bottom): frequency spectrum of the roll exciting moment

frequency). The log-log plot of the discretization error(the difference between the exact solution and numerical solution) with the mesh size is provided in Fig 3.11.

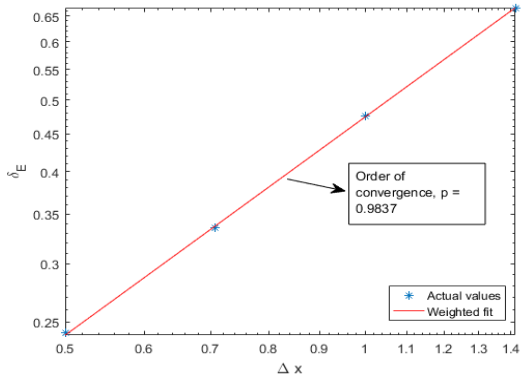

Figure 3.11: Log-log plot of the discretization error with the mesh size

With this confidence, we start to look into the next step: development of Nonlinear radiation program.

Nonlinear radiation program

We do not intend to reproduce the boundary conditions for a nonlinear radiation program. They have already been described. We will through a light on the brief steps to be followed and the way we find the intersection point. The brief steps that are undertaken for a time step:

1. We use Constant Panel Method(CPM) to estimate the velocity field(we mean the potential and its gradients). This is required for time stepping the evolution equations on the free surface and the lateral boundaries.

2. Using the input from the present step, we set up the boundary value problem for the acceleration potential and evaluate the roll moment associated with it.

3. Remesh all the surfaces after finding the intersection points of the body and the free surface.

4. Repeat steps 1-3 until required.

Before we provide the results from the nonlinear radiation program, we would like to discuss how we find the intersection point between the free surface and the body. Let us focus on finding the instersection point on the left hand side of the body(the technique is the same for the other side of the body). We first fit a cubic smoothing spline for

the free surface elevation and extend the spline representation(extend it for a meter into the body). We can get the equation that represents the cubic spline at the corner most panel(point closest to the body), call this as 1. We have simple body(a rectangle barge) whose sides give an linear equation, call this 2. We find the intersection between 1 and 2. Since 1 is cubic, we get three roots, then to find unique value of X intersection, we look for the root that satisfies that the condition that its between particular values(these particular values are the maximum values that the body can take for maximum roll angle amplitude specified). Once, we have this unique X-intersection, we substitute this value in the cubic spline representation of the free surface to find the Y-intersection. The only problem with this technique is that at crests and troughs of the wave, the extended extrapolation is not quite accurate.

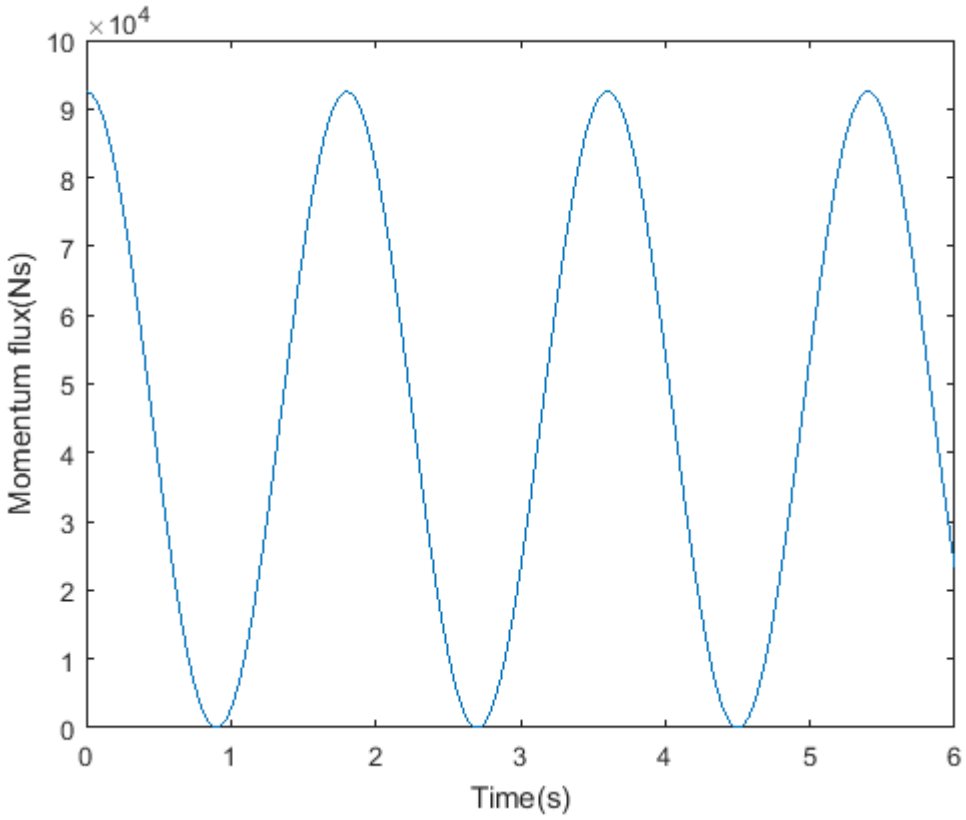

Figure 3.12: Conservation of momentum flux across the domain

Instead of presenting the results of the nonlinear radiation program here, we present them later along with the results of the Fluid Impulse Theory(derived later). Here, we

provide the plot of the momentum flux(Fig 3.12), which is conserved. This suggests as a verification for the program.

3.4 Fluid Impulse Theory

We have seen that in all the cases so far, be it linear or nonlinear code, we had to solve two boundary values at each time step: one for the velocity potential and other for its temporal gradient. This is computationally intensive. Recently, in 2012, P.D.Sclavounos[10] had used the conservation of fluid momentum principle to estimate the nonlinear loads on the structure. He evaluated the loads directly, without estimating the pressure, thus circumventing the partial time gradients of the potential. The idea of using conservation of fluid momentum to estimate the nonlinear loads on structure is esentially not new in the field of fluid dynamics, but this has not been much used in the field of ship hydrodynamics. We re-derive the expressions following along the lines of P.D.Sclavounos[10] and end up getting similar expressions. He assumes that the disturbance potential(potential generated due to the presence of body) and the ambient wave potential(incident wave potential) decay far away from the body and thus, the control surfaces at infinity are not considered in his derivation. He states that the ambient wave potential decay is similar to the calm sea condition outside the fetch zone and the decay of the disturbance potential is due to its dipole like behaviour far away from the body. But since we are dealing with two dimensional fliows, we expect that this dipole like decay is not possible. Since, in two dimensional flows, there is no directional dispersion or directional spreading of the energy, the nonlinearities extend to infinity. Thus, the control surfaces at infinty(lateral boundaries) should have contribution and we had to re-derive.

Denoting V(t) as the volume bounded by the computational domain(refer Fig 3.13), whose boundaries are given by S(t) which include the lateral boundaries(upstream(S_{UP}) and downstream(S_{DS})), Free surface(left hand side(S_{FL}) and right hand side(S_{FR}) of the body), the body(S_B) and the bottom(S_{BO}). We do not specify any boundary conditions in the begining and go about with no assumptions, until stated. By virtue of Reynold Transport Theorem, we have 3.41, where U stands for the velocity of the bounding surfaces for the control volume.

$$\frac{\mathrm{D}}{\mathrm{Dt}} \int_{V(t)} \nabla\phi \mathrm{dv} = \int_{V(t)} \frac{\partial \nabla\phi}{\partial t} \mathrm{dv} + \int_{S(t)} \nabla\phi (U \cdot \hat{n}) \mathrm{ds} \tag{3.41}$$

Applying the Gauss theorem on the left hand side and the on the first term after swaping

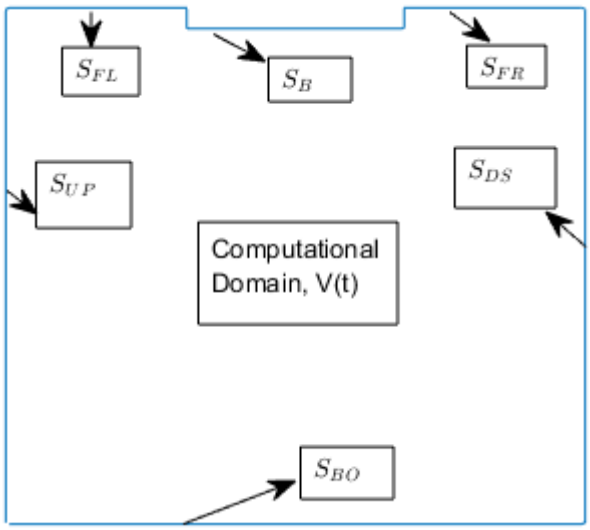

Figure 3.13: Computational Volume along with various surfaces

the time derivative with the gradient of the potential, we have:

$$\frac{\mathrm{D}}{\mathrm{Dt}}\int_{S(t)}\phi\hat{n}\mathrm{ds}=\int_{S(t)}\Big[\frac{\partial\phi}{\partial t}\hat{n}+\nabla\phi(U\cdot\hat{n})\Big]\mathrm{ds} \tag{3.42}$$

We use Eulerian representation of the free surface(that is the points are only allowed to move in Y-direction and frozen from the X- motion). The consequence of the representation is that the normal velocity of the free surface(in our representation) is not equal to the normal gradient of the velocity potential on the free surface. Also, at the upstream and downstream boundaries, the normal velocity of these surfaces is not equal to the normal gradient of the potential. So, again let us add and substract the term $\int_{S_{FSL}}\nabla\phi\frac{\partial\phi}{\partial n}\mathrm{ds}, \int_{S_{FSR}}\nabla\phi\frac{\partial\phi}{\partial n}\mathrm{ds}, \int_{S_{UP}}\nabla\phi\frac{\partial\phi}{\partial n}\mathrm{ds}, \int_{S_{DS}}\nabla\phi\frac{\partial\phi}{\partial n}\mathrm{ds}$ to the derivation(3.39) and assume that the velocity of the free surface is U for the time being(later we replace by vertical gradient of the potential). The upstream and downstream boundaries are fixed, so the velocity of these surfaces is zero(3.44).

$$\begin{aligned}\frac{\mathrm{D}}{\mathrm{Dt}}\int_{S(t)}\phi\hat{n}\mathrm{ds}&=\int_{S(t)}\Big[(\frac{\partial\phi}{\partial t}\hat{n}+\nabla\phi\frac{\partial\phi}{\partial n})\Big]\mathrm{ds}-\int_{S_{UP}}\nabla\phi\frac{\partial\phi}{\partial n}\mathrm{ds}-\int_{S_{DS}}\nabla\phi\frac{\partial\phi}{\partial n}\mathrm{ds}\\&-\int_{S_{FSL}}\nabla\phi\frac{\partial\phi}{\partial n}\mathrm{ds}-\int_{S_{FSR}}\nabla\phi\frac{\partial\phi}{\partial n}\mathrm{ds}+\int_{S_{FSL}}\nabla\phi(U\cdot\hat{n})\mathrm{ds}+\int_{S_{FSR}}\nabla\phi(U\cdot\hat{n})\mathrm{ds}\end{aligned} \tag{3.43}$$

$$U=\begin{cases}0 & \text{on Upstream and downstream boundaries}\\ \frac{\partial\phi}{\partial y} & \text{on Free surface}\end{cases} \tag{3.44}$$

Let us deal with the whole derivation, by assuming that the first two terms of the right hand side of (3.43) are present (3.45) and latter lets add the rest.

$$\frac{\mathrm{D}}{\mathrm{Dt}}\int_{S(t)}\phi\hat{n}\mathrm{ds} = \int_{S(t)}\Big[\frac{\partial\phi}{\partial t}+\nabla\phi\frac{\partial\phi}{\partial n}\Big]\mathrm{ds} \tag{3.45}$$

Re-arranging(3.45) will lead to (3.46)

$$\int_{S(t)}\frac{\partial\phi}{\partial t}\hat{n}\mathrm{ds} = \frac{\mathrm{D}}{\mathrm{Dt}}\int_{S(t)}\phi\hat{n}\mathrm{ds} - \int_{S(t)}\nabla\phi\frac{\partial\phi}{\partial n}\mathrm{ds} \tag{3.46}$$

Now adding $\int_{S(t)}\frac{1}{2}\nabla\phi\cdot\nabla\phi\hat{n}\mathrm{ds}$ and $\int_{S(t)}gZ\hat{n}\mathrm{ds}$ on to both sides of the expression above leads to (3.47).

$$\int_{S(t)}\Big[\frac{\partial\phi}{\partial t}+\frac{1}{2}\nabla\phi\cdot\nabla\phi+gZ\Big]\hat{n}\mathrm{ds} = \frac{\mathrm{D}}{\mathrm{Dt}}\int_{S(t)}\phi\hat{n}\mathrm{ds}-\int_{S(t)}\Big[\nabla\phi\frac{\partial\phi}{\partial n}-\frac{1}{2}\nabla\phi\cdot\nabla\phi\hat{n}\Big]\mathrm{ds}+\int_{S(t)}gZ\hat{n}\mathrm{ds} \tag{3.47}$$

For any closed volume, the following identity holds(refer to the Appendix for the proof):

$$\int_{S(t)}\Big[\nabla\phi\frac{\partial\phi}{\partial n}-\frac{1}{2}\nabla\phi\cdot\nabla\phi\hat{n}\Big]\mathrm{ds} = 0 \tag{3.48}$$

Substituting (3.48) into (3.47) leads to simpler expression(3.49).

$$\int_{S(t)}\Big[\frac{\partial\phi}{\partial t}+\frac{1}{2}\nabla\phi\cdot\nabla\phi+gZ\Big]\hat{n}\mathrm{ds} = \frac{\mathrm{D}}{\mathrm{Dt}}\int_{S(t)}\phi\hat{n}\mathrm{ds}+\int_{S(t)}gZ\hat{n}\mathrm{ds} \tag{3.49}$$

We want to be more specific about the details, so we deal with the left hand side and right hand side of the expression independently. We first go about with the left hand side of the expression. If we break the expression into the integrals over the surface, we see that we are simply left with expressions of the pressure(factor of density missing). This was initially the reason of adding terms(in eq 3.47) on the both sides of the equation. We recollect that the pressure on the free surface should be identically zero(Free Surface Dynamic Boundary Condition). Representing the integral of pressure over the wetted surface of the body as negative of the force exerted on the body(F_B), we finally end up

with:

$$\int_{S(t)}\Big[\frac{\partial\phi}{\partial t}+\frac{1}{2}\nabla\phi\cdot\nabla\phi+gZ\Big]\hat{n}\mathrm{ds}=\int_{S_{UP}}\Big[\frac{\partial\phi}{\partial t}+\frac{1}{2}\nabla\phi\cdot\nabla\phi+gZ\Big]\hat{n}\mathrm{ds}+\int_{S_{FL}}\Big[\frac{\partial\phi}{\partial t}+\frac{1}{2}\nabla\phi\cdot\nabla\phi+gZ\Big]\hat{n}\mathrm{ds}+\int_{S_B}\Big[\frac{\partial\phi}{\partial t}+\frac{1}{2}\nabla\phi\cdot\nabla\phi+gZ\Big]\hat{n}\mathrm{ds}$$
$$+\int_{S_{FR}}\Big[\frac{\partial\phi}{\partial t}+\frac{1}{2}\nabla\phi\cdot\nabla\phi+gZ\Big]\hat{n}\mathrm{ds}+\int_{S_{DS}}\Big[\frac{\partial\phi}{\partial t}+\frac{1}{2}\nabla\phi\cdot\nabla\phi+gZ\Big]\hat{n}\mathrm{ds}+\int_{S_{BO}}\Big[\frac{\partial\phi}{\partial t}+\frac{1}{2}\nabla\phi\cdot\nabla\phi+gZ\Big]\hat{n}\mathrm{ds}$$
$$=\int_{S_{UP}}\Big[\frac{\partial\phi}{\partial t}+\frac{1}{2}\nabla\phi\cdot\nabla\phi+gZ\Big]\hat{n}\mathrm{ds}+\int_{S_B}\Big[\frac{\partial\phi}{\partial t}+\frac{1}{2}\nabla\phi\cdot\nabla\phi+gZ\Big]\hat{n}\mathrm{ds}$$
$$+\int_{S_{DS}}\Big[\frac{\partial\phi}{\partial t}+\frac{1}{2}\nabla\phi\cdot\nabla\phi+gZ\Big]\hat{n}\mathrm{ds}+\int_{S_{BO}}\Big[\frac{\partial\phi}{\partial t}+\frac{1}{2}\nabla\phi\cdot\nabla\phi+gZ\Big]\hat{n}\mathrm{ds}=\int_{S_{UP}+S_{DS}+S_{BO}}\frac{p}{\rho}\hat{n}\mathrm{ds}-\frac{F_B}{\rho} \tag{3.50}$$

The left hand side of (3.49) simplifies to (3.51).

$$\int_{S(t)}\Big[\frac{\partial\phi}{\partial t}+\frac{1}{2}\nabla\phi\cdot\nabla\phi+gZ\Big]\hat{n}\mathrm{ds}=\int_{S_{UP}}\frac{p}{\rho}\hat{n}\mathrm{ds}+\int_{S_{DS}}\frac{p}{\rho}\hat{n}\mathrm{ds}+\int_{S_{BO}}\frac{p}{\rho}\hat{n}\mathrm{ds}-\frac{F_B}{\rho} \tag{3.51}$$

Substituting (3.51) into (3.49), re-arranging the terms and adding the terms that were skipped in (3.45) leads to the (3.52).

$$F_B=\int_{S_{UP}}p\hat{n}\mathrm{ds}+\int_{S_{DS}}p\hat{n}\mathrm{ds}+\int_{S_{BO}}p\hat{n}\mathrm{ds}-\rho\frac{\mathrm{D}}{\mathrm{Dt}}\int_{S(t)}\phi\hat{n}\mathrm{ds}-\rho\int_{S(t)}gZ\hat{n}\mathrm{ds}$$
$$-\rho\int_{S_{UP}}\nabla\phi\frac{\partial\phi}{\partial n}\mathrm{ds}-\rho\int_{S_{DS}}\nabla\phi\frac{\partial\phi}{\partial n}\mathrm{ds}-\rho\int_{S_{FSL}}\nabla\phi\frac{\partial\phi}{\partial n}\mathrm{ds}-\rho\int_{S_{FSR}}\nabla\phi\frac{\partial\phi}{\partial n}\mathrm{ds}$$
$$+\rho\int_{S_{FSL}}\nabla\phi(U\cdot\hat{n})\mathrm{ds}+\rho\int_{S_{FSR}}\nabla\phi(U\cdot\hat{n})\mathrm{ds} \tag{3.52}$$

This(3.52) is the final expression for the nonlinear load on the structure. But, this still needs some refinements, so that we can apply it to our problem at hand. Before, we see, how the expression shapes out for our computational domain, we would like to see, how the expression will be in the linear problem. We proove that the expression for the force is the same as that of Direct Pressure Integration in the linear case. Since, we assume linear, all the terms involving the product of the gradient of the potential and the normal gradient of the potential can be neglected(third, fourth, fifth, sixth). In the linear setting the velocity(U) of the free surface is supposed to be zero. Then, we expand the pressure term on the right hand side(3.53).

$$F_B=\rho\int_{S_{UP}+S_{DS}+S_{BO}}\Big[\frac{\partial\phi}{\partial t}+\frac{1}{2}\nabla\phi\cdot\nabla\phi+gZ\Big]\hat{n}\mathrm{ds}-\rho\frac{\mathrm{D}}{\mathrm{Dt}}\int_{S(t)}\phi\hat{n}\mathrm{ds}-\rho\int_{S(t)}gZ\hat{n}\mathrm{ds} \tag{3.53}$$

Since, we assume linear, the quadratic term of the pressure should be small and is neglected. We can cancel few terms form the hydrostatic components of the pressure. This will lead to an expression for the linear force(F_{BL}) on the body(3.54).

$$F_{BL} = \rho \int_{S_{UP}} \frac{\partial \phi}{\partial t} \hat{n} \mathrm{ds} + \rho \int_{S_{DS}} \frac{\partial \phi}{\partial t} \hat{n} \mathrm{ds} + \rho \int_{S_{BO}} \frac{\partial \phi}{\partial t} \hat{n} \mathrm{ds} - \rho \frac{\mathrm{D}}{\mathrm{Dt}} \int_{S(t)} \phi \hat{n} \mathrm{ds} - \rho \int_{S_B} gZ \hat{n} \mathrm{ds} - \rho \int_{S_{FSL}} gZ \hat{n} \mathrm{ds} - \rho \int_{S_{FSR}} gZ \hat{n} \mathrm{ds} \quad (3.54)$$

We can further simplify (3.54). Since, we assume linear, the time derivative which is outside the integral can be pushed inside(more strictly speaking, we can use the fundamental theorem of calculus: Leibnitz theorem, noting that limits are not a function of time, will lead to time derivative inside the integral). Since, the problem is solved linearly, the normal is time-independent and can be pushed out of derivative(refer eq 3.55)

$$\rho \frac{\mathrm{D}}{\mathrm{Dt}} \int_{S(t)} \phi \hat{n} \mathrm{ds} = \rho \int_{S(t)} \frac{\partial}{\partial t} (\phi \hat{n}) \mathrm{ds} = \rho \int_{S(t)} \frac{\partial \phi}{\partial t} \hat{n} \mathrm{ds} \quad (3.55)$$

Substituting this back and cancelling the common terms out from $S(t)$, leads to (3.56).

$$F_{BL} = -\rho \int_{S_{FSL}} \frac{\partial \phi}{\partial t} \hat{n} \mathrm{ds} - \rho \int_{S_B} \frac{\partial \phi}{\partial t} \hat{n} \mathrm{ds} - \rho \int_{S_{FSR}} \frac{\partial \phi}{\partial t} \hat{n} \mathrm{ds} - \rho \int_{S_B} gZ \hat{n} \mathrm{ds} - \rho \int_{S_{FSL}} gZ \hat{n} \mathrm{ds} - \rho \int_{S_{FSR}} gZ \hat{n} \mathrm{ds} \quad (3.56)$$

Lets us combine the terms with respect to the free surface and body seperately(3.57).

$$F_{BL} = -\rho \int_{S_{FL}+S_{FR}} \Big[\frac{\partial \phi}{\partial t} + gZ \Big] \hat{n} \mathrm{ds} - \rho \int_{S_B} \Big[\frac{\partial \phi}{\partial t} + gZ \Big] \hat{n} \mathrm{ds} \quad (3.57)$$

We, see that, we end up with the linearized pressure on the free surface. If we recollect the linearized dynamic free surface boundary condition, the linearized pressure on the free surface is identically zero. This simplifies (3.57) to (3.58).

$$F_{BL} = -\rho \int_{S_B} \Big[\frac{\partial \phi}{\partial t} + gZ \Big] \hat{n} \mathrm{ds} \quad (3.58)$$

Since, we are only looking for the hydrodynamic force(be it radiation or the excitation force), we neglect hydrostatic component and represent the linearized hydrodynamic force by $(F_{BL})^{HD}$ in (3.59).

$$(F_{BL})^{HD} = -\rho \int_{S_B} \frac{\partial \phi}{\partial t} \hat{n} \mathrm{ds} \quad (3.59)$$

If we look at the expression carefully, we have an expression which is identical to the Direct Pressure Integration. This ends our proof of similarity between the Fluid Impulse

Boundary	n_x	n_y	$\frac{\partial\phi}{\partial x}$	$\frac{\partial\phi}{\partial y}$
Upstream	-1	0	$-\frac{\partial\phi}{\partial n}$	$\frac{\partial\phi}{\partial y}$
Free surface left	n_x	n_y	$\frac{\partial\phi}{\partial x}$	$\frac{\partial\phi}{\partial y}$
Body	n_x	n_y	$\frac{\partial\phi}{\partial x}$	$\frac{\partial\phi}{\partial y}$
Free surface right	n_x	n_y	$\frac{\partial\phi}{\partial x}$	$\frac{\partial\phi}{\partial y}$
Dowsntream	1	0	$\frac{\partial\phi}{\partial n}$	$\frac{\partial\phi}{\partial y}$
Bottom	0	-1	$\frac{\partial\phi}{\partial x}$	0

Table 3.11: Boundaries of the domain along with the values: X-component of the normal(n_x), Y component of normal(n_y), and partial gradients of the potential

Theory(FIT) and the Direct Pressure Integration(DPI) in the linear setting. It would be quite handy, if we could proove it analytically in the nonlinear setting. But, this seems impossible. Instead, in the case of nonlinear simulations, we are going to proove that the Fluid Impulse Theory(FIT) and the Direct Pressure Integration(DPI) are similar using numerical simulations. So, we need to simplify the complete nonlinear expression(3.52), such that we can use it in our code.We expand the pressure in (3.52) and cancel out the common hydrostatic constributions, which simplifies(3.48) to (3.60).

$$\begin{aligned} F_B = \rho \int_{S_{UP}} \Big[\frac{\partial\phi}{\partial t} + \frac{1}{2}\nabla\phi\cdot\nabla\phi\Big]\hat{n}\mathrm{ds} + \rho\int_{S_{DS}} \Big[\frac{\partial\phi}{\partial t} + \frac{1}{2}\nabla\phi\cdot\nabla\phi\Big]\hat{n}\mathrm{ds} \\ + \rho\int_{S_{BO}} \Big[\frac{\partial\phi}{\partial t} + \frac{1}{2}\nabla\phi\cdot\nabla\phi\Big]\hat{n}\mathrm{ds} - \rho\frac{\mathrm{D}}{\mathrm{Dt}}\int_{S(t)}\phi\hat{n}\mathrm{ds} - \rho\int_{S_B} gZ\hat{n}\mathrm{ds} \\ - \rho\int_{S_{FSL}} gZ\hat{n}\mathrm{ds} - \rho\int_{S_{FSR}} gZ\hat{n}\mathrm{ds} \end{aligned} \quad (3.60)$$

Neglecting the hydrostatic component, representing the hydrodynamic force by $(F_B)^{HD}$, we get (3.61) from (3.60).

$$\begin{aligned} (F_B)^{HD} = \rho \int_{S_{UP}} \Big[\frac{\partial\phi}{\partial t} + \frac{1}{2}\nabla\phi\cdot\nabla\phi\Big]\hat{n}\mathrm{ds} + \rho\int_{S_{DS}} \Big[\frac{\partial\phi}{\partial t} + \frac{1}{2}\nabla\phi\cdot\nabla\phi\Big]\hat{n}\mathrm{ds} \\ + \rho\int_{S_{BO}} \Big[\frac{\partial\phi}{\partial t} + \frac{1}{2}\nabla\phi\cdot\nabla\phi\Big]\hat{n}\mathrm{ds} - \rho\frac{\mathrm{D}}{\mathrm{Dt}}\int_{S(t)}\phi\hat{n}\mathrm{ds} - \rho\int_{S_{FSL}} gZ\hat{n}\mathrm{ds} - \rho\int_{S_{FSR}} gZ\hat{n}\mathrm{ds} \end{aligned} \quad (3.61)$$

Now, we make a table - 3.11 which provides the values of various quantities on the boundaries, which are substituted into the expression that simplifies (3.61) to (3.62).

$$(F_B)^{HD} = \rho \int_{S_{UP}} \Big[\frac{\partial \phi}{\partial t} + \frac{1}{2}((\frac{\partial \phi}{\partial n})^2 + (\frac{\partial \phi}{\partial y})^2)\Big]\hat{n}\mathrm{ds} + \rho \int_{S_{DS}} \Big[\frac{\partial \phi}{\partial t} + \frac{1}{2}((\frac{\partial \phi}{\partial n})^2 + (\frac{\partial \phi}{\partial y})^2)\Big]\hat{n}\mathrm{ds} + \rho \int_{S_{BO}} \Big[\frac{\partial \phi}{\partial t} + \frac{1}{2}((\frac{\partial \phi}{\partial n})^2 + (\frac{\partial \phi}{\partial x})^2)\Big]\hat{n}\mathrm{ds} - \rho \int_{S(t)} \phi \hat{n}\mathrm{ds} - \rho \int_{S_{FSL}} gZ\hat{n}\mathrm{ds} - \rho \int_{S_{FSR}} gZ\hat{n}\mathrm{ds} \tag{3.62}$$

Since, we are interested in the roll moment, we have to introduce the generalized normal by a cross product of position vector(defined from the co-ordinate system placed on the centerline of the mean position of the body and on the free surface) and the components of the normals. The final expression for the nonlinear hydrodynamic roll moment on the body is obtained after the substituting for the generalized normals and some trivial mathemathics(3.63).

$$\begin{aligned}(F_B)^{HD} = {} & \rho \int_{S_{UP}} \Big[\frac{\partial \phi}{\partial t} + \frac{1}{2}((\frac{\partial \phi}{\partial n})^2 + (\frac{\partial \phi}{\partial y})^2)\Big] y\mathrm{ds} - \\ & \rho \int_{S_{DS}} \Big[\frac{\partial \phi}{\partial t} + \frac{1}{2}((\frac{\partial \phi}{\partial n})^2 + (\frac{\partial \phi}{\partial y})^2)\Big] y\mathrm{ds} - \rho \int_{S_{BO}} \Big[\frac{\partial \phi}{\partial t} + \frac{1}{2}(\frac{\partial \phi}{\partial y})^2\Big](x - x_G)\mathrm{ds} \\ & - \rho \frac{\mathrm{D}}{\mathrm{Dt}} \int_{S_{UP}} \phi y\mathrm{ds} + \rho \frac{\mathrm{D}}{\mathrm{Dt}} \int_{S_{DS}} \phi y\mathrm{ds} - \rho \frac{\mathrm{D}}{\mathrm{Dt}} \int_{S_{FSL}} \phi\Big[(x - x_G)n_y - yn_x\Big]\mathrm{ds} \\ & - \rho \frac{\mathrm{D}}{\mathrm{Dt}} \int_{S_B} \phi\Big[(x - x_G)n_y - yn_x\Big]\mathrm{ds} + \rho \frac{\mathrm{D}}{\mathrm{Dt}} \int_{S_{BO}} \phi(x - x_G)\mathrm{ds} - \rho \frac{\mathrm{D}}{\mathrm{Dt}} \int_{S_{FSR}} \phi\Big[(x - x_G)n_y - yn_x\Big]\mathrm{ds} \\ & - \rho \int_{S_{FL}} gZ\Big[(x - x_G)n_y - yn_x\Big]\mathrm{ds} - \rho \int_{S_{FSR}} gZ\Big[(x - x_G)n_y - yn_x\Big]\mathrm{ds}\end{aligned} \tag{3.63}$$

The last term of the expression can be replaced by the terms consisting of the potential on the free surface by using the dynamic free surface boundary condition. This is done as the numerical scheme employed is semi-implicit when it comes to evaluating the potential on the free surface and thus accurate than using the free surface elevation. So, now the

final expression is depicted in (3.64).

$$
\begin{aligned}
(F_B)^{HD} = \rho \int_{S_{UP}} \Big[\frac{\partial \phi}{\partial t} + \frac{1}{2}((\frac{\partial \phi}{\partial n})^2 + (\frac{\partial \phi}{\partial y})^2)\Big] y \mathrm{ds} - \\
\rho \int_{S_{DS}} \Big[\frac{\partial \phi}{\partial t} + \frac{1}{2}((\frac{\partial \phi}{\partial n})^2 + (\frac{\partial \phi}{\partial y})^2)\Big] y \mathrm{ds} - \rho \int_{S_{BO}} \Big[\frac{\partial \phi}{\partial t} + \frac{1}{2}(\frac{\partial \phi}{\partial y})^2\Big](x - x_G)\mathrm{ds} \\
- \rho \frac{\mathrm{D}}{\mathrm{Dt}} \int_{S_{UP}} \phi y \mathrm{ds} + \rho \frac{\mathrm{D}}{\mathrm{Dt}} \int_{S_{DS}} \phi y \mathrm{ds} - \rho \frac{\mathrm{D}}{\mathrm{Dt}} \int_{S_{FSL}} \phi \Big[(x - x_G)n_y - y n_x\Big] \mathrm{ds} \\
-\rho \frac{\mathrm{D}}{\mathrm{Dt}} \int_{S_B} \phi \Big[(x - x_G)n_y - y n_x\Big] \mathrm{ds} + \rho \frac{\mathrm{D}}{\mathrm{Dt}} \int_{S_{BO}} \phi (x - x_G) \mathrm{ds} - \rho \frac{\mathrm{D}}{\mathrm{Dt}} \int_{S_{FSR}} \phi \Big[(x - x_G)n_y - y n_x\Big] \mathrm{ds} \\
+\rho \int_{S_{FSL}} (\frac{\partial \phi}{\partial t} + \frac{1}{2}\nabla\phi \cdot \nabla\phi) \Big[(x - x_G)n_y - y n_x\Big] \mathrm{ds} + \rho \int_{S_{FSR}} (\frac{\partial \phi}{\partial t} + \frac{1}{2}\nabla\phi \cdot \nabla\phi) \Big[(x - x_G)n_y - y n_x\Big] \mathrm{ds}
\end{aligned}
\tag{3.64}
$$

Now let us add back the terms left out in eq (3.45) back to (3.64) and get (3.65).

$$
\begin{aligned}
(F_B)^{HD} = \rho \int_{S_{UP}} \Big[\frac{\partial \phi}{\partial t} + \frac{1}{2}((\frac{\partial \phi}{\partial n})^2 + (\frac{\partial \phi}{\partial y})^2)\Big] y \mathrm{ds} - \\
\rho \int_{S_{DS}} \Big[\frac{\partial \phi}{\partial t} + \frac{1}{2}((\frac{\partial \phi}{\partial n})^2 + (\frac{\partial \phi}{\partial y})^2)\Big] y \mathrm{ds} - \rho \int_{S_{BO}} \Big[\frac{\partial \phi}{\partial t} + \frac{1}{2}(\frac{\partial \phi}{\partial y})^2\Big](x - x_G)\mathrm{ds} \\
- \rho \frac{\mathrm{D}}{\mathrm{Dt}} \int_{S_{UP}} \phi y \mathrm{ds} + \rho \frac{\mathrm{D}}{\mathrm{Dt}} \int_{S_{DS}} \phi y \mathrm{ds} - \rho \frac{\mathrm{D}}{\mathrm{Dt}} \int_{S_{FSL}} \phi \Big[(x - x_G)n_y - y n_x\Big] \mathrm{ds} \\
-\rho \frac{\mathrm{D}}{\mathrm{Dt}} \int_{S_B} \phi \Big[(x - x_G)n_y - y n_x\Big] \mathrm{ds} + \rho \frac{\mathrm{D}}{\mathrm{Dt}} \int_{S_{BO}} \phi (x - x_G) \mathrm{ds} - \rho \frac{\mathrm{D}}{\mathrm{Dt}} \int_{S_{FSR}} \phi \Big[(x - x_G)n_y - y n_x\Big] \mathrm{ds} \\
+\rho \int_{S_{FSL}} (\frac{\partial \phi}{\partial t} + \frac{1}{2}\nabla\phi \cdot \nabla\phi) \Big[(x - x_G)n_y - y n_x\Big] \mathrm{ds} + \rho \int_{S_{FSR}} (\frac{\partial \phi}{\partial t} + \frac{1}{2}\nabla\phi \cdot \nabla\phi) \Big[(x - x_G)n_y - y n_x\Big] \mathrm{ds} \\
- \rho \int_{S_{UP}} \nabla\phi \frac{\partial \phi}{\partial n} \mathrm{ds} - \rho \int_{S_{DS}} \nabla\phi \frac{\partial \phi}{\partial n} \mathrm{ds} - \rho \int_{S_{FSL}} \nabla\phi \frac{\partial \phi}{\partial n} \mathrm{ds} - \rho \int_{S_{FSR}} \nabla\phi \frac{\partial \phi}{\partial n} \mathrm{ds} \\
+ \rho \int_{S_{FSL}} \nabla\phi (U \cdot \hat{n}) \mathrm{ds} + \rho \int_{S_{FSR}} \nabla\phi (U \cdot \hat{n}) \mathrm{ds}
\end{aligned}
\tag{3.65}
$$

Let us have look at the last term of (3.65) seperately and re-arrange it(3.66).

$$
\nabla\phi (U \cdot \hat{n}) \mathrm{ds} = U \times (\nabla\phi \times r \times \hat{n}) + (r \times \hat{n}) \nabla\phi \cdot U \tag{3.66}
$$

The first term(right hand side) of (3.66) will be zero because the flow is irrotational($\nabla\phi \times r = -r \times \nabla\phi = 0$) and this eventually leads to (3.67).

$$
\nabla\phi (U \cdot \hat{n}) \mathrm{ds} = (r \times \hat{n}) \nabla\phi \cdot U \tag{3.67}
$$

Substitute back in (3.63) and use the velocity of the free surface(3.44) as vertical gradient of the velocity potential leads to the final expression for the hydrodynamic roll moment

on the body(3.68).

$$
\begin{aligned}
(F_B)^{HD} = \rho \int_{S_{UP}} \Big[\frac{\partial \phi}{\partial t} + \frac{1}{2}((\frac{\partial \phi}{\partial n})^2 + (\frac{\partial \phi}{\partial y})^2)\Big] y \mathrm{ds} - \\
\rho \int_{S_{DS}} \Big[\frac{\partial \phi}{\partial t} + \frac{1}{2}((\frac{\partial \phi}{\partial n})^2 + (\frac{\partial \phi}{\partial y})^2)\Big] y \mathrm{ds} - \rho \int_{S_{BO}} \Big[\frac{\partial \phi}{\partial t} + \frac{1}{2}(\frac{\partial \phi}{\partial y})^2\Big](x - x_G)\mathrm{ds} \\
- \rho \frac{\mathrm{D}}{\mathrm{Dt}} \int_{S_{UP}} \phi y \mathrm{ds} + \rho \frac{\mathrm{D}}{\mathrm{Dt}} \int_{S_{DS}} \phi y \mathrm{ds} - \rho \frac{\mathrm{D}}{\mathrm{Dt}} \int_{S_{FSL}} \phi \Big[(x - x_G)n_y - y n_x\Big] \mathrm{ds} \\
-\rho \frac{\mathrm{D}}{\mathrm{Dt}} \int_{S_B} \phi \Big[(x - x_G)n_y - y n_x\Big] \mathrm{ds} + \rho \frac{\mathrm{D}}{\mathrm{Dt}} \int_{S_{BO}} \phi (x - x_G) \mathrm{ds} - \rho \frac{\mathrm{D}}{\mathrm{Dt}} \int_{S_{FSR}} \phi \Big[(x - x_G)n_y - y n_x\Big] \mathrm{ds} \\
+\rho \int_{S_{FSL}} (\frac{\partial \phi}{\partial t} + \frac{1}{2}\nabla\phi \cdot \nabla\phi) \Big[(x - x_G)n_y - y n_x\Big] \mathrm{ds} + \rho \int_{S_{FSR}} (\frac{\partial \phi}{\partial t} + \frac{1}{2}\nabla\phi \cdot \nabla\phi) \Big[(x - x_G)n_y - y n_x\Big] \mathrm{ds} \\
- \rho \int_{S_{UP}} \nabla\phi \frac{\partial \phi}{\partial n} \mathrm{ds} - \rho \int_{S_{DS}} \nabla\phi \frac{\partial \phi}{\partial n} \mathrm{ds} - \rho \int_{S_{FSL}} \nabla\phi \frac{\partial \phi}{\partial n} \mathrm{ds} - \rho \int_{S_{FSR}} \nabla\phi \frac{\partial \phi}{\partial n} \mathrm{ds} \\
+ \rho \int_{S_{FSL}} (\frac{\partial \phi}{\partial y})^2 \Big[(x - x_G)n_y - y n_x\Big] \mathrm{ds} + \rho \int_{S_{FSR}} (\frac{\partial \phi}{\partial y})^2 \Big[(x - x_G)n_y - y n_x\Big] \mathrm{ds} \quad (3.68)
\end{aligned}
$$

3.4.1 Physical Interpretation of the terms in Fluid Impulse Theory

Before, discussing the application of the Fluid Impulse Theory for the nonlinear program, lets us try tounderstand the physical interpretation of the terms in the expression. Then, we provide some information on evaluation of the terms in the expression.

We define Impulse(see 3.69) on a surface as the integral of the product of potential and the generalized normal on that surface. According to the fundamental laws of physics, the time derivative of the impulse provides the generalized forces on the body.

$$I = \int_S \phi \hat{n} \mathrm{dS} \tag{3.69}$$

Let us have a close look at the final expression (3.52), we can see that the force on the body is the contribution of the pressure forces(The first three terms of the 3.52), the time derivative of the impulse(the fourth term of (3.52) and defined clearly in 3.69) and the gravity force(fifth term of 3.46). To make it clear that the last term is the gravity force, let us apply the divergence theorem to that specific term and we will end up with (3.70)

$$\int_{S_t} gZ\hat{n} \mathrm{dS} = \int_{\partial V} \nabla(gZ) \mathrm{dV} = g \int_{\partial V} \nabla(Z) \mathrm{dV} \tag{3.70}$$

The term is the same as the gravity force contribution in any momentum equations(Be it NS equations, Euler equations). But since, it has gravity associated with it and after

simplifications in the derivations, only has contribution from the free surface for the hydrodynamic force, we call it as hydrostatic contribution to the roll moment from the free surface, from now on. The rest of the terms sprang up as a consequence of not tracking the fluid particles themselves(eulerian representation) and they all represent the momentum flux through the upstream, downstream and the free surface.

We have understood the various terms, so far. But, we have not looked into computation of the various terms. We will start by examining how we are finding the time derivative of Impulse. Since, we just wanted to show that we arrive at similar results with the Fluid Impulse Theory and the Direct Pressure Integration, we use simple techniques for time derivative of the impulse. Let I_2 be the impulse at time step t^n and I_1 be the impulse at time step t^{n-1}, then the time derivative of Impulse at time step 'n' is given by 3.71.

$$\left(\frac{\mathrm{dI}}{\mathrm{dt}}\right)^n = \frac{I_2 - I_1}{\Delta t} \tag{3.71}$$

Now, for the evaluation of the temporal gradients of the various terms, we need to consider the remeshing of the various surfaces. For example, if we consider the remeshing on the upstream boundary, then the temporal gradient of the potential is given by (3.72), where U includes the panel velocity given by (3.73).

$$\frac{\partial \phi}{\partial t} = \frac{\phi(t + \Delta t) - \phi(t)}{\Delta t} + U \cdot \nabla \phi \tag{3.72}$$

If at time step t, the location of a point(panel collocation point) is at Y_1 and this changes after remeshing to Y_2 for time step $t + \Delta t$, then the panel velocity is given by (3.73).

$$U = \frac{Y_2 - Y_1}{\Delta t} \tag{3.73}$$

Now a question that may incur in mind is why do not we use the definition of (3.72) for time derivative of impulse. It is quite simple to recognize that the impulse is an integral quantity and thus we can simply use backward differences.We have many integrals that have to be numerically evaluated. We have used the Newtons cotes formula(simpsons rule and the trapezoidal rule), Guass Legendre rules(10th and 15th order) and finally the MATLAB in built Adaptive Guass Kronrod Quadrature for evaluating the integrals and the last choice seemed to be the best. Now, we have understood the physical significance of various terms, along with their numerical computations, so we are now ready for some numerical simulations.

3.4.2 FIT applied to a nonlinear diffraction program

We first present the results of applying FIT for nonlinear diffraction program for the parameters provided in table - 3.12. The output of the program is provided in Fig 3.14, where we have the as usual time trace of the moment along with its frequency content.

Variable	Value
Wave Amplitude	0.1m
Wave Length	20m
Length of the computational domain	80m
Water depth	150m
Width of the body	30m
Draft of the body	6m
X-center of gravity	40m
Y-center of gravity	0m
CFL number	0.28

Table 3.12: Input parameters for the Nonlinear diffraction program

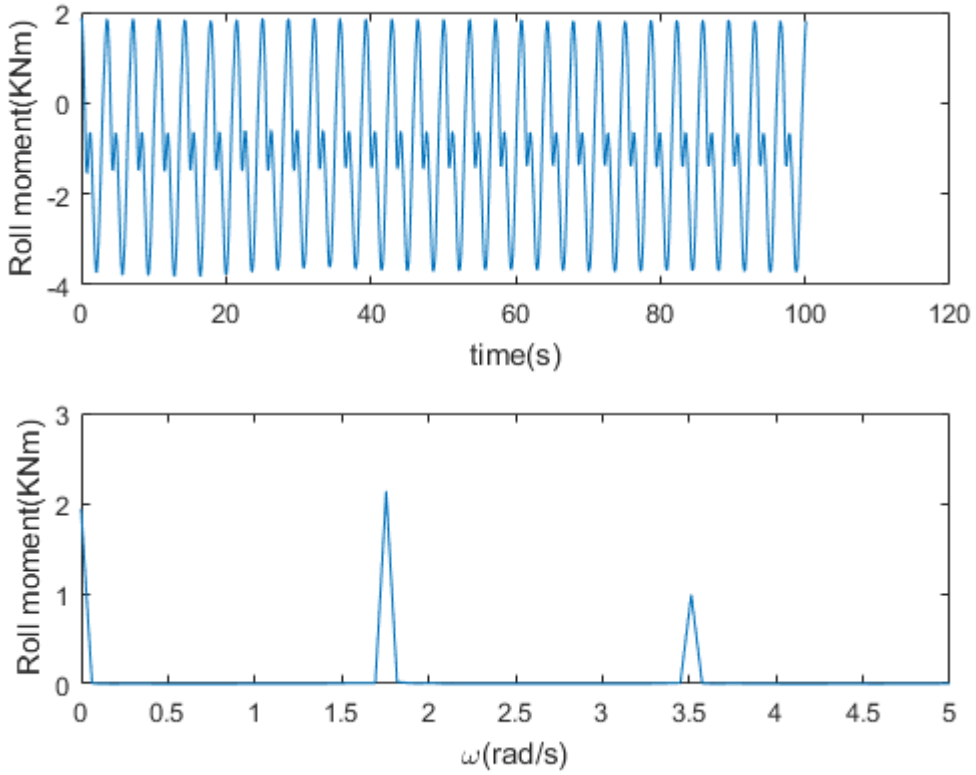

Figure 3.14: (Top): Moment time trace of the nonlinear diffraction program for wave height of 0.2m and wavelength of 20m using FIT, (Bottom): Frequency content of the Moment using FIT

Before we go by comparing, we would like to show that the major contribution to the final moment is provided by the body impulse, free surface impulse and the hydrostatic contribution from the free surface(Fig 3.15). In fig 3.15, the free surface impulse and the hydrostatic contribution have been combined together as they are individually really large values and they would not clearly show the body impulse and the total moment, but in Fig 3.16, these are shown independently.

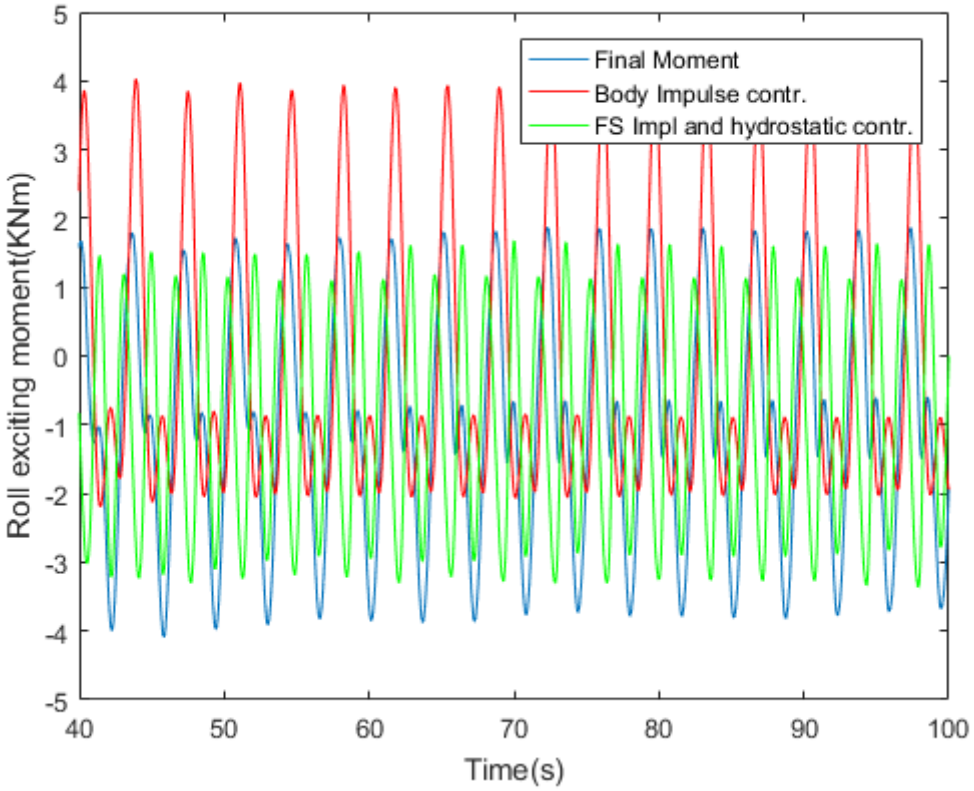

Figure 3.15: The total moment and the contributions of the body impulse, free surface impulse and hydrostatic component

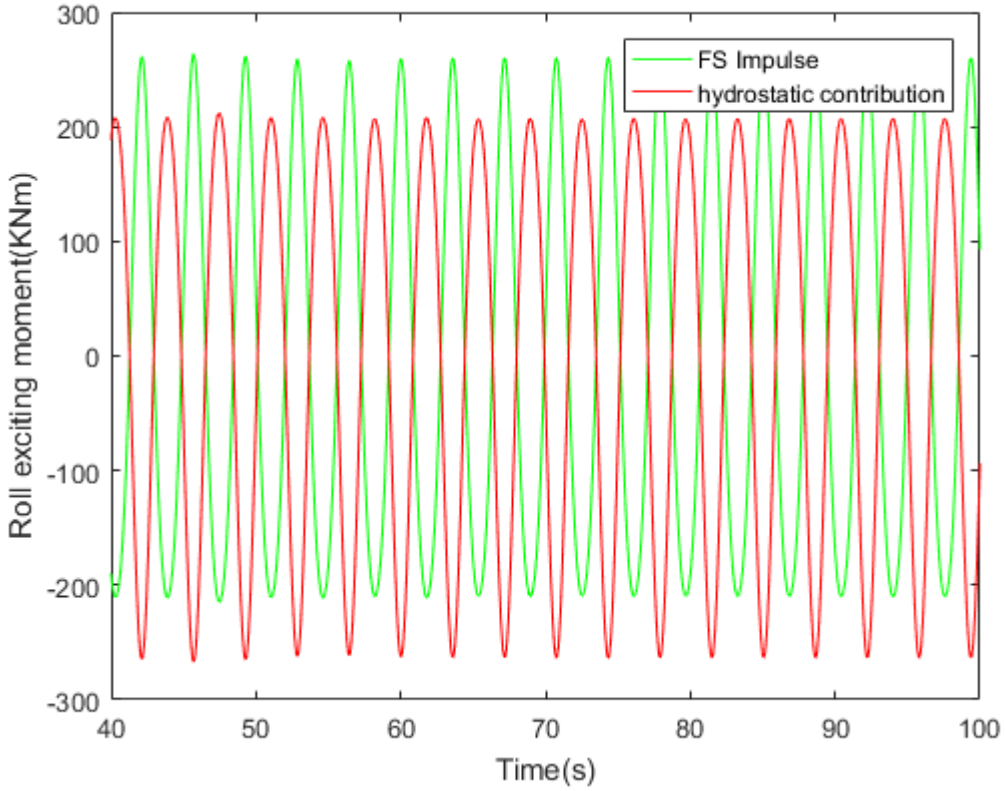

Figure 3.16: The contribution of the free surface impulse and the hydrostatic term to the total final roll exciting moment

From Fig 3.16, we can see clearly see the importance of the free surface contributions. This implies that the answer is quite sensitive to the free surface representation and any slight change on the free surface, will effect the answer. We have tried an experiment here: In the results presented so far, we have provided the potential on the intersection of the free surface and the upstream boundary as the value extrapolated from the nearby free surface elevation, but we have also carried out simulations were the potential at the same intersection point is provided as the input wave potential(well, this is not exactly correct, as the upstream boundary should behave like a Generating Absorbing Boundary Condition, but we just wanted to proove that the answer varies with this change). In the first case, we are making the intersection point behave as that it only belongs to the free surface and in the second case, we make it as part of the upstream boundary only. But, in reality, it behaves as its part of both the free surface and the upstream boundary, which

we could not enforce. This is one of the consequences of using Constant Panel Method. We refer P2 as the case where the potential on the intersection boundary is specified as the upstream potential value and P1 as the case where we use free surface extrapolation. We show in table 3.13, the results from the program, where the sensistivity of the reformulated Fluid Impulse Theory to the Free surface representation can be clearly seen.

	Moment(KNm)		
Case	Mean	Linear	Sum
P1	1.941	2.136	0.9899
P2	0.498	2.16	1.95

Table 3.13: The sensitivity of the results of FIT to the representation of the free surface

Now, in Fig 3.17, we give a frequency comparison between the results of FIT and DPI for the case in table -3.12. The results are also tabulated in table - 3.14 for various steepness and non-dimensional wavelengths. We produce a more clearer comparison between the Direct Pressure Intergation(DPI) and the Fluid Impulse Theory(FIT) by comparing them in time domain(Fig 3.18a) and in the frequency domain(Fig 3.18b) for waves of wave height 0.1m and wavelength of 12m. This clearly shows that the results between both the theories are close enough.

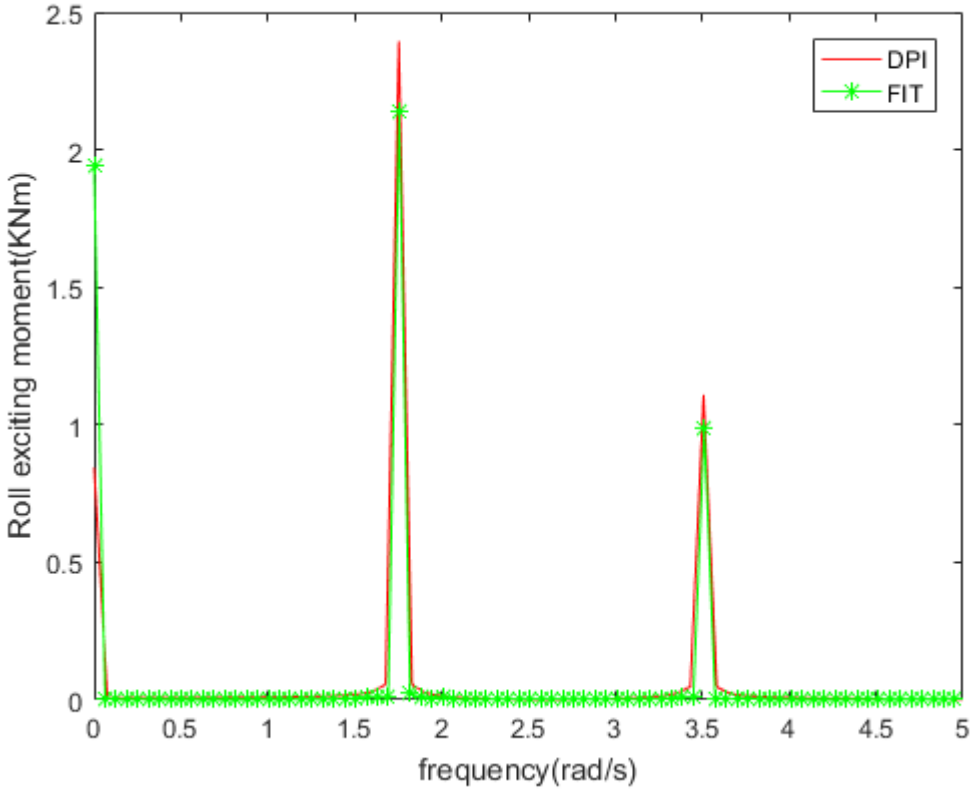

Figure 3.17: Frequency content of the moment time traces obtained from the Direct Pressure Integration(DPI) and Fluid Impulse Theory(FIT) for wave of wave height 0.2m and wavelength of 20m

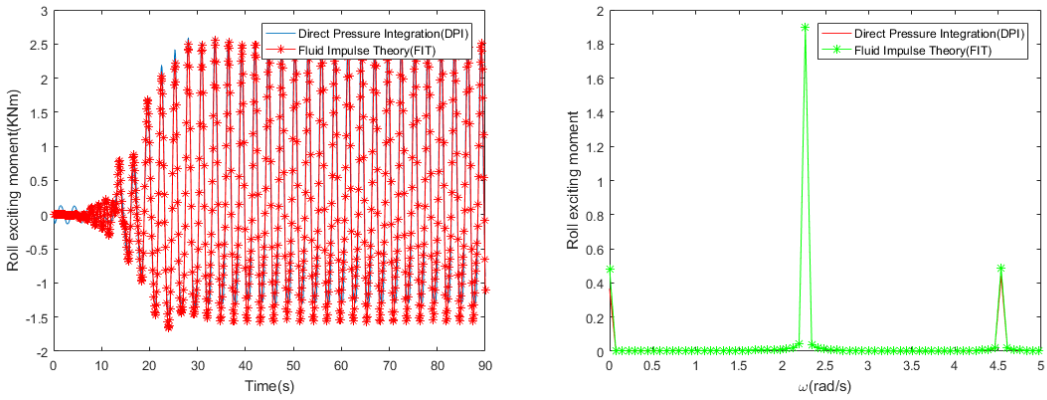

(a) Roll exciting moment on a barge (b) Frequency comparison between the two theories

Figure 3.18: Roll moments on barge of beam B=30m and draft T=6m by waves of waveheight of 0.1m and wavelength 12m

					$\frac{M}{\rho B^2 T \frac{g}{2} \frac{H}{\lambda}}$		
Order	Wave steepness	$\frac{B}{\lambda}$	$\omega\sqrt{\frac{B}{g}}$	Technique	Mean	Linear	Sum
5	0.00833	2.5	3.96	DPI	0.001773	0.009959	0.00144328
5	0.00833	2.5	3.96	FIT	0.002584	0.010026	0.001844
5	0.00769	2.308	3.81	DPI	0.001735	0.010435	0.0020644
5	0.00769	2.308	3.81	FIT	0.00416	0.010431	0.00416
5	0.005	1.5	3.07	DPI	0.003418	0.00862	0.001889
5	0.005	1.5	3.07	FIT	0.00164	0.0086647	0.0020279
5	0.01	1.5	3.07	DPI	0.0032816	0.0086647	0.0040558
5	0.01	1.5	3.07	FIT	0.006931	0.007742935	0.009587
5	0.0066	2	3.55	DPI	0.0016	0.0112	0.0020502
5	0.066	2	3.55	FIT	0.00246	0.0112	0.002334
5	0.004	1.2	2.75	DPI	0.001451	0.000987	0.002743
5	0.004	1.2	2.75	FIT	0.0069133	0.000959	0.0069677
5	0.01	3	4.34	DPI	0.0018	0.006449	0.0024
5	0.01	3	4.34	FIT	0.0018	0.006383	0.0030

Table 3.14: Comparison of the results of Direct Pressure Integration(DPI) and the Fluid Impulse Theory(FIT), Linear implies the contribution to the Moment at wave frequency, sum implies the contribution to the Moment at twice the wave frequency

As we can see from the table - 3.14, the sum and the linear component match quite well between the Direct Pressure Integration(DPI) and Fluid Impulse Theory(FIT), whereas the mean component predicted from the Fluid Impulse Theory differs slightly from the value from the Direct Pressure Integration(DPI). As already stated, there are three main contributors to the final moment:

1. The Body Impulse
2. The Free surface impulse
3. The hydrostatic contribution

The free surface impulse and the hydrostatic contribution are quite high compared with the body impulse. So, we try to club them as total free surface contribution, so as to

study its contributions to the final moment. The body impulse is mainly responsible for the linear component and small contribution at twice frequency, whereas the free surface provides the complete mean component of the moment and small contributions at linear and sum frequencies. Thus, the different mean component between the Fluid Impulse Theory(FIT) and the Direct Pressure Integration(DPI) is because of the free surface representation. We have used a quite coarse mesh, as refining the mesh produces wiggles which eventually break the code. These wiggles develop at the wave-body intersection, due to the incompatibility at the intersection. The intersection is found by extrapolating data from the free surface only, whereas in reality, this intersection point remains common to the body and the free surface. A way to get over this incompatibility has been clearly explained in the works of H. Xu and D.Yue[30] and they recommend using the double node technique suggested by Lin[2] with a Higher Order Boundary Element Method(HOBEM).

As already stated in chapter 2, these wiggles have been observed in the works of many researchers and they get over it by smoothing functions, but that would complicate things here, because that would lead to messy terms which have to be incorporated in our derivation of fluid impulse theory. Thus, we do not use any such smoothing function. May be an arguable choice, would be to develop a Higher Order Boundary Element Method(HOBEM) and capture the exact value of the potential and the free surface elevation at all intersection point by using double node technique. Also, we need not mesh fine in HOBEM, because they would have quadratic convergence.

After the wave gets diffracted from the body, in the linear program, we get standing waves for the wavelength considered here, whereas in the nonlinear program, we do not get exact standing waves. It is because the scheme is designed to be upwind for the incoming wave, but for the diffracted wave, it is not so and this causes slight numerical dispersion. We have showed already the sensitivity of the Fluid Impulse Theory to the representation of the free surface. Thus, we need higher order finite difference schemes for the computation of all necessary gradients on the free surface. An other consequence of using an upwind scheme, is that the wiggles that are developed close to the wave-body intersection, travel into the computational domain and this causes the program to break.

An interesting observation from the table 3.14 would be the difference between the results of the Fluid Impulse Theory and the Direct Pressure Integration is higher when the waves are longer. This is an another cause of the employing the constant panel

Variable	Value
Wave height	0.1m
Wave length	12m
Barge beam	12m
Barge draft	2.4m
Computational domain length	60m
Computational domain depth	150m

Table 3.15: Dimensions of the body and domain for the case where the wavelength is chosen to be the same as the body beam

method. There is an incompatibility of the boundary conditions usually at the intersection of the lateral boundaries and the bottom boundary. As long as the waves are small, the waves do not feel the bottom, so this incompatibility does not cause much problems. But, as the waves grow longer, this incompatibility is responsible for small wiggles at the upstream-free surface intersection. Since, the nature of finite differencing is upstream, these appear like, they are travelling back out of the domain. As we have already seen that the results of the Fluid Impulse Theory are dependent on the free surface representation, thus, as the waves become longer, the answers vary. But, still the answers are close enough. Again, the remedy would be to employ an Higher Order Boundary Element Method(HOBEM) and use the double node technqiue, so as to ensure compatibility between the lateral and bottom boundaries.

Before, we sum up our dicsussion of the application of the re-formulated Fluid Impulse Theory, we study a last test case where the wavelength is the same as the body beam. Many nonlinear effects become predominant at this condition(example: added resistance in waves). Since, we have stated already the problems with simulating long waves, we make the body dimensions smaller so that the it matches the wavelength. The dimensions of the body and the domain are tabulated in Table - 3.15. We provide the time trace of the roll exciting moment computed on the barge along with the frequency content in Fig 3.19(a) and 3.19(b) respectively, using Direct Pressure Integration(DPI) and the reformulated Fluid Impulse Theory(FIT, with two different CFL numbers). The results match quite well. Also, the sensitivity of the Fluid Impulse Theory to time step is cleary seen. An interesting point is that with increasing time step, the CFL number

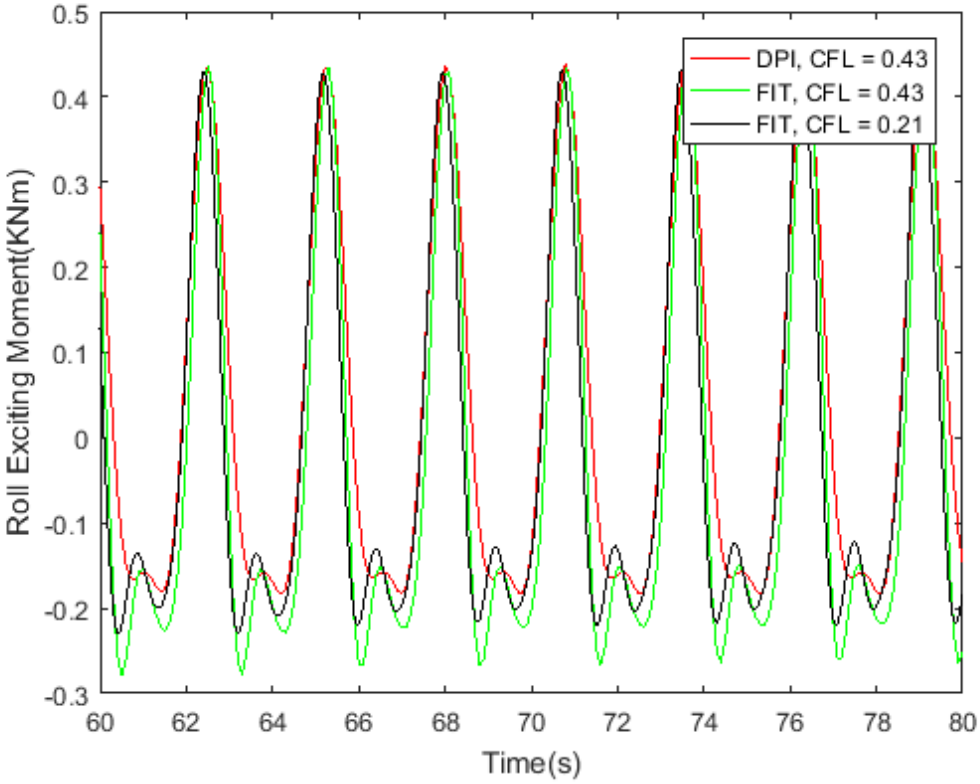

(a) Roll exciting moment on a barge

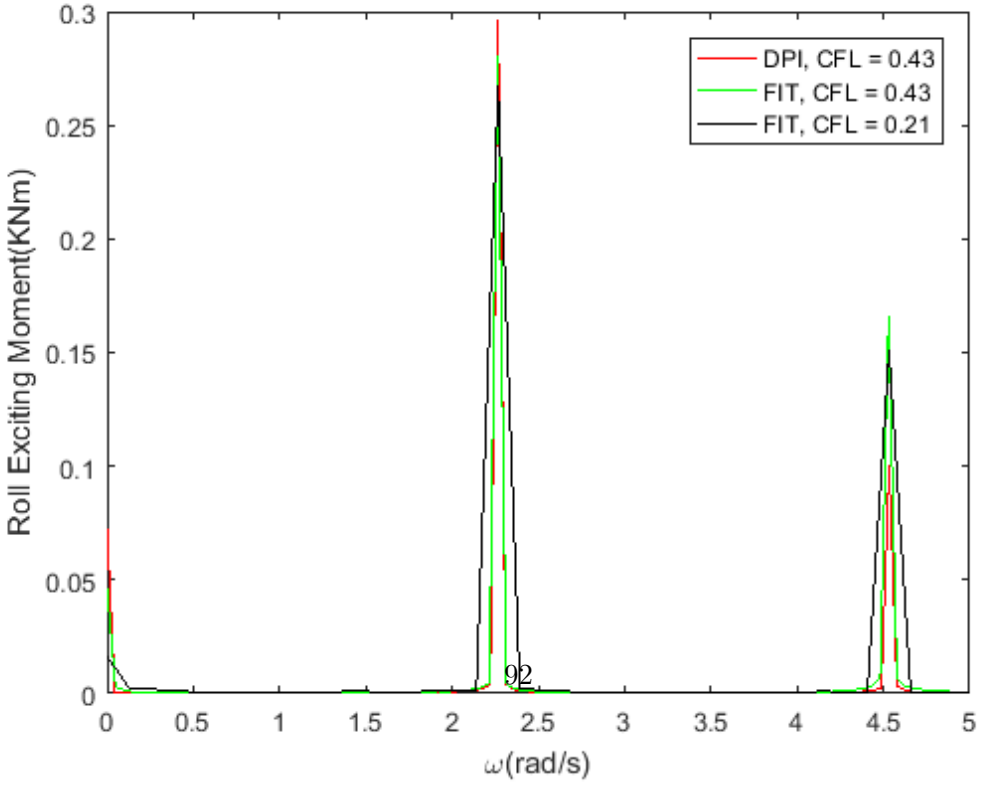

(b) Frequency comparison between the two theories

Figure 3.19: Roll moments on barge of beam B=12m and draft T=2.4m by waves of waveheight of 0.1m and wavelength 12m

Variable	Value
Length of computational domain	150m
height of the computational domain	150m
Width of the body	30m
Draft of the body	6m
X-center of gravity	75m
Y-center of gravity	0m
Amplitude of oscillation	0.005rad
CFL	0.2

Table 3.16: Inputs to the nonlinear radiation program for comparison with the linear results

increases and thus the numerical diffusion in the simualtion of the waves on the free surface decreases. But, the consequence of having higher time step is that the accuracy of the time derivative of the impulses reduces as we use backward differences in time to estimate them. So, one should be really careful with the choice of time step.

Though all these are some hindcasts of our nonlinear diffraction program, we are glad that the results from our nonlinear diffraction program using Direct Pressure Integration(DPI) and the Fluid Impulse Theory(FIT) match quite well. We will suggest some future suggestions in later chapter, which will improve the technique.

3.4.3 Application of the Fluid Impulse Theory to nonlinear radiation program

The evaluation of terms is no different and everything that has been presented, so far in the Fluid Impulse Theory is employed here. The table 3.16 gives the parameters which served as an input to the program. The amplitude of oscillation is provided small, as to compare and verify the programs with respect to how they behave when in linear regime. This serves as a tool for verification purpose. In Fig 3.20, we provide the results of various radiation programs and as we can see these all match quite well. A question that might be puzzling, is how did we find the speed of the wave forehand for finding the CFL number. We used the formula of Eckhart and Fenton[31], for estimaing the wavenumber of the wave(3.74). Though, this is for the linear waves, we still use it for

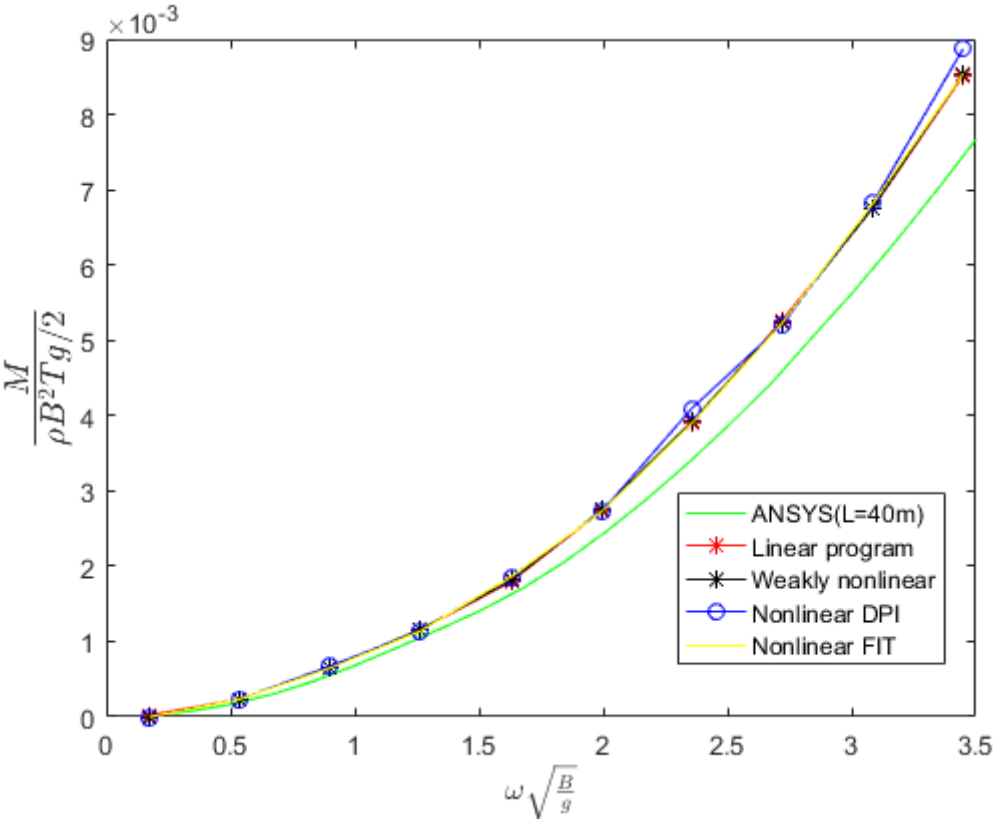

Figure 3.20: Comparison between the various nonlinear radiaition programs: Linear, weakly nonlinear, nonlinear DPI and nonlinear FIT for the parameters provided in Table -15

our estimation of the wave number, and the wave speed.

$$k = \frac{1}{d}\frac{\alpha + \beta^2 \cosh(\beta)^{-2}}{\tanh\beta + \beta\cosh(\beta)^{-2}} \tag{3.74}$$

They were always wiggles close to the body, especially when there was a crest or trough near the body. We associate them to the way, we estimate the intersection point between the wave and the body. Now, we carry out simulations at a frequency of 0.76rad/s(the roll natural frequency of the body) and an amplitude of 0.05rad(inputs to the program in Table 3.17) and in Fig 3.21, we have plot demonstrating the both techniques for these wave conditions. The results match quite well.

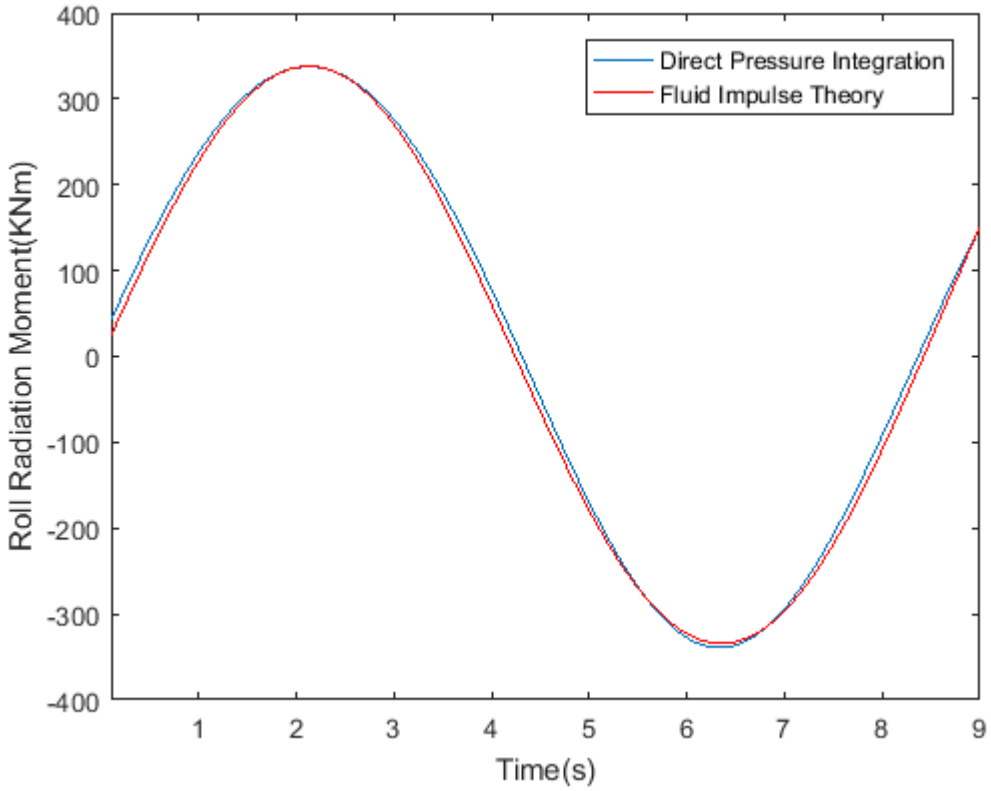

Figure 3.21: Comparison of FIT and DPI results for roll amplitude of 0.05rads at roll natural frequency(0.76rad/s)

Variable	Value
Length of computational domain	150m
Height of computational domain	150m
Width of the body	30m
Draft of the body	6m
X-center of gravity	75m
Y-center of gravity	0m
Amplitude of roll motion	0.05rad
CFL	0.025
ω	0.76rad/s

Table 3.17: Inputs to the nonlinear radiation program for roll motion of 0.05rads at roll natural frequency

Chapter 4

Conclusions and Recommendations

After sucessful proof and validation of the results of Fluid Impulse Theory(FIT) with the Direct Pressure Integration(DPI), we would like to state the advantages/disadvantages of the Fluid Impulse Theory(FIT) as compared to Direct Pressure Integration(DPI) and follow it up with future recommendations.

4.1 Advantages of the Fluid Impulse Theory over Direct Pressure Integration

1. In DPI, we need to find the pressure and then integrate it over the wetted surface, to find the load on the structure. This involves estimating the temporal gradient of the potential and its spatial gradients on the body. Estimating the temporal gradient of the potential is not that straight forward as employing backward differences in complete nonlinear program gives numerical errors. The reason being that the ship and the water are always in state of dynamic equilibrium at every instant and using the information of the last time instant may lead to numerical instabilities. So, we need to set up an other boundary value problem(one of the four techniques used for finding the temporal gradient) for the temporal gradient. Thus, every time instant, we need to solve two boundary value problems, which is time consuming. In FIT, we evaluate the potential on the various surfaces and use this information to find the moment by using Reynolds Transport Theorem on the fluid momentum in the computational domain, thereby getting the moment on the body. This involves only one boundary value problem. Thus, this should be less time consuming. A

formal proof with a computational efficiency calculated is quite difficult to state, as this computational time may itself have to do with the numerical schemes employed than the technique itself. Either ways, the application of the Fluid Impulse Theory makes a two step procedure(potential to pressure and then to Moment) as a single step procedure(potential to Moment).

4.2 Disadvantages of the Fluid Impulse Theory over Direct Pressure Integration

1. The FIT procedure is quite sensitive to the representation of the free surface, so quite care must be taken with getting a proper free surface representation. This implies a lower time step, finer mesh, accurate time stepping and spatial gradient evaluations and a Higher Order Boundary Element Method(HOBEM). This may partially appear to outweigh the advantage, but any ways as the nonlinearity of the wave or the wave steepness becomes higher, we need to use a Higher Order Boundary Element Method(even for DPI), so this should not outweigh the advantage.

2. When we want to optimize the hull form locally, we need to evaluate the pressure on the hull surface(an example would be to optimize the hull form for having lower resistance in waves) and the FIT does not provide the pressure. This implies that FIT cannot be used for cases where pressure is required on the hull surface.

4.3 Recommendations for Future work

1. We have stated two disadvantages over one advantage, but the advantage would dominate, especially, when we have a three dimensional nonlinear program, FIT should be more efficient than the DPI. So, the next step should be to verify the theory that is derived in this work for a three dimensional case as it seems promising.

2. A step that could be performed before carrying out the previous one, is to use a Higher Order Boundary Element Methods(HOBEM), higher order time stepping techniques and have more concrete proof of the theory in two dimensions.

3. Forward speed problems, especially in the case of container ships play an important role and could be dealt with fluid impulse theory when compared to DPI and viscous codes. So, extending the theory so that it includes the forward speed is quite important.

4. It was seen that they have been wiggles in the generation of waves in the 2D-NWT generated and also in few cases in the nonlinear diffraction program. Though, this has been documented in the works of many researchers, a definative answer has not been arrived at and this requires some attention.

Chapter 5

Appendix

Appendix-A

The derivation for integral equation is revisited here briefly. For more,thorough understanding,works of Lamb[32] and Kellogg[13] can be shed into light.

Consider a 2D simply connected region, u and w be two scalar fields which are second order continuous, then the greens theorem states:

$$\iiint_{\Omega}(u\nabla^2 w - w\nabla^2 u)\mathrm{d}\Omega = \iint_{S}[-w\frac{\partial u}{\partial n_\zeta} + u\frac{\partial w}{\partial n_\zeta}]\mathrm{dS}_\zeta \tag{5.1}$$

where, n refers to the normal which is out of the computational domain Ω. Now, one can replace u with the unknown potential($\phi(\zeta)$) and w with the Green's function:

$$G(\zeta; x) = \frac{1}{2\pi}\log|\zeta - x| \tag{5.2}$$

Let the field point, x where the greens function is logarithmically singular be a point in the domain or on the boundary. The control domain is pictured in figure 5.1. The singular point is located in the domain, and a circle is placed around the point. This circle is made to meet the outer domain through two surfaces S_1 and S_2. Now invoking the definitions for u,v and splitting the surface S into the constituent surfaces leads to (5.3):

$$\iiint_{\Omega}[\phi\nabla^2 G - G\nabla^2\phi]\mathrm{d}\Omega = \iint_{dS+S_1+S_\zeta+S_2}[\phi\frac{\partial G}{\partial n} - \frac{\partial\phi}{\partial n}G]\mathrm{dS}_\zeta \tag{5.3}$$

Since, the unknown potential and the Greens function satisfy the Laplace equation, the left hand side of the (5.3) is identically zero. The normal direction on S_1 and

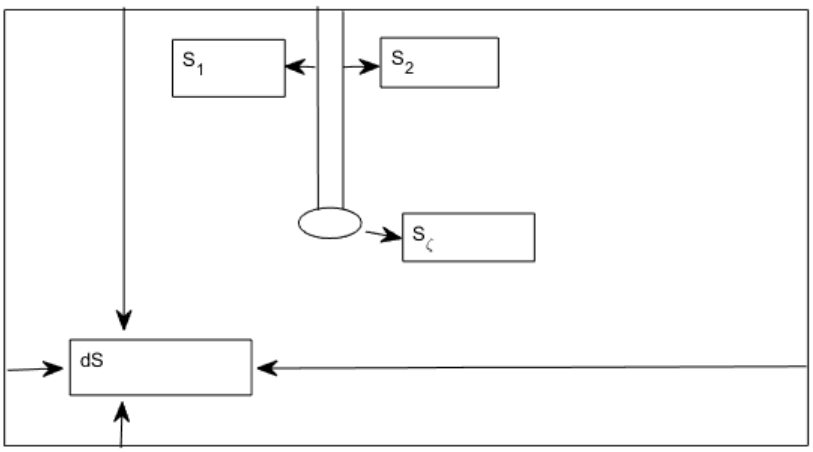

Figure 5.1: Control domain

S_2 are opposite and provided that they are quite close to each other, the difference of values of potential and Greens function between these surfaces are negligible, thus the contributions of the integral on the right hand side to these surface are equal and opposite, canceling each other. Now, one will be left with the exterior domain and the surface S_ζ. This simplifies the equations to (5.4).

$$\iint_{dS}[\phi\frac{\partial G}{\partial n}-\frac{\partial \phi}{\partial n}G]\mathrm{dS}_\zeta+\iint_{S_\zeta}[\phi\frac{\partial G}{\partial n}-\frac{\partial \phi}{\partial n}G]\mathrm{dS}_\zeta=0 \tag{5.4}$$

Now,let us consider the second term of the (5.4) separately. Since, this is circle, dS=rdθ, where r refers to the radius of the circle.

$$\iint_{S_\zeta}[\phi\frac{\partial G}{\partial n}-\frac{\partial \phi}{\partial n}G]r\mathrm{d}\theta \tag{5.5}$$

Also, note that the radius of the circle is exactly in the opposite direction to the normal.

$$\frac{\partial G}{\partial n}=-\frac{1}{2\pi r} \tag{5.6}$$

One needs to note that ϕ in the integral(5.5) is the value on the circle and this whole integral resembles the contribution of the singular point as the radius tends to zero. Now substituting (5.6) in (5.5) and noting that the negative sign is due to the opposite directions of normal and r leads to (5.7).

$$\iint_{S_\zeta}[-\phi\frac{1}{2\pi r}-\frac{1}{2\pi}\frac{\partial \phi}{\partial n}\log r]r\mathrm{d}\theta \tag{5.7}$$

Now, as r $\rightarrow$ 0, we get:

$$\lim r \rightarrow 0(\int_0^{2\pi}[-\frac{\phi}{2\pi}]\mathrm{d}\theta - \int_0^{2\pi}\frac{1}{2\pi}\frac{\partial\phi}{\partial n}r\log r\mathrm{d}\theta \tag{5.8}$$

The second part of (5.8) goes to zero as r approaches zero, leaving:

$$\iint_{S_\zeta}[\phi\frac{\partial G}{\partial n} - \frac{\partial\phi}{\partial n}G]r\mathrm{d}\theta = -\phi(x) \tag{5.9}$$

If the singular point is on the boundary, we only integrate it on the half circle, thus getting (5.10) for singular point on the boundary.

$$\iint_{S_\zeta}[\phi\frac{\partial G}{\partial n} - \frac{\partial\phi}{\partial n}G]r\mathrm{d}\theta = -\frac{\phi(x)}{2} \tag{5.10}$$

Now back substituting the contribution of second integral in (5.4) will yield (5.11).

$$\iint_{dS}[\phi\frac{\partial G}{\partial n} - \frac{\partial\phi}{\partial n}G]\mathrm{dS}_\zeta - \frac{1}{2}\phi(x) = 0 \tag{5.11}$$

Thus, the final integral equation for potential takes the form:

$$\frac{\phi(x)}{2} = \iint_{dS}[\phi(\zeta)\frac{\partial G(\zeta;x)}{\partial n_\zeta} - \frac{\partial\phi(\zeta)}{\partial n_\zeta}G(\zeta;x)]\mathrm{dS}_\zeta \tag{5.12}$$

In the case of three dimensions, the Greens function changes, but the steps of the derivation will be essentially same, except that instead of a circle, we have a sphere of radius ϵ.

Appendix-B

Assuming that the disturbance(η) of the free surface is small, then the potential on the free surface at the disturbed free surface can be Taylor expanded.

$$\phi|_{y=\eta} = \phi|_{y=0} + \eta\frac{\partial\phi}{\partial z}|_{y=0} + \frac{\eta^2}{2}\frac{\partial^2\phi}{\partial^2 z}|_{y=0} + \frac{\eta^3}{3!}\frac{\partial^3\phi}{\partial^3 z}|_{y=0} + \cdots \tag{5.13}$$

Now, using expressions (2.41), we can find the quantities required in (5.13) and by using the first four terms in the expressions leads to (5.14). In the expression (5.14), the potential ϕ_0 refers to linear wave potential on $y = 0$(5.15).

$$\phi_I = \phi_0(1 + \eta\tanh(kh) + \frac{\eta^2}{2!} + \frac{\eta^3}{3!}\tanh(kh)) \tag{5.14}$$

$$\phi_0 = \frac{Ag}{\omega}\cos(\omega t - kx) \tag{5.15}$$

The phase velocity of the wave is necessary to enforce the Sommerfeld radiation condition at the downstream. For linear Airy wave theory, using the Kinematic Free Surface Boundary Condition(KFSBC), one can arrive at the analytical dispersion relation. So, by Taylor expanding the KFSBC, we find the dispersion relation. The KFSBC is displayed in (5.16).

$$\frac{\partial\eta}{\partial t} + \nabla\eta\cdot\nabla\phi = \frac{\partial\phi}{\partial y} \tag{5.16}$$

Since, we deal with one dimensional wave propagation, (5.16) simplifies to (5.17).

$$\frac{\partial\eta}{\partial t} + \frac{\partial\eta}{\partial x}\frac{\partial\phi}{\partial x} - \frac{\partial\phi}{\partial y} = 0 \tag{5.17}$$

The second term($\frac{\partial\phi}{\partial x}$) and third term($\frac{\partial\phi}{\partial y}$) can be Taylor expanded.

$$\begin{aligned}(\frac{\partial\eta}{\partial t} + \frac{\partial\eta}{\partial x}\frac{\partial\phi}{\partial x} - \frac{\partial\phi}{\partial y})|_{y=\eta} = \frac{\partial\eta}{\partial t} + \frac{\partial\eta}{\partial x}(\frac{\partial\phi}{\partial x}|_{y=0} + \eta\frac{\partial^2\phi}{\partial^2 x}|_{y=0} + \frac{\eta^2}{2!}\frac{\partial^3\phi}{\partial^3 x}|_{y=0} + \frac{\eta^3}{3!}\frac{\partial^4\phi}{\partial^4 x}|_{y=0} + \cdots)\\ - (\frac{\partial\phi}{\partial y}|_{y=0} + \eta\frac{\partial^2\phi}{\partial^2 y}|_{y=0} + \frac{\eta^2}{2!}\frac{\partial^3\phi}{\partial^3 y}|_{y=0} + \frac{\eta^3}{3!}\frac{\partial^4\phi}{\partial^4 y}|_{y=0} + \cdots)\end{aligned} \tag{5.18}$$

Then, substituting for all terms in the equations and correcting leads to the following dispersion relation.

$$\omega = \sqrt{gk\tanh(kh)(1 + \frac{k^2\eta^2}{4})} \tag{5.19}$$

The phase velocity follows from (5.20):

$$c = \frac{\omega}{k} \tag{5.20}$$

The free surface wave profile assumed to be incorporated in (5.18) is still a linear sinusoidal wave profile(5.21).

$$\eta = A\sin(\omega t - kx) \tag{5.21}$$

The expressions (5.14) are used to specify the incident wave potential on the upstream boundary and initially on the free surface boundary and downstream boundary of the computational domain in nonlinear wave simulations. The wave speed for nonlinear wave simulations is provided by (5.20).

Derivation of the normal acceleration of the fluid particle

The derivation is reproduced from the works of Van Daalen[5], Tanizawa[25] and Berkvens[27]. The description is in the X-Z co-ordinate system and S-N co-ordinate system. For the following derivation, we use s_1 as the tangential co-ordinate and s_2 is the normal pointing out of the fluid. The third co-ordinate which is out of the plane containing S-N is the same for both the co-ordinate systems. θ represents rotation about the Y co-ordinate. The acceleration of the point in the fluid is defined as (5.22).

$$\ddot{x} = \frac{\mathrm{d}\dot{\mathrm{x}}}{\mathrm{dt}} = \frac{\mathrm{d}}{\mathrm{dt}}(\sum_{k=1}^{2}(\dot{x}\cdot s_k)s_k) \tag{5.22}$$

Using the product rule for the derivative in the parenthesis yields (5.23).

$$\ddot{x} = (\frac{\mathrm{d}}{\mathrm{dt}}(\sum_{k=1}^{2}\dot{x}\cdot s_k))s_k + \sum_{k=1}^{2}\dot{x}\cdot s_k\frac{\mathrm{ds_k}}{\mathrm{dt}} \tag{5.23}$$

The magnitude of the vectors in a rotating reference frame is given by (5.24).

$$\frac{\mathrm{dS}}{\mathrm{dt}} = \dot{\theta}\times S \tag{5.24}$$

From (5.24), we have (5.25) and (5.26).

$$\frac{\mathrm{ds_1}}{\mathrm{dt}} = \dot{\theta}\times s_1 = \dot{\theta}s_2 \tag{5.25}$$

$$\frac{\mathrm{ds_2}}{\mathrm{dt}} = \dot{\theta}\times s_2 = -\dot{\theta}s_1 \tag{5.26}$$

Further expanding the summations in (5.23) leads to (5.27).

$$\ddot{x} = \frac{\mathrm{d}}{\mathrm{dt}}(\dot{x}\cdot s_1)s_1 + \frac{\mathrm{d}}{\mathrm{dt}}(\dot{x}\cdot s_2)s_2 + (\dot{(x)}\cdot s_1)(\dot{\theta}s_2) + (\dot{x}\cdot s_2)(-\dot{\theta}s_1) \tag{5.27}$$

Taking scalar product of (5.27) with the outward normal leads to (5.28).

$$\ddot{x} \cdot s_2 = \frac{\mathrm{d}(\dot{\mathrm{x}} \cdot \mathrm{s}_2)}{\mathrm{dt}} + (\dot{x} \cdot s_1)\dot{\theta} \tag{5.28}$$

Let us deal with the first term of the expression (5.28). If we represent the velocity of the fluid by the gradient of the velocity potential and then express the gradient in the tangential co-ordinate system.

$$\frac{\mathrm{d}(\dot{\mathrm{x}} \cdot \mathrm{s}_2)}{\mathrm{dt}} = \frac{\mathrm{d}(\nabla\phi \cdot \mathrm{s}_2)}{\mathrm{dt}} = \frac{\mathrm{d}}{\mathrm{dt}}(\Big[\frac{1}{h_1}\frac{\partial\phi}{\partial s_1}s_1 + \frac{1}{h_2}\frac{\partial\phi}{\partial s_2}s_2\Big] \cdot s_2) \tag{5.29}$$

The values h represent the scale factors(Lame co-efficients). Using the product rule for differentiation and substituting (5.25) yields (5.32).

$$\frac{\mathrm{d}(\dot{\mathrm{x}} \cdot \mathrm{s}_2)}{\mathrm{dt}} = \frac{\mathrm{d}}{\mathrm{dt}}(\frac{1}{h_1}\frac{\partial\phi}{\partial s_1}s_1 + \frac{1}{h_2}\frac{\partial\phi}{\partial s_2}s_2) \cdot s_2 + (\frac{1}{h_1}\frac{\partial\phi}{\partial s_1}s_1 + \frac{1}{h_2}\frac{\partial\phi}{\partial s_2}s_2) \cdot \frac{\mathrm{ds}_2}{\mathrm{dt}} \tag{5.30}$$

$$\frac{\mathrm{d}}{\mathrm{dt}}(\frac{1}{h_1}\frac{\partial\phi}{\partial s_1}s_1 + \frac{1}{h_2}\frac{\partial\phi}{\partial s_2}s_2) \cdot s_2 + (\frac{1}{h_1}\frac{\partial\phi}{\partial s_1}s_1 + \frac{1}{h_2}\frac{\partial\phi}{\partial s_2}s_2) \cdot (-\dot{\theta}s_1) \tag{5.31}$$

$$= \frac{\mathrm{d}}{\mathrm{dt}}(\frac{1}{h_1}\frac{\partial\phi}{\partial s_1}s_1 + \frac{1}{h_2}\frac{\partial\phi}{\partial s_2}s_2) \cdot s_2 - \frac{1}{h_1}\frac{\partial\phi}{\partial s_1}\dot{\theta} \tag{5.32}$$

Now substituting (5.32) back into (5.27) leads to (5.33).

$$\ddot{x}\cdot s_2 = \frac{\mathrm{d}}{\mathrm{dt}}(\frac{1}{h_1}\frac{\partial\phi}{\partial s_1}s_1+\frac{1}{h_2}\frac{\partial\phi}{\partial s_2}s_2)\cdot s_2-\frac{1}{h_1}\frac{\partial\phi}{\partial s_1}\dot{\theta}+(\dot{x}\cdot s_1)\dot{\theta} = \frac{\mathrm{d}}{\mathrm{dt}}(\frac{1}{h_1}\frac{\partial\phi}{\partial s_1}s_1+\frac{1}{h_2}\frac{\partial\phi}{\partial s_2}s_2)\cdot s_2+\Big[(\dot{x}\cdot s_1)-\frac{1}{h_1}\frac{\partial\phi}{\partial s_1}\Big]\dot{\theta} \tag{5.33}$$

The material derivative of a function f as expressed in the S-N co-ordinate system is derived in (5.34).

$$\frac{\mathrm{df}}{\mathrm{dt}} = \frac{\partial f}{\partial t} + \nabla f \cdot \dot{x} = \frac{\partial f}{\partial t} + \dot{x} \cdot (\sum_{k=1}^{2} \frac{1}{h_k}\frac{\partial f}{\partial s_k}s_k) = \frac{\partial f}{\partial t} + (\dot{x} \cdot s_1)\frac{1}{h_1}\frac{\partial f}{\partial s_1} + (\dot{x} \cdot s_2)\frac{1}{h_2}\frac{\partial f}{\partial s_2} \tag{5.34}$$

Now, consider the first term of the equation (5.33) and apply (5.34) will yield (5.35).

$$\frac{\mathrm{d}}{\mathrm{dt}}(\frac{1}{h_1}\frac{\partial\phi}{\partial s_1}s_1) = \frac{\partial}{\partial t}(\frac{1}{h_1}\frac{\partial\phi}{\partial s_1}s_1)+(\dot{x}\cdot s_1)\frac{1}{h_1}\frac{\partial}{\partial s_1}(\frac{1}{h_1}\frac{\partial\phi}{\partial s_1}s_1)+(\dot{x}\cdot s_2)\frac{1}{h_2}\frac{\partial}{\partial s_2}(\frac{1}{h_1}\frac{\partial\phi}{\partial s_1}s_1) \tag{5.35}$$

Expanding the terms in (5.35) leads to (5.36).

$$\frac{\mathrm{d}}{\mathrm{dt}}(\frac{1}{h_1}\frac{\partial\phi}{\partial s_1}s_1) = \frac{1}{h_1}\frac{\partial^2\phi}{\partial t\partial s_1}s_1 + (\dot{x} \cdot s_1)\frac{1}{h_1}\frac{\partial}{\partial s_1}(\frac{1}{h_1}\frac{\partial\phi}{\partial s_1})s_1 + (\dot{x} \cdot s_1)\frac{1}{{h_1}^2}\frac{\partial\phi}{\partial s_1}\frac{\partial s_1}{\partial s_1}+ (\dot{x} \cdot s_2)\frac{1}{h_2}\frac{\partial}{\partial s_2}(\frac{1}{h_1}\frac{\partial\phi}{\partial s_1})s_1 + (\dot{x} \cdot s_2)\frac{1}{h_1 h_2}\frac{\partial\phi}{\partial s_1}\frac{\partial s_1}{\partial s_2} \tag{5.36}$$

Using the definitions of the derivatives of unit vectors in curvilinear co-ordinates as shown in (5.37-5.38) and collecting the terms leads to (5.39).

$$\frac{\partial s_1}{\partial s_1} = -s_2 \frac{1}{h_2} \frac{\partial}{\partial s_2}(h_1) \tag{5.37}$$

$$\frac{\partial s_1}{\partial s_2} = s_2 \frac{1}{h_1} \frac{\partial}{\partial s_1}(h_2) \tag{5.38}$$

$$\begin{aligned}
\frac{\mathrm{d}}{\mathrm{dt}}(\frac{1}{h_1}\frac{\partial \phi}{\partial s_1}s_1) &= \Big[\frac{1}{h_1}\frac{\partial^2 \phi}{\partial t \partial s_1} + (\dot{x}\cdot s_1)\frac{1}{h_1}\frac{\partial}{\partial s_1}(\frac{1}{h_1}\frac{\partial \phi}{\partial s_1}) + (\dot{x}\cdot s_2)\frac{1}{h_2}\frac{\partial}{\partial s_2}(\frac{1}{h_1}\frac{\partial \phi}{\partial s_1})\Big]s_1 \\
&+ \Big[(\dot{x}\cdot s_1)\frac{1}{{h_1}^2}\frac{\partial \phi}{\partial s_1}(-\frac{1}{h_2}\frac{\partial}{\partial s_2}(h_1)) + (\dot{x}\cdot s_2)\frac{1}{h_1 h_2}\frac{\partial \phi}{\partial s_1}(\frac{1}{h_1}\frac{\partial}{\partial s_1}(h_2))\Big]s_2 \\
&= \Big[\frac{1}{h_1}\frac{\partial^2 \phi}{\partial t \partial s_1} + (\dot{x}\cdot s_1)\frac{1}{h_1}\frac{\partial}{\partial s_1}(\frac{1}{h_1}\frac{\partial \phi}{\partial s_1}) + (\dot{x}\cdot s_2)\frac{1}{h_2}\frac{\partial}{\partial s_2}(\frac{1}{h_1}\frac{\partial \phi}{\partial s_1})\Big]s_1 \\
&+ \Big[\frac{1}{{h_1}^2 h_2}\frac{\partial \phi}{\partial s_1}\big[(\dot{x}\cdot s_2\frac{\partial}{\partial s_1}(h_2) - (\dot{x}\cdot s_1)\frac{\partial}{\partial s_2}(h_1))\big]\Big]s_2
\end{aligned} \tag{5.39}$$

The scale factor is defined accordingly as (5.40).

$$\frac{1}{{h_k}^2} = \sum_{k=1}^{2} \frac{\partial x_m}{\partial q_k} \tag{5.40}$$

Now taking scalar product of (5.39) with s_2 yields the first term of (5.32).

$$\frac{\mathrm{d}}{\mathrm{dt}}(\frac{1}{h_1}\frac{\partial \phi}{\partial s_1}s_1)\cdot s_2 = \Big[\frac{1}{{h_1}^2 h_2}\frac{\partial \phi}{\partial s_1}\big[(\dot{x}\cdot s_2)\frac{\partial h_2}{\partial s_1} - (\dot{x}\cdot s_1)\frac{\partial h_1}{\partial s_2}\big]\Big] \tag{5.41}$$

without the derivation presented here, the second term has also something similar and presented in (5.42).

$$\frac{\mathrm{d}}{\mathrm{dt}}\Big[\frac{1}{h_2}\frac{\partial \phi}{\partial s_2}s_2\Big]\cdot s_2 = \Big[\frac{1}{h_2}\frac{\partial^2 \phi}{\partial t \partial s_2} + (\dot{x}\cdot s_1)\frac{1}{h_1}\frac{\partial}{\partial s_1}(\frac{1}{h_2}\frac{\partial \phi}{\partial s_2}) + (\dot{x}\cdot s_2)\frac{1}{h_2}\frac{\partial}{\partial s_2}(\frac{1}{h_2}\frac{\partial \phi}{\partial s_2})\Big] \tag{5.42}$$

By back substituting (5.41) and (5.42) into (5.32), we get (5.43).

$$\begin{aligned}
&\ddot{x}\cdot s_2 = \Big[\frac{1}{{h_1}^2 h_2}\frac{\partial \phi}{\partial s_1}\big[(\dot{x}\cdot s_2)\frac{\partial h_2}{\partial s_1} - (\dot{x}\cdot s_1)\frac{\partial h_1}{\partial s_2}\big]\Big] + \\
&\Big[\frac{1}{h_2}\frac{\partial^2 \phi}{\partial t \partial s_2} + (\dot{x}\cdot s_1)\frac{1}{h_1}\frac{\partial}{\partial s_1}(\frac{1}{h_2}\frac{\partial \phi}{\partial s_2}) + (\dot{x}\cdot s_2)\frac{1}{h_2}\frac{\partial}{\partial s_2}(\frac{1}{h_2}\frac{\partial \phi}{\partial s_2})\Big] + \Big[(\dot{x}\cdot s_1) - \frac{1}{h_1}\frac{\partial \phi}{\partial s_1}\Big]\dot{\theta}
\end{aligned} \tag{5.43}$$

By referring to the work of P.J.F Berkvens[12], the scaling of the co-ordinate system is taken at will; we take:

$$h_i = 1, \frac{\partial h_i}{\partial s_i} = 0, i = 1, 2 \tag{5.44}$$

$$\frac{\partial h_2}{\partial s_1} = 0, \frac{1}{R} = -\frac{1}{h_1}\frac{\partial h_1}{\partial s_2} \tag{5.45}$$

Now, substituting (5.45) and (5.44) into (5.43) leads to (5.46).

$$\ddot{x}\cdot s_2 = \frac{1}{h_2}\frac{\partial^2\phi}{\partial t\partial s_2} + \frac{1}{{h_1}^2 h_2}\frac{\partial\phi}{\partial s_1}\big[-(\dot{x}\cdot s_1)(-\frac{h_1}{R})\big] + (\dot{x}\cdot s_1)\frac{1}{h_1}(\frac{\partial h_2}{\partial s_1}\frac{\partial\phi}{\partial s_2} + h_2\frac{\partial^2\phi}{\partial s_1\partial s_2}) +$$
$$(\dot{x}\cdot s_2)\frac{1}{h_2}(\frac{\partial h_2}{\partial s_2}\frac{\partial\phi}{\partial s_2} + h_2\frac{\partial^2\phi}{\partial^2 s_2}) + \Big[(\dot{x}\cdot s_1) - \frac{1}{h_1}\frac{\partial\phi}{\partial s_1}\Big]\dot{\theta} = \frac{1}{h_2}\frac{\partial^2\phi}{\partial t\partial s_2} + \frac{1}{h_1 h_2}\frac{\partial\phi}{\partial s_1}(\dot{x}\cdot s_1)\frac{1}{R} +$$
$$(\dot{x}\cdot s_1)\frac{1}{h_1 h_2}\frac{\partial^2\phi}{\partial s_1\partial s_2} + (\dot{x}\cdot s_2)\frac{1}{{h_2}^2}\frac{\partial^2\phi}{\partial^2 s_2} + \Big[(\dot{x}\cdot s_1) - \frac{1}{h_1}\frac{\partial\phi}{\partial s_1}\Big]\dot{\theta} \tag{5.46}$$

Now, the Laplace equation is S-N co-ordinate system is as expressed in(5.47). This has been derived in

$$\nabla^2\phi = \frac{1}{h_1 h_2}\Big[\frac{\partial}{\partial s_1}(h_2\frac{\partial\phi}{\partial s_1}) + \frac{\partial}{\partial s_2}(h_1\frac{\partial\phi}{\partial s_2})\Big] \tag{5.47}$$

Re-arranging we can get the following expression and note that the potential has to satisfy the Laplace equation.

$$h_1\frac{\partial^2\phi}{\partial^2 s_2} = h_1 h_2\nabla^2\phi - h_2\frac{\partial^2\phi}{\partial^2 s_1} + \frac{h_1}{R}\frac{\partial\phi}{\partial s_2} \tag{5.48}$$

Substituting (5.44) and (5.45) into (5.48) and then substituting (5.48) into (5.46) leads to the final expression (5.49).

$$\frac{\partial^2\phi}{\partial s_2\partial t} = \ddot{x}\cdot s_2 - ((\dot{x}\cdot s_1) - \frac{\partial\phi}{\partial s_1})\dot{\theta} - (\dot{x}\cdot s_1)\big[\frac{\partial\phi}{\partial s_1}\frac{1}{R} + \frac{\partial^2\phi}{\partial s_1\partial s_2}\big] + (\dot{x}\cdot s_2)\big[\frac{\partial^2\phi}{\partial^2 s_1} - \frac{1}{R}\frac{\partial\phi}{\partial s_2}\big] \tag{5.49}$$

Let us replace n for s_2 into (5.49) leads us to an final expression(5.50).

$$\frac{\partial^2\phi}{\partial n\partial t} = \ddot{x}\cdot n - ((\dot{x}\cdot s) - \frac{\partial\phi}{\partial s})\dot{\theta} - (\dot{x}\cdot s)\big[\frac{\partial\phi}{\partial s}\frac{1}{R} + \frac{\partial^2\phi}{\partial s\partial n}\big] + (\dot{x}\cdot n)\big[\frac{\partial^2\phi}{\partial^2 s} - \frac{1}{R}\frac{\partial\phi}{\partial n}\big] \tag{5.50}$$

Derivation for the Dynamic Boundary Condition on the Rigid body

To begin with, the normal acceleration of fluid particle on the body has been derived already in the previous attachment. Here, we will be looking into the normal acceleration of the rigid body. Two co-ordinate systems have been used here for the derivation: The earth fixed co-ordinate system(x,z) and the body fixed co-ordinate system(x',z') which rotates and translates with the body, centered at the center of gravity of the body. Let R be the position vector of point P(x_p,z_p) when viewed from the earth fixed co-ordinate system, r be the position vector of the same point, when viewed from the body fixed co-ordinate system and R_0 be the position vector of the center of gravity when viewed

with the earth fixed co-ordinate system. The relation between the position vectors is presented in (1).

$$R = R_0 + r \tag{5.51}$$

Taking the derivative of (1) leads to expression for velocity, we have to remember ourself that the derivative of vector in a rotating co-ordinate system is as expressed in (2).

$$\frac{\mathrm{Dr}}{\mathrm{Dt}} = \dot{r} + \dot{\theta_G} \times r = \dot{r} + \omega_G \times r \tag{5.52}$$

Now carrying out the derivative of (1) leads to expression (3).

$$V = V_0 + v + \omega_G \times r \tag{5.53}$$

Here V_0 represents the steady translating velocity, v refers to the velocity of the point P due to freedom of vessel to perform translational motions and the last term represents the velocity of the point P due to the rotations of the vessel.

Taking the derivative of (3) leads to an expression of acceleration of the point P on the ship.

$$A = A_0 + a + 2\omega_G \times v + \dot{\omega_G} \times r + \omega_G \times (\omega_G \times r) \tag{5.54}$$

The first two terms represents the steady translational acceleration and acceleration at a point due to the translational modes of motion, the second term is associated with the coriolis acceleration, the third term is due to the acceleration at a point due to rotational modes and the last term is associated with the centripetal acceleration. For the body, we impose no steady velocity and the translational velocities, but we have rotational velocities. This simplifies the expression (4) to (5).

$$A = \dot{\omega_G} \times r + \omega_G \times (\omega_G \times r) \tag{5.55}$$

Taking the derivative of (5) with respect to the generalized normal leads to (6).

$$A \cdot \hat{n} = (\dot{\omega_G} \times r) \cdot \hat{n} + (\omega_G \times (\omega_G \times r)) \cdot \hat{n} \tag{5.56}$$

Using (7) into (6) yields (8).

$$A \times (B \times C) = (A \cdot C)B - (A \cdot B)C \tag{5.57}$$

$$A \cdot \hat{n} = (\dot{\omega_G} \times r) \cdot \hat{n} + ((\omega_G \cdot r)\omega_G - (\omega_G \cdot \omega_G)r) \cdot \hat{n} \tag{5.58}$$

The expression for the normal gradient of the acceleration potential is reproduced here as (9).

$$\frac{\partial^2\phi}{\partial n\partial t} = \ddot{x}\cdot n - ((\dot{x}\cdot s) - \frac{\partial\phi}{\partial s})\dot{\theta} - (\dot{x}\cdot s)\big[\frac{\partial\phi}{\partial s}\frac{1}{R} + \frac{\partial^2\phi}{\partial s\partial n}\big] + (\dot{x}\cdot n)\big[\frac{\partial^2\phi}{\partial^2 s} - \frac{1}{R}\frac{\partial\phi}{\partial n}\big] \quad (5.59)$$

Substituting (8) into (9) leads to (10).

$$\frac{\partial^2\phi}{\partial n\partial t} = (\dot{\omega_G}\times r)\cdot\hat{n} + ((\omega_G\cdot r)\omega_G - (\omega_G\cdot\omega_G)r)\cdot\hat{n} - ((\dot{x}\cdot s) - \frac{\partial\phi}{\partial s})\dot{\theta} - (\dot{x}\cdot s)\big[\frac{\partial\phi}{\partial s}\frac{1}{R} + \frac{\partial^2\phi}{\partial s\partial n}\big] + (\dot{x}\cdot n)\big[\frac{\partial^2\phi}{\partial^2 s} - \frac{1}{R}\frac{\partial\phi}{\partial n}\big] \quad (5.60)$$

Using the Newtons law, the moment can be expressed as the temporal gradient of angular momentum.

$$I\ddot{\theta_G} = L \quad (5.61)$$

The angular momentum can be expressed as the integral of the pressure as in (12).

$$L = \iint_S p(\zeta)(r(\zeta)\times n(\zeta))\mathrm{d}\zeta \quad (5.62)$$

Substituting (12) back in (11) leads to (13).

$$\ddot{\theta_G} = \iint_S \frac{p(\zeta)}{I}(r(\zeta)\times n(\zeta))\mathrm{d}\zeta \quad (5.63)$$

Now substituting (13) in (8) leads to (14).

$$\begin{aligned}\frac{\partial^2\phi}{\partial t\partial n} = &\Big(\Big(\iint_S \frac{p(\zeta)}{I}(r(\zeta)\times n(\zeta))\mathrm{d}\zeta\Big)\times r\Big)\cdot\hat{n} + ((\omega_G\cdot r)\omega_G - (\omega_G\cdot\omega_G)r)\cdot\hat{n} \\ &- ((\dot{x}\cdot s) - \frac{\partial\phi}{\partial s})\dot{\theta} - (\dot{x}\cdot s)\big[\frac{\partial\phi}{\partial s}\frac{1}{R} + \frac{\partial^2\phi}{\partial s\partial n}\big] + (\dot{x}\cdot n)\big[\frac{\partial^2\phi}{\partial^2 s} - \frac{1}{R}\frac{\partial\phi}{\partial n}\big] \quad (5.64)\end{aligned}$$

Using the identity (15) further simplifies (14) to (16).

$$(A\times B)\cdot C = A\cdot(B\times C) \quad (5.65)$$

$$\begin{aligned}\frac{\partial^2\phi}{\partial t\partial n} = &\iint_S \frac{p(\zeta)(r(\zeta)\times n(\zeta))}{I}\cdot(r(x)\times n(x))\mathrm{dS}\zeta + ((\omega_G\cdot r)\omega_G - (\omega_G\cdot\omega_G)r)\cdot\hat{n} \\ &- ((\dot{x}\cdot s) - \frac{\partial\phi}{\partial s})\dot{\theta} - (\dot{x}\cdot s)\big[\frac{\partial\phi}{\partial s}\frac{1}{R} + \frac{\partial^2\phi}{\partial s\partial n}\big] + (\dot{x}\cdot n)\big[\frac{\partial^2\phi}{\partial^2 s} - \frac{1}{R}\frac{\partial\phi}{\partial n}\big] \quad (5.66)\end{aligned}$$

The expression for pressure is provided in (17).

$$p(\zeta) = -\rho(\frac{\partial\phi(\zeta)}{\partial t} + \frac{1}{2}\nabla\phi(\zeta)\cdot\nabla\phi(\zeta) + g\zeta_2) \quad (5.67)$$

Introduce (17) into (16) which yields (18).

$$\frac{\partial^2\phi}{\partial t\partial n} = \iint_S \frac{-\rho(\frac{\partial\phi(\zeta)}{\partial t} + \frac{1}{2}\nabla\phi(\zeta)\cdot\nabla\phi(\zeta) + g\zeta_2)(r(\zeta)\times n(\zeta))}{I}\cdot(r(x)\times n(x))\mathrm{dS}\zeta$$
$$+ ((\omega_G\cdot r)\omega_G - (\omega_G\cdot\omega_G)r)\cdot\hat{n}$$
$$- ((\dot{x}\cdot s) - \frac{\partial\phi}{\partial s})\dot{\theta} - (\dot{x}\cdot s)\big[\frac{\partial\phi}{\partial s}\frac{1}{R} + \frac{\partial^2\phi}{\partial s\partial n}\big] + (\dot{x}\cdot n)\big[\frac{\partial^2\phi}{\partial^2 s} - \frac{1}{R}\frac{\partial\phi}{\partial n}\big] \quad (5.68)$$

The term associated with the temporal gradient of the potential can be bought into the left hand side. By clubbing all the rest terms on the right hand side as $\gamma(x)$, we get (19) from (18).

$$\phi_{tn}(x) + \iint_S K(x,\zeta)\phi_t(\zeta) = \gamma(x) \quad (5.69)$$

$$K(x,\zeta) = \frac{(r(\zeta)\times n(\zeta))\cdot(r(x)\times n(x))}{I} \quad (5.70)$$

The discretized version of (19) can be expressed as (21).

$$(\phi_{tn})^i + \sum_{j=1}^{N_s} C_k^{ij}\phi_t{}^i = \gamma^i \quad (5.71)$$

Here, the variables have the following the expression:

$$C_k^{ij} = \rho\Delta S_j\Big[\frac{(r^i\times n^i)\cdot(r^j\times n^j)}{I}\Big] \quad (5.72)$$

$$\gamma^i = (\omega_G\cdot r^i)(\omega_G\cdot n^i) - (\omega_G\cdot\omega_G)(r^i\cdot n^i) - \sum_{j=1}^{N_s} C_k^{ij}(\frac{1}{2}\nabla\phi^j\cdot\nabla\phi^j) + \nu^i \quad (5.73)$$

$$\nu^i = -((\dot{x^i}\cdot s^i) - (\frac{\partial\phi}{\partial s})^i)\dot{\theta^i} - (\dot{x^i}\cdot s)\big[(\frac{\partial\phi}{\partial s})^i\frac{1}{R^i} + (\frac{\partial^2\phi}{\partial s\partial n})^i\big] + (\dot{x^i}\cdot n)\big[(\frac{\partial^2\phi}{\partial^2 s})^i - \frac{1}{R^i}(\frac{\partial\phi}{\partial n})^i\big] \quad (5.74)$$

Since, we use flat panels to represent the body, the curvature of these panels is zero, which further simplifies (24) into (25).

$$\nu^i = -((\dot{x^i}\cdot s^i) - (\frac{\partial\phi}{\partial s})^i)\dot{\theta^i} - (\dot{x^i}\cdot s)\big[(\frac{\partial^2\phi}{\partial s\partial n})^i\big] + (\dot{x^i}\cdot n)\big[(\frac{\partial^2\phi}{\partial^2 s})^i\big] \quad (5.75)$$

The works of Van Daalen[5] and Tanizawada[25] served as excellent source for the derivation presented above. The derivation is quite similar to that of Van Daalen[5], except the difference of sign before the quadratic terms of potential in (23), which the author believes to be a typo in Daalen's[5] derivation.

Normal gradient of Incident wave potential for weak scatterer diffraction problem

After solving the Boundary Value Problem for the incident wave potential(Numerical Wave Tank solution), we have incident wave potential and its normal gradient on all the bounding surfaces. Using these values, the incident wave potential can be calculated at any point by using (121).

$$\phi(\overrightarrow{x}) = \iint_{\partial S} \big(\phi(\overrightarrow{\zeta})\frac{\partial G}{\partial n}(\overrightarrow{x}, \overrightarrow{\zeta}) - \frac{\partial \phi(\overrightarrow{\zeta})}{\partial n} G(\overrightarrow{x}, \overrightarrow{\zeta})\big)\mathrm{dS} \tag{5.76}$$

Choosing $\overrightarrow{x}$ to be points on the instantaneous body wetted surface(with respect to the incident wave profile) and $\overrightarrow{\zeta}$ to be the points all across the boundaries(upstream, Free surface, downstream and bottom) that form the part of the Numerical Wave Tank, we can find the incident wave potential along the wetted body surface. But, we do not need the potential itself. We rather need the normal gradient of the incident wave potential. We introduce a set of points exterior to the body such that every point on the body has a point associated with this artificial surface(refer to fig 22) and find the gradients. Since, the body is fixed, the normals are simply X-gradients on the left vertical lines and Y-gradients of the bottom. Thus, they can be evaluated with finite difference schemes. In reality, the term on the left hand side of the above equation is to have a fctor of half(see chapter -2), but since we are evaluating the potential on the points inside the computation domain and not on the boundary itself, that factor does not come.

Appendix-E

$$\iint_S (\nabla_i \phi(\nabla_j \phi \cdot n_j) - \frac{1}{2}(\nabla_j \phi \cdot \nabla_j \phi) n_i)\mathrm{dS} \tag{5.77}$$

Rearranging this equation,by using A(B.C)=AB.C for the first of the integrand,we get (2)

$$\iint_S ((\nabla_i \phi \nabla_j \phi) \cdot n_j - \frac{1}{2}(\nabla_j \phi \cdot \nabla_j \phi) n_i)\mathrm{dS} \tag{5.78}$$

Applying the divergence theorem:

$$\iiint_V (\nabla_j(\nabla_i \phi \nabla_j \phi) - \frac{1}{2}\nabla_i(\nabla_j \phi \cdot \nabla_j \phi))\mathrm{dv} \tag{5.79}$$

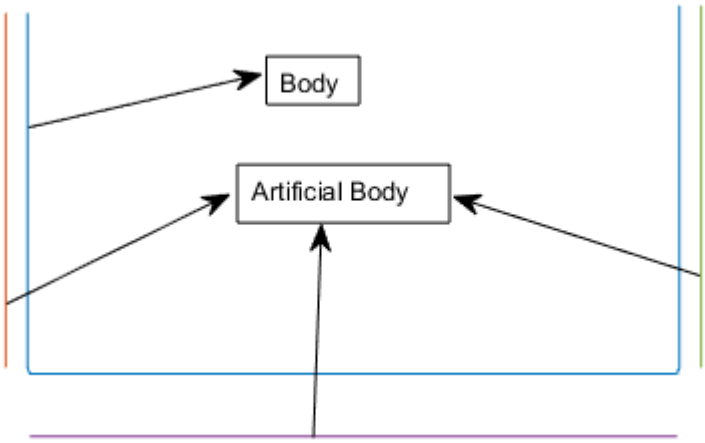

Figure 5.2: Artificial body along with the actual body

Expanding the first term using d(AB)=dA B + dB A,we get:

$$\iiint_V (\frac{\partial^2 \phi}{\partial {x_j}^2} \nabla_i \phi + \nabla_j \phi \nabla_j (\nabla_i \phi) - \frac{1}{2} \nabla_i (\nabla_j \phi \cdot \nabla_j \phi)) dv \tag{5.80}$$

Now,lets consider the third term of the integrand and expanding the del operator

$$\frac{1}{2} \nabla_i (\nabla_j \phi \cdot \nabla_j \phi) = \frac{1}{2} ((\nabla_i \nabla_j \phi) \cdot \nabla_j \phi + \nabla_j \phi \cdot (\nabla_i \nabla_j \phi)) \tag{5.81}$$

If we carefully look at the right hand side terms,they are both equal.

$$\frac{1}{2} \nabla_i (\nabla_j \phi \cdot \nabla_j \phi) = (\nabla_i \nabla_j \phi) \cdot \nabla_j \phi \tag{5.82}$$

Now,(A.B)=—A——B—cos(θ),if A=B,then A.A=—A——A—,using this in equation 6.

$$(\nabla_i \nabla_j \phi) \cdot \nabla_j \phi = \nabla_i \nabla_j \phi \nabla_j \phi \tag{5.83}$$

Now,re-arranging the indices,we get (8).

$$\frac{1}{2} \nabla_i (\nabla_j \phi \cdot \nabla_j \phi) = \nabla_j \phi \nabla_i (\nabla_j \phi) \tag{5.84}$$

Now,substituting (8) in (4),(4) reduces to (9):

$$\iiint_V (\frac{\partial^2 \phi}{\partial {x_j}^2} \nabla_i \phi + \nabla_j \phi \nabla_j (\nabla_i \phi) - \nabla_j \phi \nabla_j (\nabla_i \phi)) dv = \iiint_V (\frac{\partial^2 \phi}{\partial {x_j}^2} \nabla_i \phi) dV \tag{5.85}$$

Now,since the potential satisfies the laplace equation,the expression goes to zero.So:

$$\iint_S (\nabla_i \phi (\nabla_j \phi \cdot n_j) - \frac{1}{2} (\nabla_j \phi \cdot \nabla_j \phi) n_j) ds = 0 \tag{5.86}$$

Bibliography

[1] Longuet-Higgins and Cokelet, "The deformation of steep surface waves on water i.a numerical method of computation," *Proc. R. Soc. Lond. A.*, vol. 350, pp. 1–26, 1976.

[2] T. Vinje and P. Brevig, "Nonlinear two-dimensional ship motion," *Proceedings of the 3rd International Conference on Numerical Ship Hydrodynamics*, 1981.

[3] W.Lin, "Nonlinear motion of the free surface near a moving body," *Doctoral Thesis,MIT*, 1984.

[4] J.E.Romate, "The numerical simulations of nonlinear gravity waves in three dimensions using a higher order panel method," *Doctoral Thesis,TU Twente*, 1989.

[5] J. Broeze, "Numerical modeling of nonlinear free surface waves with a 3d panel method," *Doctoral Thesis,TU Twente*, 1993.

[6] V. Daalen, "Numerical and theoretical studies of water waves and floating bodies," *Doctoral Thesis,TU Twente*, 1993.

[7] D Sen, "A numerical method for two-dimensional studies of large amplitude motions of floating bodies in steep waves," *Doctoral Thesis,Memorial University of Newfoundland*, 1988.

[8] J. Pawlowski, "A nonlinear theory of ship motions in waves," *Proceedings of the 19th Symposium on Naval Hydrodynamics*, 1992.

[9] R. F. Beck, "Fully nonlinear water wave computations using a desingularized euler-lagrange time-domain approach," *Nonlinear Water Wave Interaction, Advances in Fluid Mechanics*, pp. 1–59, 1999.

[10] P.D.Sclavounous, "Nonlinear impulse of ocean waves on floating bodies," *J. Fluid Mech.*, vol. 697, pp. 316–337, 2012.

[11] P. S.Lee, "A fluid impulse nonlinear theory of ship motions and sea loads," *International Shipbuilding Progress*, vol. 60, pp. 555–577, 2013.

[12] J.-H. Westhuis, "The numerical simulation of nonlinear waves in a hydrodynamical model test basin," *Doctoral Thesis,TU Twente*, 2001.

[13] Kellogg, "Foundations of potential theory," 1929.

[14] R. H. Courant, "Methods of mathematical physics, ii.," *Interscience Publishers, New York*, 1962.

[15] G. Jawson M.A; Symm, "Integral equation methods in potential theory and and electrostatics," *Academic Press, London*, 1977.

[16] B Hunt, "The panel method for subsonic aerodynamic flows: A survey of mathematical formulations and numerical models, and an outline of the new british aerospace scheme.," *VKI lecture series 1978-4 on Computational Fluid Dynamics*,

[17] M.M.Rienecker and J.D.Fenton, "A fourier approximation method for steady water waves," *J. Fluid Mech.*, vol. 104, pp. 119–137, 1981.

[18] Cointe, "Remarks on the numerical treatment of the intersection point between a rigid body and a free surface," *International Workshop on Water Wave and Floating Bodies(IWWWWFB)*, 1988.

[19] Greenhow and Lin, "Nonlinear free surface effects: Experiments and theory," *Report, MIT*, 1983.

[20] T. Vada and D. Nakos, "Time-marching schemes for ship motion simulations," *Proceedings of the 8th International Workshop on Water Waves and Floating Bodies*, 1993.

[21] W.Koo and M.H.Kim, "Freely floating-body simulation by a 2d fully nonlinear numerical wave tank," *Ocean Engineering*, vol. 31(16), pp. 2011–2046, 2004.

[22] R.Cointe, "Quelques aspects de la simulation numerique d'un canal a houle(284 pages in french)," *Doctoral thesis, Ecole Nationale des Pnts et Chaussees, Paris, France*, 1989.

[23] R. Y.Cao and W.W.Schultz, "Nonlinear computaion of wave loads and motions of floating bodeis in incident waves," *Proceedings of the 9th International Workshop on Water Waves and Floating Bodies(IWWWFB)*, 1994.

[24] G. Wu and R.Eatock-Taylor, "Transient motion of a floating body in steep water waves," *Proceedings of the 11th International Workshop on Water Waves and Floating Bodies(IWWWWFB)*, 1996.

[25] K. Tanizawa, "A nonlinear simulation method of 3d body motions in waves," *Journal of Society of Naval Architects of Japan*, vol. 178, pp. 179–191, 1995.

[26] M. Kashiwagi, *Fully-nonlinear simulations of hydrodynamic forces on a heaving two-dimensional body*, 1996.

[27] P. Berkvens, "Floating bodies interacting with water waves," *Doctoral thesis, Technical University of Twente*, 1998.

[28] W. J.M.J Journee and R. Huijmans, "Offshore hydromechanics," *Course notes, Delft University of Technology*,

[29] L.Eca and M.Hoekstra, "A procedure for the estimation of the numerical uncertainity of cfd calculations based on grid refinement studies," *Journal of Computational Physics*, vol. 262, pp. 104–130, 2014.

[30] D. Y. H.Xu, "Computations of fully-nonlinear three-dimensional water waves," *Nineteenth Symposium on Naval Hydrodynamics*, 1992.

[31] Leo.H.Holthuijsen, "Waves in oceanic and cosatal waters," *Cambridge University Press*, 2007.

[32] H.Lamb, "A treatise on the mathematical theory of the motion of the fluids," *Cambridge University Press*, 1879.